



**Politecnico
di Torino**

Collegio di Ingegneria Chimica e dei Materiali
Corso di Laurea Magistrale in Ingegneria dei Materiali

Cantilever deflection measurement for thin film stress evaluation for MEMS applications

Relatore:
Prof. Stefano Bianco

Candidato:
Niccolò Bottauscio

Relatore esterno:
Dott. Luca Lamagna

Anno Accademico 2022/2023
Sessione di Laurea novembre 2023

Acknowledgments

Ci tengo a ringraziare il gruppo R&D MEMS di STMicroelectronics per avermi dato l'opportunità di svolgere il mio lavoro di tesi presso la sede di Agrate Brianza (MB).

Ringrazio il prof. Stefano Bianco per il suo lavoro di supervisione e il dott. Luca Lamagna e la dott.ssa Laura Castoldi per avermi seguito in tutte le fasi dell'attività in azienda.

Ringrazio il dott. Igor Varisco, il dott. Andrea Nomellini, la dott.ssa Federica Capra, la dott.ssa Federica Dusi, il dott. Andrea Casanova, il dott. Mattia Pallaro, la dott.ssa Angelica Baldini, il dott. Riccardo Tacchini, la dott.ssa Anita Previdi, la dott.ssa Alessandra Sciutti, il dott. Davide Assanelli, la dott.ssa Rossella Chiara, il dott. Andrea Picco, il dott. Marco Dosi, il dott. Francesco Revello, il dott. Matteo Bisogni e il dott. Filippo Formoso per avermi seguito durante le fasi di processo e di misurazione.

Ringrazio il dott. Fabrizio Cerini e il dott. Roberto Carminati per le consulenze riguardo il modello utilizzato.

Infine, un ringraziamento generale a tutti coloro con cui ho condiviso questi mesi in azienda.

Abstract

This experimental work is focused on the study of residual stress in thin films deposited by Chemical Vapor Deposition (CVD) techniques and used for the fabrication of micro-electromechanical systems (MEMS) sensors and actuators. The research activity has been carried out in the STMicroelectronics site located in Agrate Brianza (MB), working within the R&D MEMS process and technology development team. The activity has been focused on the fabrication of MEMS test structures, processed inside the ST clean room on 8" wafers, the stress characterization and the discussion of the results.

Residual stress of thin films is a critical aspect which has to be carefully taken into account during both design and manufacturing of MEMS devices. The reference technique in MEMS industry to evaluate the residual stress of thin films is the scanning laser method, which is commonly used in every front-end production line. This method provides the mean residual stress of a thin film from the measurement of the curvature of the wafer by using Stoney's equation. The main limitation of this approach is that it does not provide a local measurement and therefore any information on the distribution of the stress variation on the wafer surface. Therefore, it is not possible to study the center-to-edge variability which is an extremely useful information in the framework of semiconductor processing and fabrication.

In this work, an alternative method to evaluate the residual stress of thin films has been applied on different dielectric thin films deposited by CVD industrial techniques. This method is based on the characterization of an array of cantilevers which are fabricated on silicon wafers employing a simplified MEMS process flow. The fabrication process of the MEMS cantilevers is thoroughly described along the work with dedicated sections that describe the deposition, patterning and release of the structures. Upon release, cantilevers deflect to partially relieve the unbalanced residual stress in the material. The deflection of the MEMS structures has been measured on the whole wafer by employing visible light interferometry. The residual stress of the thin films integrated in the structure has been calculated from the deflection of the cantilevers.

This method differs from wafer level measurement techniques: it enables local analyses of the residual stress in microfabricated structures thus enabling the evaluation of the local and center-to-edge stress variability. The stress distribution on the wafers has been characterized for eight different films; the results have been correlated with the specific deposition technique. This alternative approach to stress evaluation, based on the use of MEMS test structures, paves the way for the study of multi-layer stacks.

Index

1. Introduction.....	1
1.1. Micro-electromechanical systems (MEMS)	
1.2. Silicon in MEMS	
1.2.1. Mechanical properties of silicon	
1.2.2. Fabrication of single-crystal wafers	
1.3. Thin films in MEMS	
1.4. Purpose of this thesis	
2. Residual stress of thin films.....	9
2.1. Thermal stress	
2.2. Intrinsic stress	
2.2.1. Origin of stress in LPCVD silicon nitride films	
2.2.2. Origin of stress in PECVD silicon nitride films	
2.2.3. Origin of stress in PECVD silicon oxide films	
2.3. Stress characterization	
3. Process flow for cantilever fabrication.....	18
3.1. Growth of the base layer	
3.1.1. Epitaxial polysilicon	
3.1.2. Chemical Mechanical Polishing	
3.2. Deposition of the thin film	
3.2.1. Low Pressure Chemical Vapor Deposition	
3.2.2. Plasma Enhanced Chemical Vapor Deposition	
3.3. Front side patterning	
3.3.1. Optical lithography	
3.3.2. Dry etching	
3.3.2.1. Reactive Ion Etching for dielectric etching	
3.3.3. Bosch process	
3.4. Release of the structures	
3.4.1. Temporary Polymer-based Bonding	
3.4.2. Back side patterning	
3.4.3. Debonding of the cap wafer	
4. Characterization of thin films.....	40
4.1. Thickness measurement	
4.1.1. Ellipsometry	
4.1.2. Reflectometry	

4.2.	Curvature measurement for stress evaluation	
4.3.	Measurement of the deflection of released structures	
5.	Theoretical model for stress evaluation from cantilever deflection	48
5.1.	Single-layer cantilever	
5.2.	Bi-layer cantilever	
6.	Fabrication and characterization of test structures	55
6.1.	Fabrication of test structures	
6.2.	Measurement setup	
6.3.	Calculation of residual stress	
6.4.	Characterization by the scanning laser method	
7.	Results and discussion	65
7.1.	Residual stress of the EPI Poly layer	
7.2.	Validation of the assumptions in the calculation of residual stress	
7.3.	Stress gradient of the EPI Poly layer	
7.4.	Residual stress of thin films: lot 2	
7.4.1.	Residual stress of LPCVD SiN tens	
7.4.2.	Residual stress of PECVD USG	
7.4.3.	Residual stress of PECVD SiN +170	
7.4.4.	Residual stress of PECVD SiN -150	
7.5.	Comparison between cantilevers of different thicknesses	
7.6.	Comparison between cantilevers of different lengths	
7.7.	Residual stress of thin films: lot 3	
7.8.	Comparison with the scanning laser method	
8.	Conclusions	88
8.1.	Achieved results	
8.2.	Outlooks	

1 | Introduction

1.1. Micro-electromechanical systems (MEMS)

Micro-electromechanical systems (MEMS) are miniaturized devices that integrate electrical and mechanical elements, commonly fabricated on silicon wafers. The well-established microfabrication techniques in semiconductor industry had a fundamental role in the development of silicon MEMS. Differently from integrated circuit (IC) technology, silicon is employed not only for its electrical properties, but also for its excellent mechanical properties. The evolution of MEMS from the last decades of the 20th century enabled the mass volume production of relatively low-cost microscopic sensors and actuators. In sensing applications, the device converts an external stimulus into an electrical signal, which is then elaborated by a microprocessor. Accelerometers are an example of MEMS sensors used to transduce acceleration into an electrical signal due to the motion of a movable silicon mass. In Figure 1, an image of a 6-axis inertial sensor, which includes an accelerometer and a gyroscope, is shown.

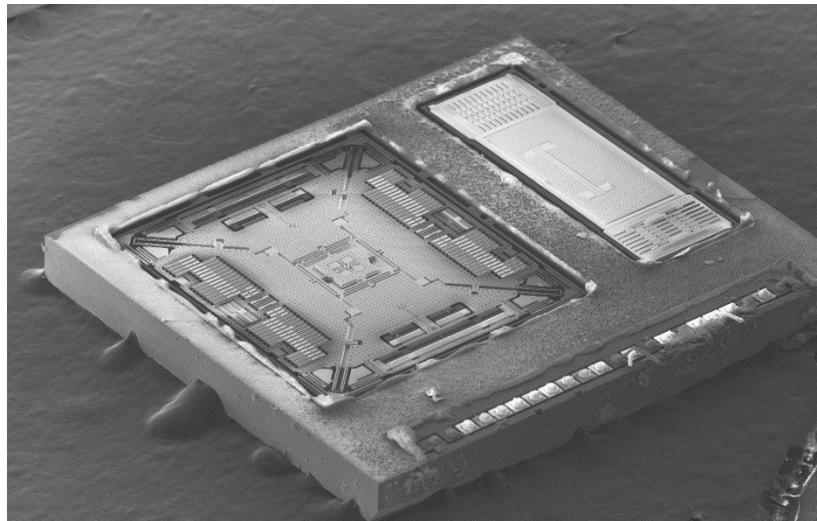


Figure 1: SEM image of a 6-axis inertial sensor.

Actuators work oppositely: the device creates mechanical motion as a consequence of an electrical input signal [1]. Micromirrors (Figure 2) are an example of MEMS actuators. Micromirrors rotate when they are actuated by the input signal, reflecting light at a different angle. MEMS actuators can rely on several different actuation principles, such as electrostatic, electromagnetic or piezoelectric.



Figure 2: SEM image of a PZT-actuated micromirror. [2]

For both sensors and actuators, MEMS must be interfaced with application-specific integrated circuits (ASIC), as shown in Figure 3. ASIC is needed to elaborate the output signal from MEMS (in sensors) or to actuate MEMS (in actuators). Therefore, devices are composed of both systems.

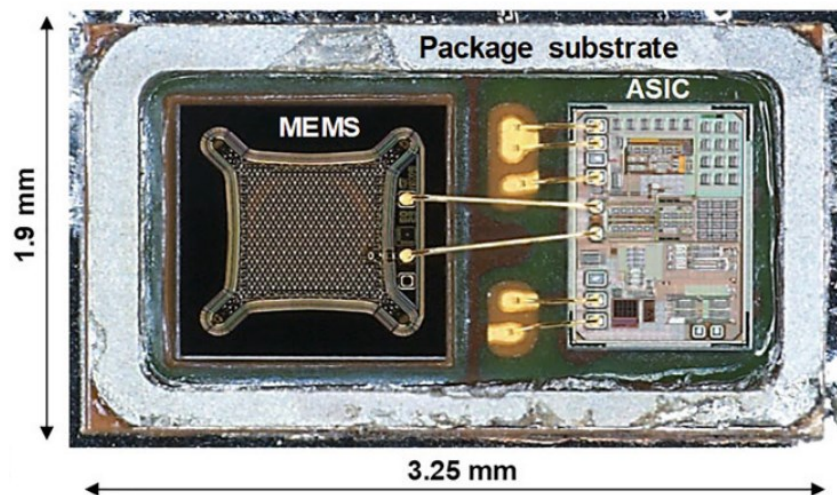


Figure 3: Image of a MEMS microphone interfaced with the ASIC by wire bonding.

The first mass volume application of MEMS was the ink jet printer, developed by IBM in the 1980s [3,4]. Ink is forced through an array of nozzles obtained employing anisotropic wet etching of silicon. Then, MEMS received a lot of interest in automotive applications with the first air pressure

sensors and accelerometers. The main challenging requirements for MEMS in the automotive industry were high reliability and high quality. In the early 21st century, new challenges arose with the development of consumer electronics, such as low power consumption, higher miniaturization, and lower cost. Wearable electronics evolved from the first wrist devices, used to measure physiological parameters, to the modern smart watches. In parallel, mobile phones evolved into smart phones. These are just a few examples of how the evolution of MEMS over the last decades affected the development of devices which have an impact on everyday life.

The MEMS structure used in this work is the cantilever which is one of the simplest structures from the fabrication and characterization point of view. Cantilevers are free-standing beams fixed on one end and suspended on the other one. This structure has been employed in several applications, such as RF switches [5], biosensors [6,7] and atomic force microscopy (AFM) probes [8]. In Figure 4, a SEM image of an array of cantilevers is shown.

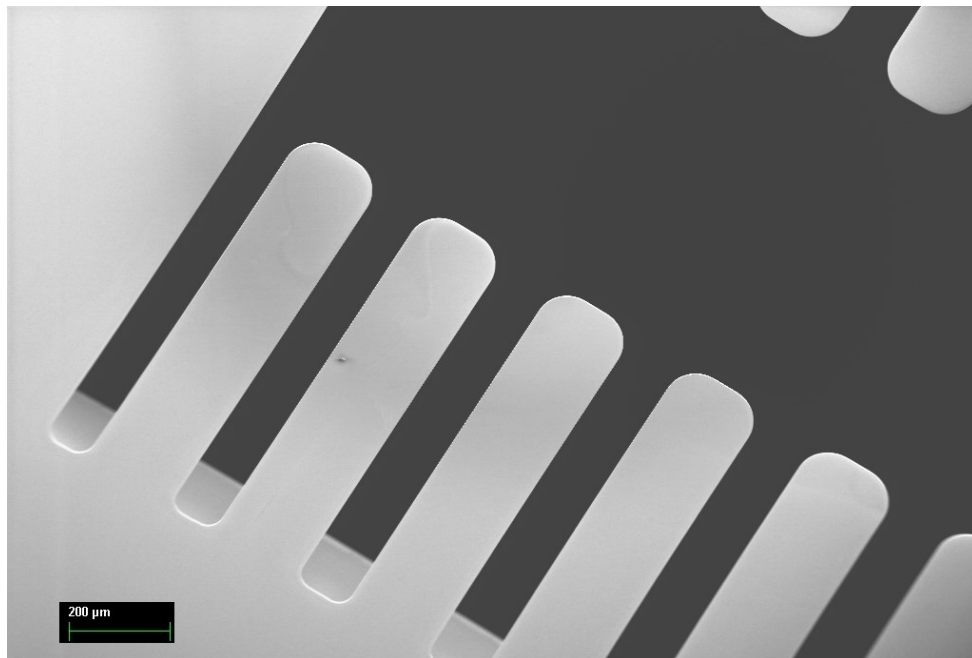


Figure 4: SEM image of an array of cantilevers.

1.2. Silicon in MEMS

Silicon is the reference substrate for MEMS fabrication [9]. The excellent mechanical properties of silicon represent a fundamental factor in the employment of this material in MEMS industry [10]. The mechanical properties of silicon are introduced in section 1.2.1, while the fabrication of single-crystal silicon wafers is briefly discussed in section 1.2.2.

1.2.1. Mechanical properties of silicon

Silicon is a hard and brittle material; thus, it undergoes fracture without showing plastic deformation at room temperature. However, it must be noted that it is not a fragile material since it is characterized by high Young's modulus and yield strength. Silicon is an ideal structural material since the excellent mechanical properties are combined with low density. In Table 1, the mechanical properties of silicon are compared with steel, known for its high Young's modulus and yield strength, and with aluminum, known for its low density. Silicon is characterized by a Young's modulus nearly equal to the Young's modulus of steel, while the yield strength is even higher. Moreover, it has a density nearly the same as aluminum. It is important to notice that silicon has a lower thermal expansion coefficient than steel and aluminum, thus it shows a higher thermal dimensional stability.

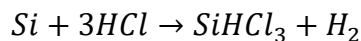
Table 1: Comparison between the thermomechanical properties of silicon, steel and aluminum [10].

	Silicon	Steel	Aluminum
Young's modulus (GPa)	$1.9 \cdot 10^2$	$2 \cdot 10^2$	$0.7 \cdot 10^2$
Yield strength (GPa)	7	2.1	0.17
Density ($\text{g} \cdot \text{cm}^3$)	2.3	7.9	2.7
Thermal expansion ($10^{-6} \cdot \text{K}^{-1}$)	2.33	17.3	25

Although single-crystal silicon has excellent mechanical properties, the apparent strength is affected by the number of defects. Therefore, it is fundamental to reduce the probability of defects generation during the processing and to integrate quality-control steps.

1.2.2. Fabrication of single-crystal wafers

Silicon is present on Earth in the form of silica. Several processes are needed to obtain high-quality single-crystal silicon from silica-rich sands, which are characterized by a high level of impurities. Firstly, silica is reduced by carbon in an electrode arc furnace to obtain metallurgical-grade (MG) polysilicon at temperatures higher than 2000°C. MG polysilicon is characterized by an impurity level of 2%, which must be further decreased for applications in semiconductor industry. Thus, it is converted to SiHCl_3 by reacting with HCl at 300°C:



Fractional distillation is used to separate SiHCl_3 from the impurity chlorides and then Siemens process is employed to decompose the liquid SiHCl_3 at 1000–1200 °C. During the process, silicon deposits on a silicon rod, resulting in electronic-grade (EG) polysilicon with an impurity concentration lower than a few parts per billion (ppb).

Czochralski method [11], illustrated in Figure 5, is the most employed technique to obtain single-crystal silicon. In a vacuum furnace, polysilicon is put into a silica crucible and then melted just above the silicon melting temperature. Then, a small single-crystal seed is dipped into the melt, resulting in a reduction of the temperature of the melt in contact with the seed. The silicon atoms in contact with the seed crystallize at the end of the seed following its crystal structure. While molten silicon solidifies, the seed and the crucible are rotated in the opposite direction to obtain cylindrical ingots.

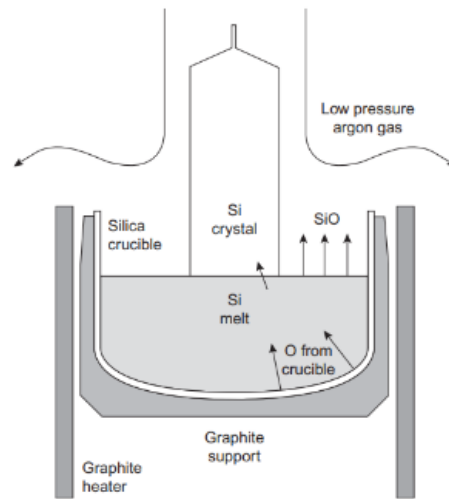


Figure 5: Schematic illustration of the fabrication of single-crystal silicon ingots employing the Czochralski method [12].

The ingot is produced with a slightly greater diameter to overcome problems related to dimensional fluctuations and deviations from the round shape. Therefore, the diameter is adjusted before slicing. The wafers obtained by slicing show sharp edges, thus they are rounded in the edge grinding step, reducing the probability of chipping. Grinding and lapping are employed to obtain macroscopically flat surfaces. The superficial damage introduced by these processes is removed by chemical etching.

1.3. Thin films in MEMS

During the fabrication of MEMS devices, several different films are deposited on the substrate to exploit their characteristic properties and to fabricate, layer after layer, the final device stack. For example, dielectric films can be employed as passivation layers [13], while piezoelectric films [14,15] as active materials enabling the functioning of sensors and actuators. Depending on their thickness, films can be classified as ultra-thin (1 nm – 50 nm), thin (50 nm – 1 μm) or thick (>1

μm). Thin films are widely used in microfabrication processes. They are commonly deposited employing Chemical Vapor Deposition (CVD) or Physical Vapor Deposition (PVD) depending on the material and the final properties required.

It is important to highlight that, in addition to their functional role in the device, thin films may affect the mechanical behavior of the microfabricated structures due to their residual stress. If it is not properly considered during the design of the device, residual stress can lead to structural failures or unexpected distortions of released structures. Moreover, a significant residual stress drift could be one of the main factors affecting the performance of devices during their lifetime. The Finite Element Method (FEM) is employed during the design of MEMS devices to predict their mechanical behavior. In order to obtain a reliable prediction, the mechanical properties of thin films must be previously evaluated and included in the model.

1.4. Purpose of this thesis

In MEMS industry, the residual stress of a thin film is commonly estimated from the bow of the wafer by Stoney's equation [16], which is discussed in section 2.3. The wafer bow is measured employing the *scanning laser method* [17], which is detailed section 4.2. However, this method exhibits several limitations. Firstly, it is a wafer level technique; therefore, it allows only the measurement of the mean residual stress of the unpatterned film. Local analyses are precluded and thus it is not possible to study the center-to-edge variability. As mentioned above, the performance of the device is affected by the overall residual stress, which must be considered during the design. The device works correctly if the residual stress of each layer is included in a range centered at the target value. The fact that the mean residual stress of a thin film deposited on an 8" wafer is included in the control range does not guarantee that for all the devices fabricated on the wafer surface the value of the residual stress is actually acceptable for the correct functioning. Secondly, the measurement is usually performed on test wafers and not directly on device wafers. Therefore, the measurement refers to the as-deposited residual stress, neglecting the effect of the following processes. For instance, thermal treatments might have a significant effect on the morphology and the composition of a thin film [18]: high temperature processes can modify the residual stress of thin films. Finally, the scanning laser method does not allow a reliable and accurate analysis of complex stacks composed of different layers. The residual stress of a thin film in a stack can be different from the value measured by Stoney's equation using a single test wafer. The difference in the coefficient of thermal expansion (CTE) between the film and the substrate is a source of residual stress, called thermal stress. The measurement of the residual stress of a thin film by Stoney's equation considers a silicon substrate; however, in a stack the deposition may occur on a layer with a different CTE than silicon, affecting the thermal stress contribution.

In this work, an alternative method to evaluate the residual stress of thin films is tested. This method is based on a test structure made of an array of cantilever beams and it is used to measure the residual stress of several dielectric films employed in MEMS devices. The residual stress is evaluated from the deflection of the cantilevers upon release. The term “release” refers to the portion of the process flow involved in obtaining free-standing structures. Upon release cantilevers deflect to partially relieve the unbalanced residual stress in the material, as shown in Figure 6. It is possible to evaluate the residual stress by employing visible light interferometry (section 4.3) to measure the deflection of the beam. This method, which is referred to as *the cantilever deflection method*, differs from wafer level measurement techniques (section 2.3) since it enables local analyses of the residual stress in microfabricated structures. The purpose of this thesis is to measure the residual stress locally, thus enabling the evaluation of its variation across the 8” wafer. The analysis is performed for eight different dielectric thin films deposited by CVD (i.e., silicon nitride, silicon oxide and silicon oxynitride). From each cantilever, the local residual stress of the film can be calculated. Therefore, this method allows to map the residual stress across the entire 8” wafer thus resulting in a localized and detailed stress characterization.

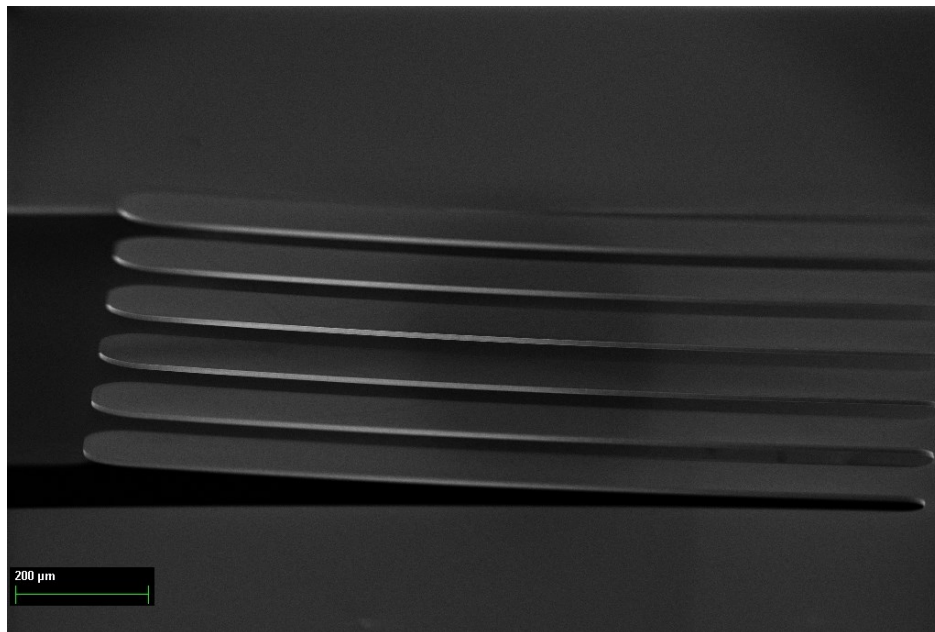


Figure 6: SEM image of an array of deflected cantilevers due to the residual stress in the structure.

References

- ¹ T.B. Jones, N.G. Nenadic; *Electromechanics and MEMS*; Cambridge University Press (2013).
- ² B. Vigna, P. Ferrari, F. F. Villa, E. Lasalandra, S. Zerbinì; *Silicon Sensors and Actuators*; Springer; chapter 18: “Micromirrors” (2022).
- ³ E. Bassous, H. H. Taub, L. Kuhn; *Ink jet printing nozzle arrays etched in silicon*; Appl. Phys. Lett. 31, 135–137 (1977).
- ⁴ L. Kuhn, E. Bassous, R. Lane; *Silicon Charge Electrode Array for Ink Jet Printing*; IEEE Transactions on Electron Devices 25, 1257–1260 (1978).
- ⁵ M. N. Mollah, N. C. Karmakar; *RF-MEMS switches: paradigms of microwave switching*; Proceedings of APMC2001, Taipei, Taiwan, 1024–1027 (2001).
- ⁶ M. Toda, N. Inomata, T. Ono, I. Voiculescu; *Cantilever Beam Temperature Sensors for Biological Applications*; IEEE Trans 12, 153–160 (2017).
- ⁷ C. Ziegler; *Cantilever-based biosensors*; Anal Bioanal Chem 379, 946–959 (2004).
- ⁸ A. Dzedzickis, J. Rožėnė, V. Bučinskis, D. Viržonis and I. Morkvėnaitė-Vilkončienė; *Characteristics and Functionality of Cantilevers and Scanners in Atomic Force Microscopy*; Materials, 16, 6379 (2023).
- ⁹ T. Ando, X.-A. Fu; *Materials: Silicon and beyond*; Sensors and Actuators A 296, 340–351 (2019).
- ¹⁰ K. E. Petersen; *Silicon as a Mechanical Material*; Proceedings of the IEEE 70, 5 (1982).
- ¹¹ J. Evers, P. Klüfers, R. Staudigl, P. Stallhofer; *Czochralski's Creative Mistake: A Milestone on the Way to the Gigabit Era*; Angew. Chem. Int. Ed., 42, 5684–5698 (2003).
- ¹² M. Tilli, T. Motooka, V. Airaksinen, S. Franssila, M. Paulasto-Kröckel, V. Lindroos; *Handbook of Silicon Based MEMS Materials and Technologies*; Elsevier (2015).
- ¹³ E. Vanhovea, A. Tsopėlaa, L. Bouscayrol, A. Desmouлина, J. Launaya, P. Temple-Boyer; *Final capping passivation layers for long-life microsensors in real fluids*; Sensors and Actuators B 178, 350–358 (2013).
- ¹⁴ S. Trolier-McKinstry, P. Murali; *Thin Film Piezoelectrics for MEMS*; Journal of Electroceramics, 12, 7–17 (2004).
- ¹⁵ I. Kanno; *Piezoelectric MEMS: Ferroelectric thin films for MEMS applications*; Japanese Journal of Applied Physics 57, 040101 (2018).
- ¹⁶ G. G. Stoney; *The tension of metallic films deposited by electrolysis*; Proc. R. Soc. London A 82, 172–173 (1909).
- ¹⁷ L. B. Freund, S. Suresh; *Thin Film Materials: Stress, Defect Formation and Surface Evolution*; Cambridge University Press; chapter 2: “Film stress and substrate curvature” (2004).
- ¹⁸ K.-S. Chen, X. Zhang, S.-Y. Lin; *Intrinsic stress generation and relaxation of plasma-enhanced chemical vapor deposited oxide during deposition and subsequent thermal cycling*; Thin Solid Films 434, 190–202 (2003).

2 | Residual stress of thin films

Stress (σ) is defined as a force per unit area. When a solid is subjected to external loadings, stress is generated as an internal resistance [1]. When loaded, all the materials undergo elastic deformation: linear strain (ϵ) is defined as the change in length per unit length. The macroscopical deformation is a consequence of the variation of the interatomic spacing [2]. Stress is related to strain by the constitutive equations of solid mechanics [3]. When the material is unloaded, the elastic deformation is recovered, and stress is relieved. However, thin films are characterized by a mismatch strain resulting in the generation of residual stress due to the substrate constraint [4]. Residual stress is defined as the internal stress of a material in absence of external loadings. It can be responsible for distortion or even failure of structures, therefore the analysis of the stress state is fundamental for the design and fabrication of devices [5]. The residual stress of a film (σ_{res}) is the consequence of two different contributions:

$$\sigma_{res} = \sigma_{th} + \sigma_i \quad (2.1)$$

where σ_{th} is the thermal stress due to a mismatch of the thermal expansion coefficients between the film and the substrate, while σ_i is the intrinsic stress of the thin film.

Commonly, stress is not uniform across the thickness of a layer due to localized effects [6]. Assuming a linear stress gradient [7], as shown in Figure 7, the residual stress can be written as a function of the y coordinate as follows:

$$\sigma = \left(\frac{\sigma_1 + \sigma_2}{2}\right) + \left(\frac{\sigma_1 - \sigma_2}{b}\right)y \quad (2.2)$$

where σ_1 and σ_2 are respectively the residual stress at the top and at the bottom of the layer, while b is the thickness of the layer.

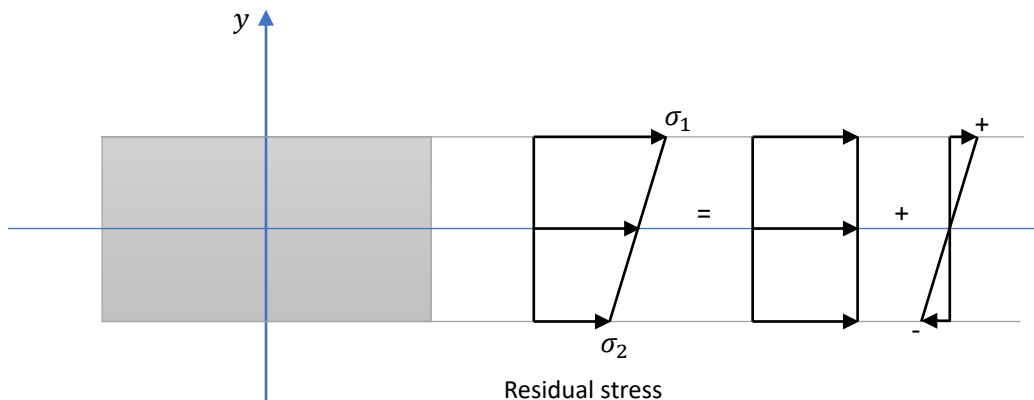


Figure 7: Variation of the residual stress across the thickness of a layer, assuming a linear stress gradient.

2.1. Thermal stress

Thermal stress is caused by the difference in thermal expansion coefficients between the film and the substrate. After the deposition, the wafer experiences a temperature drop from the deposition temperature (T_{dep}) to room temperature. Consequently, the film and the substrate should exhibit a strain (ε) which depends on the thermal expansion coefficient (α) and the temperature variation ($T - T_{dep}$). Assuming that the thermal expansion coefficient is constant in the range of temperature considered, the strain is obtained as follows:

$$\varepsilon = \alpha(T - T_{dep}) \quad (2.3)$$

Due to the different thermal expansion coefficients, a mismatch in strain occurs between the film and the substrate upon cooling. Since the strain of the film must be equal to the strain of the substrate, stress is generated resulting in net forces acting on the film (F_f) and on the substrate (F_s). Due to equilibrium of forces, F_s is equal to $(-F_f)$. Considering a portion of the film-substrate system and a state of biaxial stress, the actual strain can be obtained by using Eq. 2.4a or Eq. 2.4b [9].

$$\varepsilon = \alpha_f(T - T_{dep}) + \frac{F_f}{d_f w} \frac{(1 - \nu_f)}{E_f} \quad (2.4a)$$

$$\varepsilon = \alpha_s(T - T_{dep}) - \frac{F_f}{d_s w} \frac{(1 - \nu_s)}{E_s} \quad (2.4b)$$

The subscripts f and s refer respectively to the film and the substrate, E and ν are the Young's modulus and the Poisson's ratio, while d and w are respectively the thickness and the width of the section on which the net force acts. By equating Eq. 2.4a and Eq. 2.4b, F_f can be written as:

$$F_f = \frac{(\alpha_s - \alpha_f)(T - T_{dep})w}{\frac{(1 - \nu_f)}{d_f E_f} + \frac{(1 - \nu_s)}{d_s E_s}} \quad (2.5)$$

Assuming that $d_s E_s / (1 - \nu_s) \gg d_f E_f / (1 - \nu_f)$, the thermal stress of the film is obtained from Eq. 2.5:

$$\sigma_{th} = \frac{F_f}{d_f w} = (\alpha_s - \alpha_f)(T - T_{dep}) \frac{E_f}{(1 - \nu_f)} \quad (2.6)$$

In Figure 8, the generation of the thermal stress is shown. If α_f is greater than α_s , the film tends to shrink more than the substrate upon cooling. Therefore, the substrate constrains the shrinkage of the film resulting in a tensile thermal stress in the film (Figure 8a). On the contrary, if α_f is lower than α_s , the thermal stress in the film is compressive (Figure 8b).

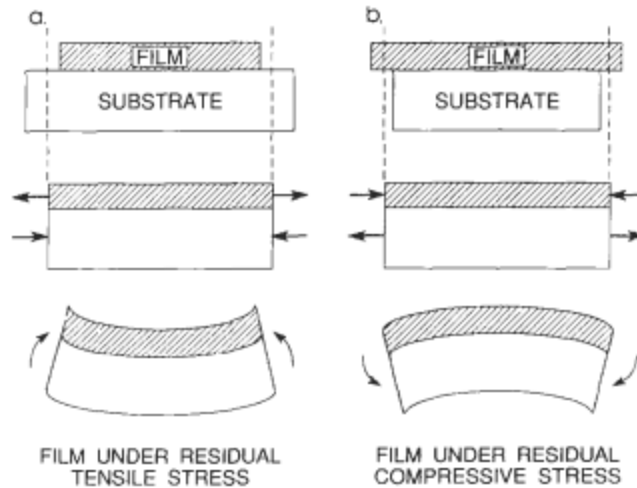


Figure 8: Generation of thermal stress in the film: (a) tensile stress, when the substrate constrains the shrinkage of the film; (b) compressive stress, when the substrate shrinks more than the film. [9]

It should be noted that, for a specific film-substrate combination, the thermal stress depends only on the deposition temperature and the temperature at which the residual stress is measured. If the wafer experiences a thermal cycle, the net change of thermal stress is zero at the end of the cycle. Therefore, a change of the residual stress upon thermal cycling is a consequence of a change of the intrinsic stress. However, stress relaxation can occur if the temperatures of the thermal cycle are sufficiently high. Consequently, the annealing temperature becomes the temperature at which the thermal stress is zero. After cooling down to room temperature, a higher thermal stress is generated in the film since the annealing temperature is higher than the deposition temperature [8].

2.2. Intrinsic stress

The intrinsic stress is the stress contribution generated during the deposition of the film. It is related to the strain of the bonds between the atoms of the layer: a tensile stress arises if the atomic spacing is higher than the nominal spacing, while a compressive stress results from a lower spacing. This variation in atomic spacing can be caused by several reasons [9]:

- Difference in interatomic spacing between the lattice of the substrate and the structural units (in case of amorphous films) or the lattice (in case of crystalline films) of the film.
- Incorporation of atoms, such as N, C, H atoms from the precursor gases.
- Incorporation of voids; in particular if depositions occur at low temperatures and atoms cannot move to their low-energy position [8].
- Ion bombardment, which occurs only in depositions assisted by plasma.

It is possible to tune the intrinsic stress by varying the deposition process parameters. For instance, in Plasma Enhance Chemical Vapor Deposition (PECVD) it is possible to modify the ion bombardment contribution by changing the power of the radio frequencies (RF) generators (commonly referred to as RF power).

Although the intrinsic stress is generated during deposition, it may change due to the post-processing conditions [10]. High temperature processes can have an impact on the chemical composition and the morphology of films. A variation in the chemical composition can modify the intrinsic stress if a depletion of incorporated atoms occurs, while the increase in atoms mobility is responsible for a variation of the morphology, such as a shrinkage of voids. Moreover, a drift in intrinsic stress may occur due to aging [22]. In the following sections, the effect of several deposition process parameters and post-processing treatments on the origin of the intrinsic stress in silicon nitride and silicon oxide films deposited by Low Pressure Chemical Vapor Deposition (LPCVD) or PECVD is discussed.

2.2.1. Origin of stress in LPCVD silicon nitride thin films

Quasi-stoichiometric LPCVD silicon nitride (Si_3N_4) is characterized by a high tensile residual stress (around +1 GPa) [11]. Since the thermal stress is slightly compressive, the resulting residual stress is due to a high tensile intrinsic stress [12]. The intrinsic stress originates from a mismatch between the structural units of Si_3N_4 (SiN_4 tetrahedra) and the lattice constant of silicon. It is possible to tune the residual stress by varying the ratio between the precursors in the inlet gas flow. Increasing the ratio dichlorosilane (DCS) and ammonia (NH_3), the concentration of silicon atoms in the film increases, resulting in a silicon-rich silicon nitride characterized by a more compressive residual stress, thus called low stress silicon nitride (LSSIN) [13,14]. In LSSIN, some of the N atoms in the tetrahedra are substituted by Si atoms, thus the structural units of LSSIN are $\text{Si}_{1+x}\text{N}_{4-x}$ tetrahedra. The volumetric distortion of the tetrahedra due to higher silicon concentrations causes a lower strain in the nitride film when deposited on a silicon substrate, resulting in a lower residual stress [15]. Figure 9 shows the residual stress as a function of the refractive index of the film, which increases with the concentration of silicon. At low values of the refractive index, the film exhibits a high tensile residual stress, which decreases rapidly with increasing the refractive index until it reaches a value of 2.23. Then, at refractive indexes higher than 2.23 the residual stress decreases with a lower slope.

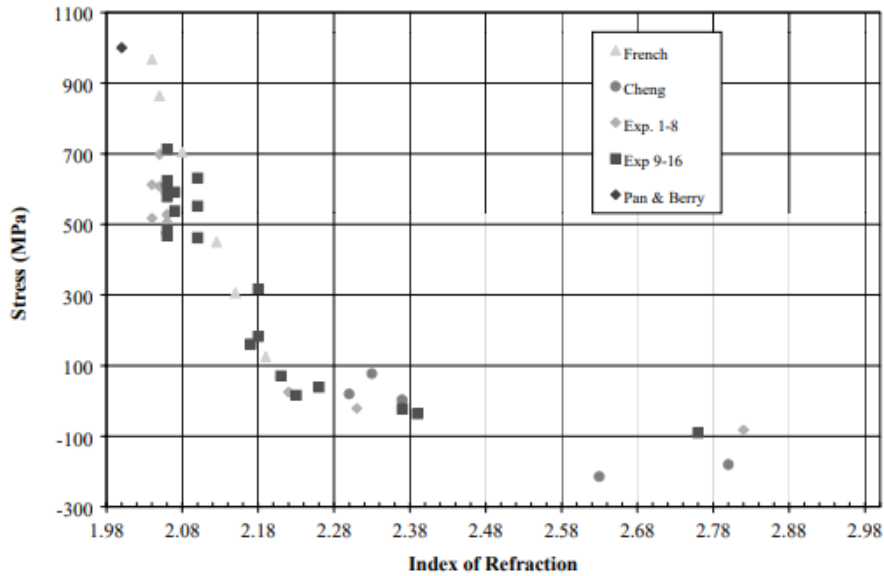


Figure 9: Residual stress of LPCVD silicon nitride as a function of the refractive index. [12]

2.2.2. Origin of stress in PECVD silicon nitride thin films

Since the thermal stress of a silicon nitride film deposited on a silicon substrate is low, the residual stress of a PECVD silicon nitride film is mainly affected by its intrinsic stress. Therefore, it is possible to tune the residual stress by varying the process parameters, which have a direct effect on the intrinsic stress. Seung Jin Oh et al. [16] deposited silicon nitride films with a residual stress ranging from tensile to compressive by increasing the RF power (from 450 to 700 W) and decreasing the total gas pressure in the deposition chamber (from 1250 mTorr to 750 mTorr). The residual stress can be tuned by varying the RF power in two different modes: high frequency (HF) mode and low frequency (LF) mode. In HF mode a higher RF power results in a higher ionization: more N^+ species are generated resulting in a higher incorporation of N atoms, which leads to a more compressive stress. In LF mode, increasing the RF power results in increasing the energy of the ions generated in the plasma. Therefore, a more compressive stress results from the higher ion bombardment and ion implantation [17,18]. High RF powers cause a higher packing of the aminosilanes of the growing film, increasing the film density. On the contrary, at low RF powers the film is characterized by a lower density. The spontaneous densification of the loose structure of the film during deposition results in a tensile residual stress [19]. As mentioned above, it is possible to tune the intrinsic stress also by modifying the total gas pressure inside the deposition chamber. In LF mode, increasing the total gas pressure results in a less compressive intrinsic stress, due to a lower ion bombardment [20]. Indeed, at high pressure the probability of inelastic collisions and homogeneous reactions increases, which results in a reduction of the average ion energy.

2.2.3. Origin of stress in PECVD silicon oxide thin films

Similarly to other PECVD thin films, the intrinsic stress of PECVD silicon oxide can be tuned by varying the process parameters. As mentioned above, the ion bombardment depends mainly on the RF power and the total gas pressure. When a high ion bombardment occurs, the arrangement of atoms results in a close packed structure, while a loose structure with voids is generated at low ion bombardments. Since the deposition occurs at relatively low temperatures, the atoms are not able to move to their zero-energy position. Therefore, a close packed structure results in a compressive intrinsic stress, while a loose structure in a tensile intrinsic stress [21]. A higher total gas pressure during deposition leads to a faster deposition and, thus, a higher incorporation of voids. However, since silicon oxide has a lower coefficient of thermal expansion than silicon, as-deposited silicon oxide films are characterized by compressive thermal stress, commonly resulting in compressive residual stress. It is possible to modify the residual stress of films by employing thermal treatments to induce structural changes [8].

Moreover, the residual stress of silicon oxide films is affected by aging. According to Haque et al. [22], moisture is responsible for aging in silicon oxide thin films due to the reaction with the strained Si-O-Si bonds on the surface, generating silanols (Si-OH) and resulting in a drift to more compressive stresses. In Figure 10, the effect of aging on the residual stress of a silicon oxide film is compared to the effect on a silicon nitride film. A thermal treatment in an environment with moisture is performed to accelerate the aging of the film. It can be noted that the residual stress of the silicon oxide film drifts towards more compressive values, while the residual stress of the silicon nitride film remains constant.

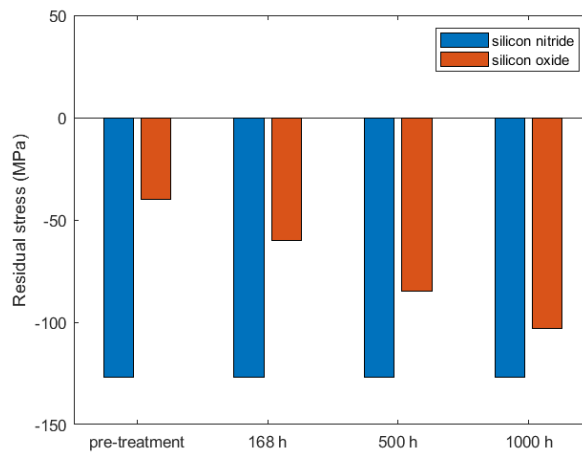


Figure 10: Comparison between the drift of residual stress of a silicon oxide film and a silicon nitride film upon aging, accelerated by a thermal treatment in an environment with moisture.

2.3. Stress characterization

The as-deposited thin films are characterized by an internal residual stress due to the strain generated during the deposition. Stress characterization of thin films is fundamental to predict the behavior of MEMS structures; however, stress cannot be measured directly. Instead, it must be evaluated from a measurable property, such as deformation, by using a proper mechanical model. The accuracy of the stress evaluation depends on the uncertainty of the measurement and on the mechanical model employed. Stress characterization of thin films is divided into three categories:

- Material level measurements
- Wafer level measurements
- Structure level measurements

Material level measurements can be nondestructive, for instance by using X-ray diffraction (XRD) [23], or destructive, for instance by using nanoindentation [24].

Wafer level measurements represent the reference residual stress evaluation techniques in a semiconductor fabrication line. The residual stress of a thin film is evaluated by measuring the curvature of the wafer after the deposition process. At equilibrium the net bending moment and the net force in the wafer must be zero, therefore the wafer bows to achieve mechanical equilibrium [25]. The radius of curvature (ρ) of the wafer is related to the residual stress of the thin film (σ_f) by Stoney's equation, which is written as follows [26]:

$$\sigma_f = \left(\frac{E_s}{1 - \nu_s} \right) \frac{t_s^2}{6\rho t_f}$$

where E_s represents the Young's modulus of the substrate, ν_s the Poisson's ratio of the substrate, t_s and t_f the thickness of the substrate and the film.

In order to apply the Stoney's equation, several assumptions are requested [27,28]:

- The substrate thickness and the film thickness are uniform.
- The film thickness is smaller than the substrate thickness: $t_f \ll t_s$.
- The substrate thickness is smaller than the diameter (d) of the wafer: $t_s \ll d$.
- The strains are infinitesimal.
- The substrate and the film are homogeneous, isotropic and linearly elastic.
- The stress state of the film is in-plane isotropic.
- The deformation of the wafer is spherical.
- The residual stress is constant on the whole surface.

However, Stoney's equation is commonly applied in cases where some of these assumptions are not respected. For example, usually the residual stress is not constant, therefore the equation is

used to estimate the average residual stress of the thin film. It must be noticed that Stoney's equation does not allow a local analysis of the stress state, but it gives an average value for the whole film.

Finally, structure level measurements represent a different approach since it involves the fabrication of test structures, such as cantilevers or membranes. The residual stress is evaluated locally from the deformation of each test structure fabricated. The cantilever deflection method applied in this work belongs to this stress characterization category.

References

-
- ¹ S.S. Bhavikatti; *Mechanics of Solids*; New Age International Ltd; chapter 8: "Simple Stresses and Strains" (2010).
 - ² W. D. Callister Jr., D. G. Rethwisch; *Material Science and Engineering*; John Wiley and Sons, Inc. (2018).
 - ³ C. A. Sciammarella, F. M. Sciammarella; *Experimental Mechanics of Solids*; John Wiley and Sons, Inc. (2012).
 - ⁴ L. B. Freund, S. Suresh; *Thin Film Materials: Stress, Defect Formation and Surface Evolution*; Cambridge University Press; chapter 2: "Film stress and substrate curvature" (2004).
 - ⁵ M. Tilli, T. Motooka, V. Airaksinen, S. Franssila, M. Paulasto-Kröckel, V. Lindroos; *Handbook of Silicon Based MEMS Materials and Technologies*; Elsevier; chapter 17: "MEMS Residual Stress Characterization: Methodology and Perspective" (2015).
 - ⁶ S. Huang, X. Zhang; *Gradient residual stress induced elastic deformation of multilayer MEMS structures*; Sensors and Actuators A 134, 177–185 (2007).
 - ⁷ T. Van der Donck, J. Proost, C. Rusu, K. Baert, C. Van Hoof, J.-P. Celis, A. Witvrouw; *Effect of deposition parameters on the stress gradient of CVD and PECVD poly-SiGe for MEMS applications*; Proceedings of SPIE 5342, 8–18 (2004).
 - ⁸ K.-S. Chen, X. Zhang, S.-Y. Lin; *Intrinsic stress generation and relaxation of plasma-enhanced chemical vapor deposited oxide during deposition and subsequent thermal cycling*; Thin Solid Films 434, 190–202 (2003).
 - ⁹ M. Ohring; *Material Science of Thin Films*; Academic Press; chapter 9: "Mechanical Properties of Thin Films" (1992).
 - ¹⁰ C.-L. Tien, T.-W. Lin; *Thermal expansion coefficient and thermomechanical properties of SiNx thin films prepared by plasma-enhanced chemical vapor deposition*; Applied Optics 51, 30, 7229 – 7235 (2012).
 - ¹¹ B. Vigna, P. Ferrari, F. F. Villa, E. Lasalandra, S. Zerbini; *Silicon Sensors and Actuators*; Springer; chapter 3: "Thin Film Deposition" (2022).
 - ¹² J. M. Olson; *Analysis of LPCVD process conditions for the deposition of low stress silicon nitride*; Materials Science in Semiconductor Processing 5, 51–60 (2002).

-
- ¹³ P.J. French, P.M. Sarro, R. Mallée, E.J.M. Fakkeldij, R.F. Wolffenbuttel; *Optimization of a low-stress silicon nitride process for surface-micromachining applications*; Sensors and Actuators A 58, 149 – 157 (1997).
- ¹⁴ M.-C. Cheng, C.-P. Chang, W.-S. Huang, R.-S. Huang; *Ultralow-Stress Silicon-Rich Nitride Films for Micro structure Fabrication*; Sensors and Materials 11, 6, 349 – 358 (1999).
- ¹⁵ S. Habermehl; *Stress relaxation in Si-rich silicon nitride thin films*; Journal of Applied Physics 83, 4672–4677 (1998).
- ¹⁶ S. J. Oh, B. S. Ma, C. Yang, T.-S. Kim; *Intrinsic Mechanical Properties of Free-Standing SiNx Thin Films Depending on PECVD Conditions for Controlling Residual Stress*; ACS Appl. Electron. Mater., 4, 3980–3987 (2022).
- ¹⁷ P. Morin, G. Raymond, D. Benoit, P. Maury, R. Beneyton; *A comparison of the mechanical stability of silicon nitride films deposited with various techniques*; Applied Surface Science 260, 69–72 (2012).
- ¹⁸ C. Iliescu, M. Avram, B. Chen, A. Popescu, V. Dumitrescu, D. P. Poenar, A. Sterian, D. Vrtacnik, S. Amon, P. Sterian; *Residual stress in thin films PECVD depositions: A review*; Journal of Optoelectronics and Advanced Materials 13, 4, 387 – 394 (2011).
- ¹⁹ M. Maeda, K. Ikeda; *Stress evaluation of radio-frequency-biased plasma enhanced chemical vapor deposited silicon nitride films*; Journal of Applied Physics 83, 7, 3865 – 3870 (1998).
- ²⁰ K. Aite, R. Koekoek, J. Holleman, J. Middelhoek; *Characterization of intrinsic stress of PECVD silicon nitride films deposited in a hot-wall reactor*; Journal de Physique Colloques 50, C5-323–C5-331 (1989).
- ²¹ M. Ghaderi, G. de Graaf, R. F. Wolffenbuttel; *Thermal annealing of thin PECVD silicon-oxide films for airgap-based optical filters*; J. Micromech. Microeng. 26 (2016).
- ²² M. S. Haque, H. A. Naseem, W. D. Brown; *Correlation of stress behavior with hydrogen-related impurities in plasma-enhanced chemical vapor deposited silicon dioxide films*; Journal of Applied Physics 82, 2922–2932 (1997).
- ²³ L. B. Freund, S. Suresh; *Thin Film Materials: Stress, Defect Formation and Surface Evolution*; Cambridge University Press; chapter 3: “*Stress in anisotropic and patterned films*” (2004).
- ²⁴ K.-S. Chen, T.-C. Chen, K.-S. Ou; *Development of semi-empirical formulation for extracting materials properties from nanoindentation measurements: residual stress, substrate effect and creep*; Thin Solid Films 516, 1931–1940 (2008).
- ²⁵ M. Tilli, T. Motooka, V. Airaksinen, S. Franssila, M. Paulasto-Kröckel, V. Lindroos; *Handbook of Silicon Based MEMS Materials and Technologies*; Elsevier; chapter 17: “*MEMS Residual Stress Characterization: Methodology and Perspective*” (2015).
- ²⁶ G. G. Stoney; *The tension of metallic films deposited by electrolysis*; Proc. R. Soc. London A 82, 172-173 (1909).
- ²⁷ D. Ngo, X. Feng, Y. Huang, A.J. Rosakis, M.A. Brown; *Thin film/substrate systems featuring arbitrary film thickness and misfit strain distributions. Part I: Analysis for obtaining film stress from non-local curvature information*; International Journal of Solids and Structures 44, 1745-1754 (2007).
- ²⁸ M. R. Ardigo, M. Ahmed, A. Besnard; *Stoney formula: Investigation of curvature measurements by optical profilometer*; Advanced Materials Research 996, 361-366 (2014).

3 | Process flow for cantilever fabrication

The typical process flow in MEMS microfabrication derives from integrated circuit (IC) microfabrication. The core of the process flow can be simplified as the repetition of the following main processes: deposition, lithography, and etching (Figure 11). A film is deposited on the wafer during the deposition step; then lithography is performed to define a pattern, exposing the portion of the film which must be removed by etching. The actual process flow is much more complex: many other process steps are required such as photoresist removal, wet cleaning, polishing, etc.

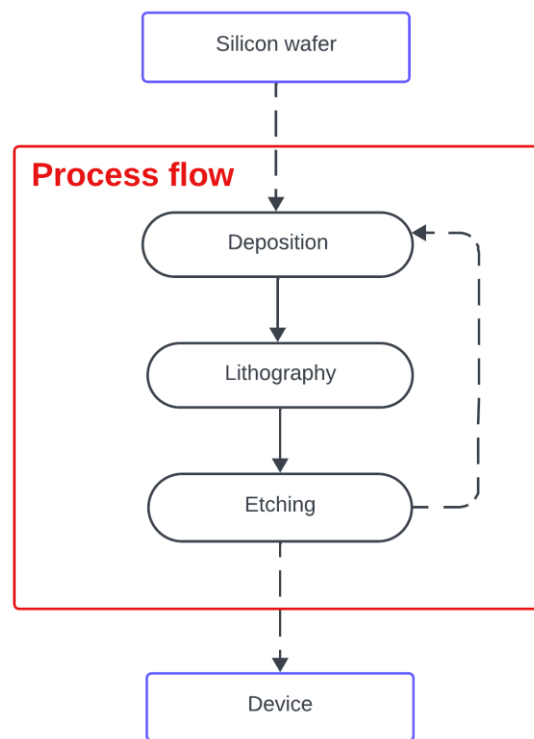


Figure 11: Scheme of the standard process flow in IC microfabrication.

More specifically, in MEMS fabrication there are two fundamental steps that are commonly required to obtain complex 3D moving structures: wafer to wafer bonding and MEMS release. The first step consists in bonding together, temporarily or permanently, two wafers; the latter consists in obtaining free-standing structures upon release of their mechanical movement.

In this chapter, the process flow employed to fabricate the test structures is described. Each test structure consists of an array of cantilevers; each cantilever is composed of a base layer and a thin film on top of it. The role of the base layer is purely structural: it must sustain the thin film that has to be characterized, which is less than 1 μm thick. The process flow consists in the growth of the base layer (section 3.1) and the deposition of the dielectric film to characterize (section 3.2). Then, the cantilever's geometry is defined on the front side by lithography and patterned removing the excess material by etching (section 3.3). Temporary bonding is needed to enable the processing of the back side of the wafer to release the cantilevers (section 3.4).

3.1. Growth of the base layer

Starting from a mono-silicon wafer Si(100) with a layer of thermal silicon oxide on its surface, a base layer film of polysilicon is grown on top of the silicon oxide layer. Polysilicon is the most used structural material in MEMS technologies and, growing it on a silicon oxide layer, it is also possible to fabricate an alternative to Silicon on Insulator (SOI) substrates [1]. Polysilicon layers can be obtained by using an LPCVD furnace or an epitaxial reactor. When the polysilicon layer must exhibit a thickness equal or higher than 10 μm , LPCVD is not employed due to the low deposition rate, in the order of tens of nm/min, and the high stress gradient and residual stress, which could be not suitable for the device [2]. When the growth of the polysilicon layer occurs in an epitaxial reactor, the layer is commonly called EPI Poly. In Figure 12, the scheme of this process is illustrated. The layer obtained is characterized by high roughness; therefore, a Chemical Mechanical Polishing (CMP) is needed to reach a mirror-like surface [3]. In the following sections, EPI Poly and CMP are discussed more in detail.

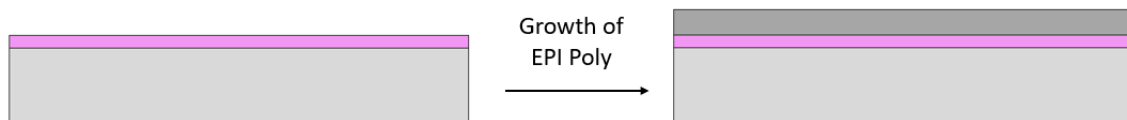


Figure 12: Scheme of the growth of epitaxial polysilicon on a monocrystalline silicon wafer with a layer of thermal silicon oxide on top of it.

3.1.1. Epitaxial polysilicon

Epitaxial polysilicon (EPI Poly) is a polycrystalline silicon layer which is grown at high temperature in a Vapor Phase Epitaxy (VPE) reactor. In VPE, gaseous silicon precursors as SiHCl_3 , SiH_2Cl_2 , SiCl_4 or SiH_4 are transported on the substrate, where they chemically react

obtaining the resulting epitaxial layer. When the precursors reach the surface of the wafer, the adsorption and the dissociation of the gaseous species occur, resulting in reactive species which diffuse on the surface to reaction sites. As shown in Figure 13, the process can work in two different regimes: the mass transport-limited and the surface reaction-limited regime. At relatively low temperatures, the surface reactions govern the growth rate of the process, thus the process works in the surface reaction-limited regime. At higher temperatures, the process works in the mass transport-limited regime, thus the growth rate is governed by the flux of reactant species through the boundary layer.

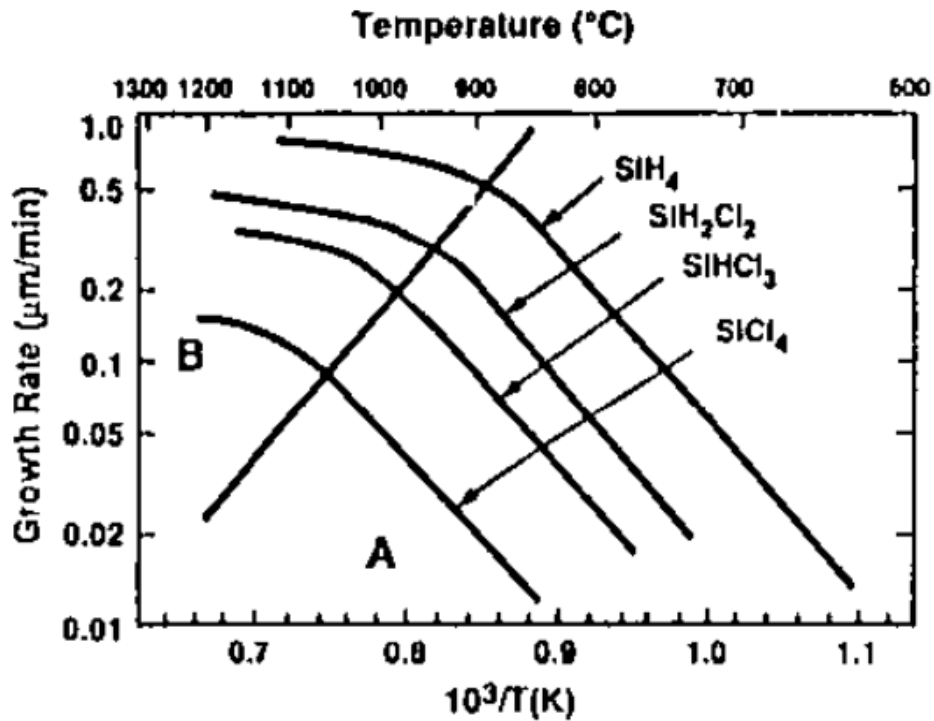


Figure 13: Plot of the growth rate as a function of $1/T$; showing two working regimes: (A) surface reaction-limited regime; (B) mass transport-limited regime. [7]

In the EPI Poly growth, a polysilicon seed layer is needed. The seed layer is previously deposited at lower temperatures using SiH_4 , because chlorosilanes precursors would produce HCl during the reaction, which limits the polysilicon nucleation. The presence of the seed ensures a uniform nucleation and growth of EPI Poly, which is grown in an atmospheric epitaxial reactor using a chlorosilanes chemistry in the range of temperatures $1050\text{--}1190^\circ\text{C}$, with a deposition rate around $1\ \mu\text{m}/\text{min}$ [4]. The seed can be deposited by LPCVD at $620\ ^\circ\text{C}$ or it can be grown in the epitaxial reactor (integrated process) in the

range of temperatures 800–900 °C. In VPE reactors, the EPI Poly growth occurs employing SiH_2Cl_2 or SiHCl_3 as gaseous precursors. Using SiH_2Cl_2 , the growth temperature is included between 1080–1100°C, while using SiHCl_3 , it is included between 1080–1190°C. Since the reactions are characterized by high growth temperatures, they are mass transport-limited, thus the growth rate of the seed layer and the EPI Poly is stable with the temperature.

EPI Poly shows excellent mechanical properties: the Young's modulus and the fracture strength range respectively from 132 to 174 GPa and from 1.2 to 2.7 GPa, comparable to steel's properties, while it has low density (2.3 g/cm^3), lower than aluminum's density. It also exhibits excellent thermal properties: high thermal conductivity and small thermal expansion coefficient. Process parameters affect the grain structure and the properties of polysilicon. The residual stress and the stress gradient depend on the following parameters: growth temperature, level of doping, growth rate and layer's thickness. Because of the high growth temperature, EPI Poly is characterized by large columnar grains, as it is shown in Figure 14. During the initial heterogeneous nucleation, the average grain size is smaller and, consequently, a compressive stress is generated in the layer. Increasing the film thickness, the grains become larger and columnar, thus the residual stress will be less compressive. Thin EPI Poly layers (as 5 μm thick) are typically compressive. The growth rate influences their stress, becoming more compressive when it increases, while increasing the growth temperature the layer will be less compressive. Differently, thick EPI Poly layers (as 35 μm thick) are tensile and are not particularly affected by the growth rate, while increasing the growth temperature they will be slightly less tensile. It is also important to consider the epitaxial reactor employed, because the residual stress is affected by the heating method. In single wafers reactors, a radiant heating method is employed, while in batch reactors it is used an induction heating method.

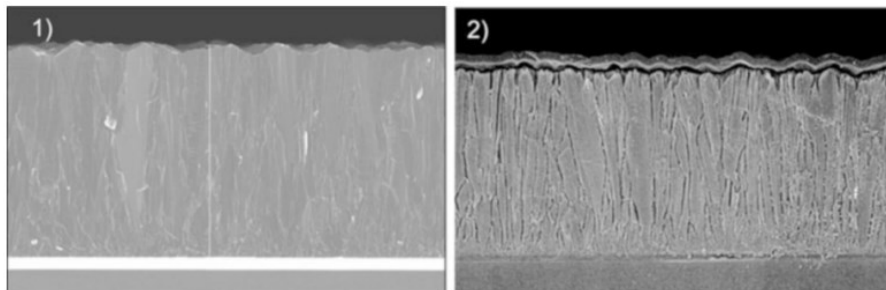


Figure 14: SEM images of the columnar grains in EPI Poly. [1]

3.1.2 Chemical Mechanical Polishing

Chemical Mechanical Polishing (CMP) is a process employed in microfabrication to smoothen or planarize surfaces. The polishing occurs because of the synergistic action of mechanical abrasion and chemical reactions on the surface of the wafer. The system configuration of this technique is shown in Figure 15. The wafer is attached to a flexible membrane using a vacuum chuck in the polishing head. Applying pressure to the back of the wafer, the front side is pressed onto the polishing pad placed on the rotating platen, which rotates in the same direction of the polishing head. The polishing pad consists of a double layer of porous polyurethane, which has to retain the slurry employed in the process. A retaining ring is placed around the wafer to avoid the wafer slippage, due to the higher pressure applied on it [5].

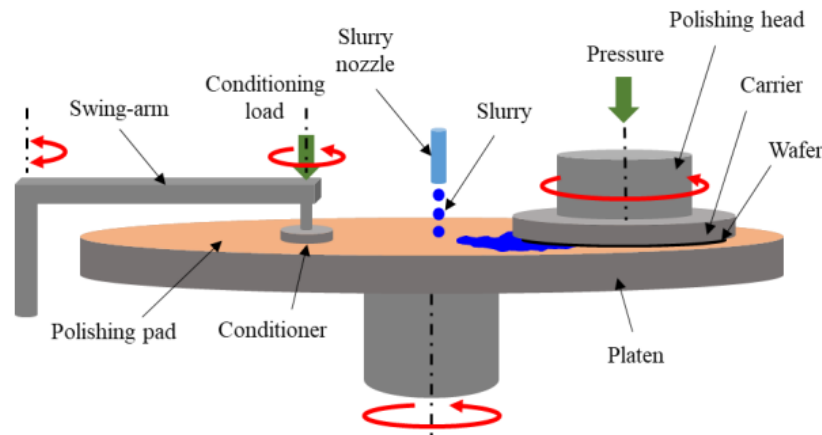


Figure 15: Schematic illustration of Chemical Mechanical Polishing. [5]

The slurry is dispensed on the polishing pad using a nozzle. The mechanical abrasion is given by nano-sized particles, typically SiO_2 , while chemical reactions occur due to the chemicals in the slurry. The aim of the reaction is to generate a chemically reacted layer on the surface, which can be easily removed by abrasion. It is important to balance properly the mechanical and the chemical actions of the slurry, as it is shown in Figure 16. Excessive removal occurs if the mechanical abrasion overcomes the effect of chemical reactions. On the contrary, when the chemical action is the main component of the polishing, the result is insufficient removal [6].

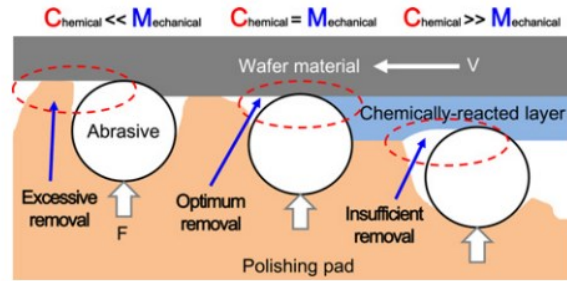


Figure 16: Illustration of the different effects of chemical mechanical polishing depending on the chemical and the mechanical actions. [6]

3.2. Deposition of the thin film

The thin film is deposited on the EPI Poly layer (Figure 17) using Chemical Vapor Deposition (CVD) techniques. In CVD, the film is obtained from gaseous precursors which react when they are activated [7]. In particular, the thin films characterized in this work are deposited by Low Pressure Chemical Vapor Deposition (LPCVD) or Plasma Enhanced Chemical Vapor Deposition (PECVD).



Figure 17: Scheme of the thin film deposition on an EPI Poly layer.

3.2.1. Low Pressure Chemical Vapor Deposition

Low Pressure Chemical Vapor Deposition (LPCVD) is a CVD technique which is used to deposit high-quality thin films with a wide range of thickness, tunable properties, and a high process repeatability. Although LPCVD is characterized by low deposition rates (from 1 nm/min to 20 nm/min), it is possible to achieve an industrial throughput because a reactor can process up to 150 wafers simultaneously. The deposition is based on the thermal decomposition of inorganic gaseous precursors, which are introduced in the reactor with carrier gases through forced convection, while unreacted gases and byproducts are removed from the reactor. The precursors diffuse towards the wafer surface and are adsorbed at the boundary layer, where they bond to the surface while

reaction products are desorbed. Usually, the deposition temperature ranges from 500 to 700 °C, while the pressure ranges from tens of mTorr to few Torr [8]. In these conditions, the reaction works in the surface reaction-limited regime. This regime is crucial to obtain a uniform film deposition along the wafer diameter, allowing to process simultaneously several closely spaced wafers in a hot wall tube type reactor [9]. The LPCVD reactor (Figure 18), also called vertical furnace, is made of a long vertical quartz tube. Heating is provided by resistivity heater elements around the reaction tube, that enable to control independently different areas of the reactor. Therefore, the process has a precise temperature control ($\pm 1^\circ\text{C}$), resulting in process uniformity and repeatability on all processed wafers.

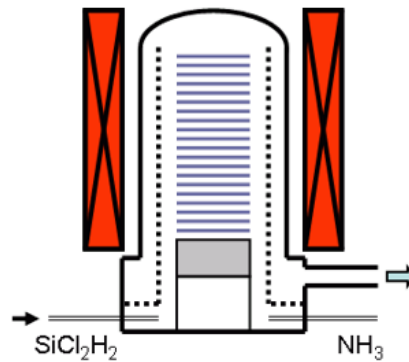
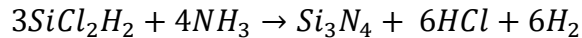


Figure 18: Schematic illustration of a vertical furnace (LPCVD reactor).

Silicon nitride (abbreviated as SiN) is a widely used thin film in MEMS devices as insulating, passivation or stopping layer. It is possible to grow high-quality thin films using SiH_2Cl_2 and NH_3 as precursors, at temperatures in the range 700-850°C and pressures in the range 100-300 mTorr. The reaction between SiCl_2H_2 and NH_3 is the following:



Due to the high energy needed to decompose the ammonia, the gas flow of NH_3 will be higher in order to obtain a quasi-stoichiometric SiN film (Si_3N_4).

As mentioned in section 2.2.1, quasi-stoichiometric LPCVD SiN is characterized by a high residual stress which limits the thickness of the film to hundreds of nm to avoid cracking [8,10]. The residual stress can be decreased by an increase of the $\text{SiCl}_2\text{H}_2/\text{NH}_3$ ratio, obtaining a silicon-rich SiN commonly called Low-Stress Silicon Nitride (LSSiN) [11,12]. The decrease in residual stress enables the deposition of thicker films, however the increase of Si concentration is associated with a decrease of insulating properties of the film.

3.2.2. Plasma Enhanced Chemical Vapor Deposition

Plasma Enhanced Chemical Vapor Deposition (PECVD) is a CVD technique assisted by plasma, which is generated in a pressure-controlled environment. It is a widely used technique in microfabrication because it is possible to tune the film properties and to employ relatively low temperatures [13]. In standard CVD reactions, high temperature is needed to provide the energy to dissociate the precursors. In PECVD the dissociation occurs because of the plasma, thus the deposition temperatures are lower and range between 100 °C and 400 °C. A low thermal budget is crucial when the device presents temperature sensitive features. Commonly, the deposition pressure is included in the range 1–10 Torr. The deposition rates are significantly higher than in LPCVD (0.3–1 $\mu\text{m}/\text{min}$), which is crucial considering that the PECVD chambers are single-wafer [8].

In Figure 19, the scheme of PECVD chambers is illustrated. The chamber consists of an aluminum body with ceramic shields and two parallel electrodes: the showerhead and the platen, where the wafer is placed. The design of the electrodes is important: it affects the distribution of gas into the chamber, influencing the shape of the plasma and the uniformity of the film. Plasma is generated between the two electrodes thanks to electrical discharge, using two radio frequencies (RF) generators: a common setup is composed of one high frequency (HF, 13.56 MHz) and one low frequency (LF, 375 kHz) generator. This approach allows direct control on film properties, such as stress and density [14]. The dissociation of the precursors is caused by the electrons present in the plasma, generating chemically reactive free radicals. Deposition occurs because the radicals react together and diffuse to the substrate [15].

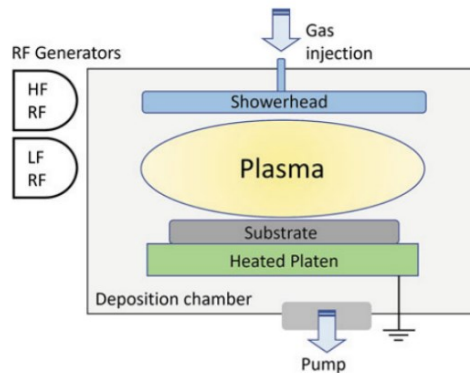


Figure 19: Schematic illustration of a PECVD chamber. [8]

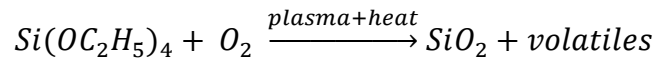
A PECVD process is characterized by three phases. Firstly, a pre-deposition occurs without the presence of the wafer to condition the chamber. Then, when the gas flow and the

pressure are stable, the wafer is introduced in the chamber and the actual deposition occurs. The last phase starts when the wafer is removed and consists of a cleaning process of the chamber, which is an in-situ etching based on C_3F_8 and O_2 . The removal of the deposited material on the sidewalls is crucial, because otherwise the impedance of the chamber could change, resulting in an incorrect plasma formation.

PECVD plays a fundamental role in MEMS fabrication when films must be characterized by a certain stress value to provide a specific contribution to the mechanical behavior of structures. This is due to the possibility of directly tuning the film stress through the process parameters and changing, for example, the power of the two generators.

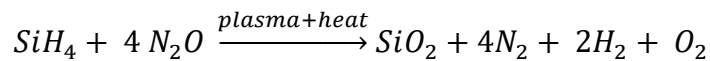
In order to deposit silicon oxide films using PECVD tetraethyl orthosilicate (TEOS) and SiH_4 are commonly employed. Films obtained with TEOS are called TEOS films, while films obtained with SiH_4 are called Undoped Silicon Glass (USG).

TEOS films are obtained due to the following reaction between TEOS and oxygen:



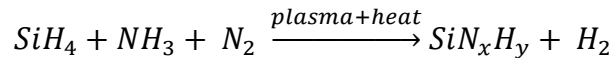
They show a higher conformality than USG films. TEOS can be used as a compensation layer, tuning its mechanical properties to balance the warpage of the wafer.

USG is commonly used as a passivation layer or as a structural dielectric with a controlled low stress. SiH_4 and N_2O are the standard precursors employed for the deposition; the reaction is:

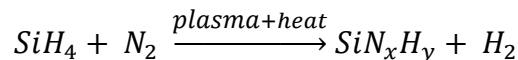


USG films can be characterized by the presence of bonded hydrogen [16] which typically leads to compressive intrinsic stress in the as-deposited films [17].

PECVD silicon nitride is commonly used as passivation layer due to its moisture diffusion barrier properties. It is commonly deposited using SiH_4 , NH_3 and N_2 as precursors:



PECVD SiN layers do not have a stoichiometric composition (Si/N ratio equal to 0.75); indeed, they commonly have a Si/N ratio between 1.12 and 1.15 [8]. However, in some cases SiN layers with low hydrogen content are required. Therefore, NH_3 -free SiN has been developed, using only SiH_4 and N_2 as precursors:



3.3. Front side patterning

After the deposition of the thin film, the front side of the wafer is patterned to define the test structure, as shown in Figure 20. Optical lithography is employed to pattern a photosensitive material, called photoresist (PR), which is previously dispensed on the surface of the wafer. The areas not covered by the photoresist are etched and removed by wet or dry etching. In this process flow, Reactive Ion Etching (RIE) and the silicon etch Bosch process are respectively employed to etch the thin film and the EPI Poly layer. Then, the residual photoresist mask is removed by an oxygen plasma ashing treatment.

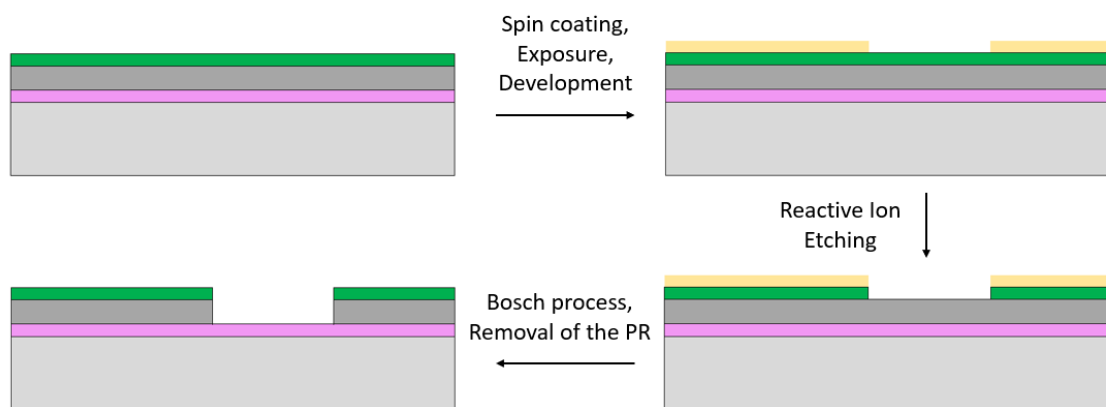


Figure 20: Scheme of the front side patterning: (a) definition of the front side pattern employing optical lithography; (b) etching of the dielectric film; (c) anisotropic etching of the EPI Poly layer employing the Bosch process.

3.3.1. Optical lithography

Optical Lithography is the technique used to transfer a particular pattern from a mask to a photoresist by irradiating with a light source. The mask is made of glass, and it is patterned with a chromium layer which is opaque to the wavelengths used [18]. Photoresists are photosensitive polymers which interact with the radiation employed [19]. The interaction between the photoresist and the radiation leads to different reactions, depending on its chemical formulation. Positive photoresists undergo partial degradation in the exposed regions, which become soluble and are removed during the development step using a development solution (Figure 21a). Differently, negative photoresists cross-link where they are irradiated by a specific wavelength. The exposed regions become insoluble to the development solution, resulting in the dissolution of the unexposed regions (Figure 21b).

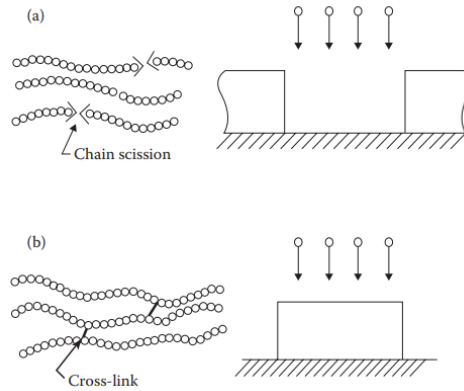


Figure 21: Comparison between the behavior upon exposure of (a) positive photoresists and (b) negative photoresists. [20]

Before the deposition of the PR, an adhesion promoter is chemically bonded to the surface to obtain a hydrophobic surface improving the PR adhesion to the wafer. The resist coating is usually performed by spin coating. A soft bake step occurs to evaporate the solvent, followed by the exposure to the light source. In some cases, a hard bake step is implemented after the development step to slope and strengthen the resist.

The exposure methods are classified as in contact, in proximity and in projection [21], as shown in Figure 22. In both contact and proximity methods the whole wafer is exposed to the radiation in a single shot, thus the mask reproduces the entire pattern to transfer. In the first method, the mask and the wafer are in contact, while in the second one there is a gap (20–50 μm) between the mask and the wafer. Higher resolutions are achievable employing contact printing, but the risk of mask rusting and damage is higher than in proximity printing. The resolution of proximity printing is limited by diffraction phenomena. In both methods, the magnification of the mask is 1X. The tools which employ these methods are called mask aligners. In the case of projection printing, the exposure system is more complex: optical lenses are used to focus and reduce the reticle image after the light passes through the mask. Thus, higher magnifications of the mask are possible, such as 2X, 4X and 5X. In one shot just a portion of the wafer is exposed, the other regions are exposed in the following shots repeating the pattern of the reticle on the whole wafer. Two different tools employ this exposure technique: steppers and scanners. In steppers, the wafer moves from a shot location to another, where the reticle is printed in the whole region. In scanners, an exposure slit is placed under the mask, so that just a portion of the reticle can be transferred. The wafer still moves from one location to another, but also the mask moves in order to transfer the whole reticle pattern before

repeating this process in another location. With steppers and scanners, it is possible to achieve higher resolutions and alignment accuracies.

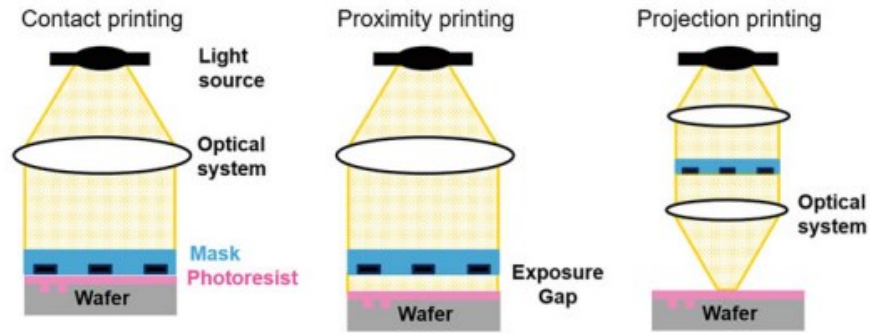


Figure 22: Schematic illustration of the three exposure methods employed in optical lithography: (a) in contact; (b) in proximity; (c) in projection. [18]

3.3.2. Dry etching

Dry etching is a class of etching techniques in which a solid surface is removed (i.e., etched away) by gaseous species of a plasma inside a reactor. There are many different types of plasma reactors [23]; in this work, a capacitively conductive plasma (CCP) reactor is employed. In a CCP reactor the feed gas is injected between two parallel electrodes, and it is ionized by applying an RF voltage between the electrodes. Ions are accelerated towards the lower electrode, on which the wafer is placed, due to a negative voltage [23].

Depending on the characteristics of the plasma, determined by process parameters set in the reactor (for instance types of feeding gas, pressure in the reactor and RF power), three different etching regimes can be attained: ion-beam milling, chemical plasma etching and reactive ion etching (RIE) [22]. In the first case, material is removed from the substrate due to the ion bombardment provided by inert ions (as Ar^+) in the plasma. The mechanism of this technique is purely physical since it occurs due to the momentum transfer between the energetic Ar^+ ions and the substrate. The etching profile is anisotropic because ions imping on the surface vertically, but it is characterized by low etch rates (thickness of the etched layer removed per unit time) and low selectivity (ratio of etch rates between two different materials). On the contrary, the mechanism of chemical plasma etching is, as the name implies, purely chemical. Plasma is needed to provide reactive neutral species, such as radicals, which diffuse to the substrate and react with the superficial atoms generating volatile products. It enables higher etch rates and higher selectivity; however, the removal

of material is isotropic and the etching profile is not straight. The comparison between the typical isotropic profile and the anisotropic profile is shown in Figure 23. In RIE, both chemical and physical etching mechanisms occur at the same time; this is the most common process employed to pattern conductor, metal and dielectric films. Indeed, by tuning the plasma condition, it is possible to achieve straight (more anisotropic plasma) or sloped (more isotropic plasma) etching profiles [22].

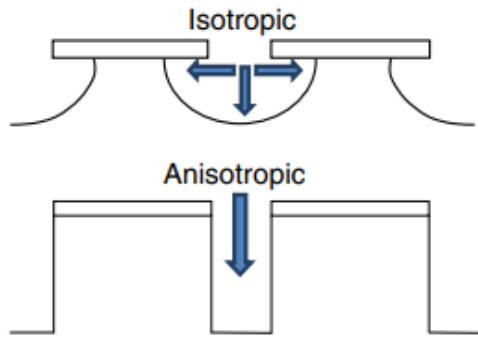


Figure 23: Comparison between isotropic etching and anisotropic etching. [23]

3.3.2.1. Reactive Ion Etching for dielectric etching

RIE with fluorocarbon chemistry is employed to etch dielectrics films, such as silicon oxide and silicon nitride, selectively over silicon. The most common feed gases used for dielectric etch include fluorocarbons (as CF_4 , C_4F_8 , C_5F_8 or C_4F_6) and some additives (commonly O_2 , Ar, CO_2 and CO). Hydrofluorocarbons (as CHF_3) can be employed to increase the selectivity over silicon.

During a SiO_2 RIE process, the generation of neutral CF_x in the plasma leads to the formation of a fluorocarbon passivation layer over the substrate. This layer acts both as a protective layer, as the energy delivered by Ar sputtering is reduced, and deliverer of fluorocarbon species activated by ion bombardment, which react with SiO_2 to form COF_x and SiF_x [24, 25]. The composition of the film and its deposition rate depend on the chemistry of the feed gas. The deposition rate must be nearly equal to the etching rate to obtain a constant steady-state thickness of the film, which enables the etching of the substrate at a constant rate. If the deposition rate is much higher than the etching rate, the thickness of the film increases continuously, and the etching of the substrate does not occur [26]. The etching rate decreases with the thickness of the fluorocarbon film, enabling the selectivity over silicon. In Figure 24 a schematic representation of the etching process is reported.

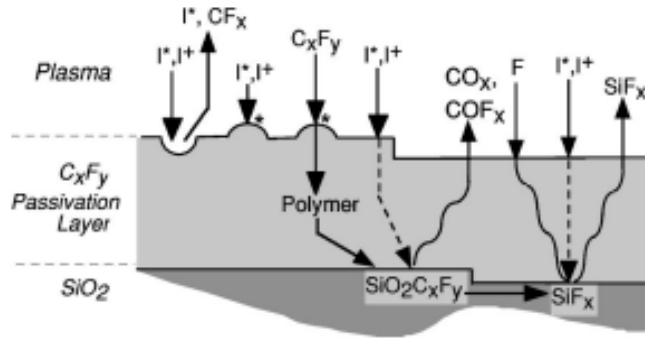


Figure 24: Schematic illustration of the activation of reactive species from the fluorocarbon film upon ion bombardment in RIE, where I^+ represent energetic ions, while I^* energetic neutral species. [24]

3.3.3. Bosch process

The Bosch process is a *Deep Reactive Ion Etching (DRIE)* technique used to etch thick layers of silicon. Standard plasma etching techniques, as RIE, use chloride and bromide chemistry to etch silicon. The plasma generated with this chemistry is able to perform an anisotropic etching, but the etch rate is too slow for deep silicon etching. On the contrary, fluorinated gases (as SF_6) show a high etch rate (up to $30 \mu\text{m}/\text{min}$), but their action is isotropic. In order to overcome the isotropic etching of fluorinated chemistry, the Bosch process was developed [27, 28]. As shown in Figure 25, this process is divided into three steps characterized by different plasma chemistries. In the first step (also called *deposition step*), a polymerizing chemistry based on fluorocarbons (as C_4F_8) is employed to deposit a Teflon-like passivation film. The second one consists of a physical etching of the polymeric film from the bottom of the structure, while it is not removed from the sidewalls. In the third step (*etch step*), silicon is etched from the bottom by a SF_6 plasma, while the Teflon-like film prevents the etching of the sidewalls.

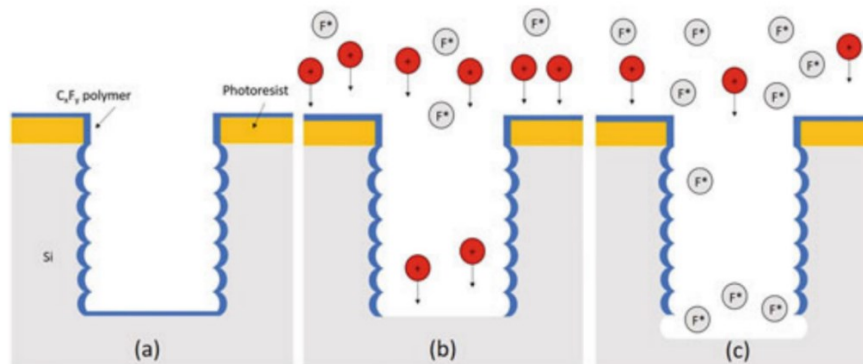


Figure 25: Schematic illustration of the three steps employed in the Bosch process: (a) deposition step, (b) removal of passivation layer step, (c) etch step. [27]

These steps must be repeated several times during the process because the new silicon exposed on the sidewalls, which is not covered by the Teflon-like film, is etched due to the isotropic action of SF_6 . The result is the characteristic profile made of the so-called *scallops* (Figure 26), which are generated during each etch step. To obtain more smooth sidewalls, thus smaller scallops, the etch step time of each cycle must be reduced [29, 30].

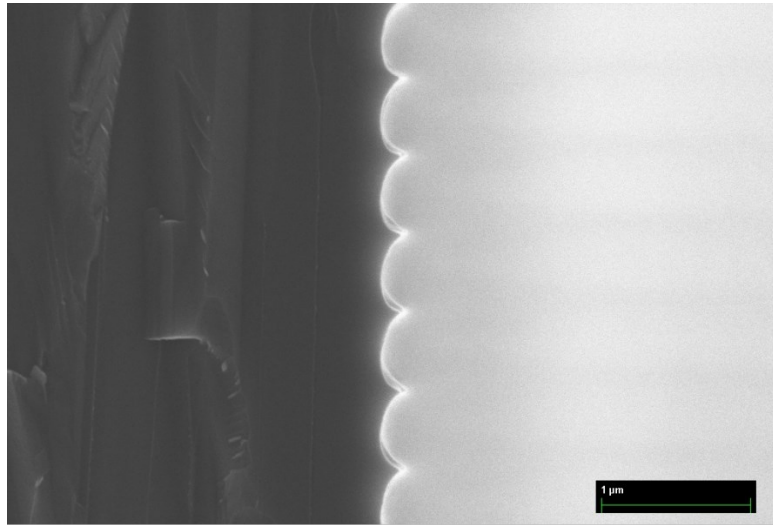


Figure 26: SEM image of the scalloping on the sidewalls of a silicon cavity opened employing the Bosch process.

3.4. Release of the structure

In order to obtain freestanding cantilevers, the wafers must be processed on the back side to open cavities under the test structures. The patterned wafer, which is called *device wafer*, is bonded to a silicon wafer, called *cap wafer*, on its front side employing a temporary polymer-based bonding. The cap wafer enables the handling of the device wafer during the backside patterning, without damaging the frontside. After the opening of the cavities on the backside, the debonding of the cap wafer occurs thanks to the *flip-flop process*. In Figure 27, the processes employed for the release of the cantilevers are illustrated.

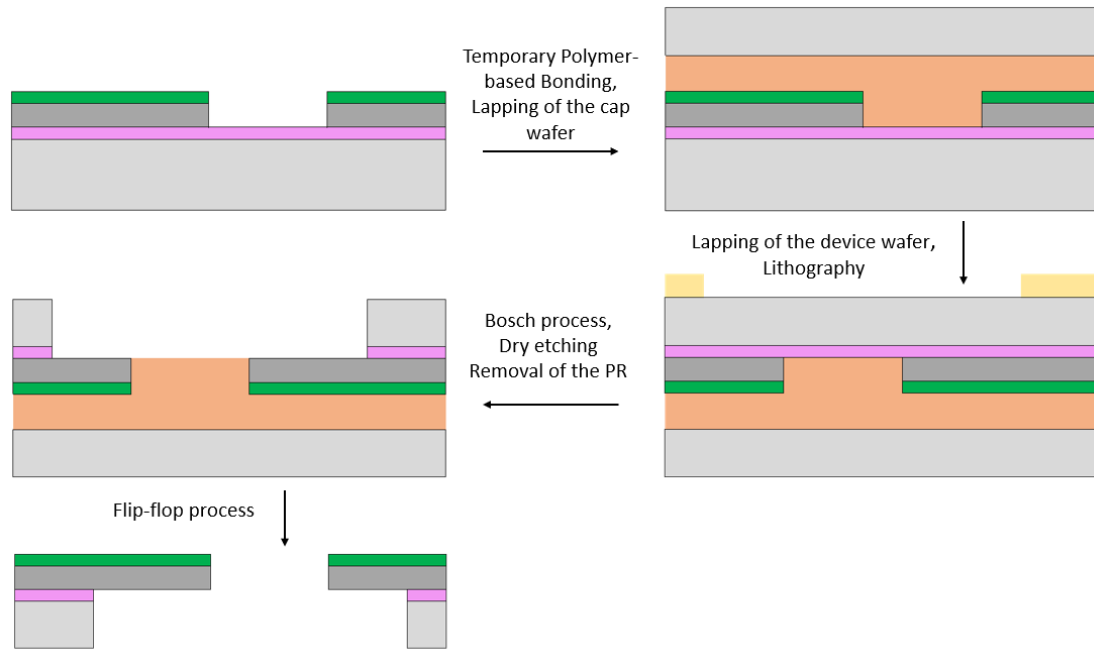


Figure 27: Scheme of the cantilever release: (a) temporary bonding of the cap wafer on the front side of the device wafer; (b) lapping of the device wafer and patterning of the back side by optical lithography; (c) Opening of the cavity on the backside by Bosch process and etching of the thermal oxide; (d) release of the cantilevers by flip-flop process.

3.4.1. Temporary Polymer-based Bonding

Wafer-to-wafer temporary bonding is widely used during MEMS processing because it can enable the micromachining of the back side of device wafers. Depending on the adhesive material, temporary bonding techniques can be divided into two major classes: tape-based and polymer-based [31]. In polymer-based techniques, adhesion occurs due to the intimate contact between the surface of the wafer and an intermediate polymeric layer. Secondary interactions, such as van der Waals interactions, are responsible for adhesion when the distance between two surfaces is lower than 0.5 nm along the whole bonding area. Due to roughness, the mean distance between two polished surfaces is higher, thus the intermediate polymeric layer is needed to provide adhesion. The thermoplastic polymer, dissolved in a solvent, is commonly coated on the cap wafer and device wafer surfaces by spin coating. As shown in Figure 28, the wettability of the surfaces must be improved to avoid the formation of voids at the bond interface, which are detrimental for adhesion [32].

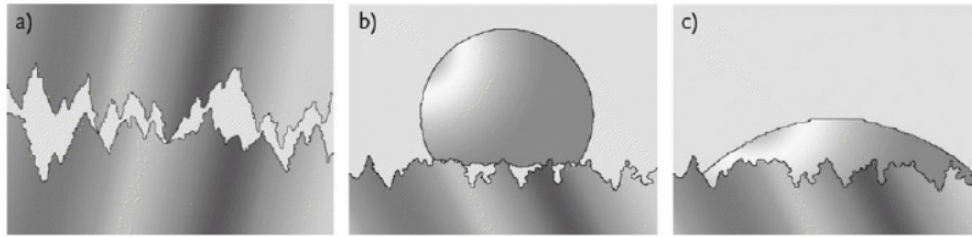


Figure 28: Schematic illustration of the effect of wettability in the formation of voids: (a) without an adhesive material the formation of voids is due to the roughness of the polished surfaces; (b) low wettability of the surface results in voids formation at the interface with the adhesive material; (c) high wettability of the surface results in intimate contact with the adhesive material. [32]

The presence of contaminants on the surface may decrease the wettability, therefore a cleaning step is implemented before spin coating. A soft-bake step is needed to remove the solvent, obtaining a solid layer (glassy state) on top of both wafers. Then, the cap wafer and the device wafer are placed into the vacuum bond chamber, where joining occurs applying pressure with the bond chucks while they are heated to soften the polymer. Vacuum conditions are required to avoid voids at the bond interface [33]. Due to heating, the temperature overcomes the glass transition temperature (T_g) of the polymer, which leads to a rubber-like state of the intermediate layer. Low viscosity is needed to allow the reflow of the adhesive material which adapts to the topography of the surface to obtain intimate contact while pressure is applied. The pressure must be released only after cooling, to ensure the correct polymer solidification.

3.4.2. Back side patterning

Before the actual patterning of the backside of the device wafer, the thickness of the substrate must be decreased removing around 300 μm of silicon by lapping. Then, the Bosch process (briefly discussed in section 2.3.3) is employed to open cavities in the silicon substrate. Since the thickness of silicon to remove is around 400 μm , a photoresist thicker than 10 μm must be employed. During spin coating, at the same value of rpm a polymer with higher viscosity gives a thicker coating. Thus, the viscosity must be high enough to obtain a thick coating. High sensitivity to the radiation is also requested since the reactions in the exposed regions must occur along the whole thickness of the photoresist. Therefore, chemically amplified photoresists (CARs) are employed. CARs are composed of a photochemical acid generator (PAG) and a polymer with an acid-labile protecting group pendant. During exposure, photolysis of PAG occurs and a photoacid is generated. The photoacid reacts with the pendants of the polymer, resulting in a conversion of the

lipophilic pendant in a hydrophilic group [34]. The exposed regions become hydrophilic, while the unexposed regions remain lipophilic. During development, a positive tone image is obtained using an aqueous base developer with tetramethylammonium hydroxide (TMAH), which dissolves the polar regions of the resist [35]. The reaction occurs during a post-exposure bake (PEB) at temperatures in the range 90–150 °C, depending on the activation energy of the reaction. Higher PEB temperatures enhance the sensitivity since the diffusion of the photoacid enables the reaction with unreacted pendants, although an excessive diffusion leads to lower resolutions [36,37].

3.4.3. Debonding of the cap wafer

Once the cavities are opened on the back side, the debonding of the cap wafer must occur. When the cap wafer is bonded by temporary polymer-based bonding, the debonding process is critical since shear forces must be applied to slide off the cap wafer. Therefore, the device wafer, which is thin due to lapping and patterned on the back side, must be supported using a *carrier wafer*. After the debonding of the cap wafer, the carrier wafer can also be removed. This process is commonly called *flip-flop process*, its scheme is illustrated in Figure 29.

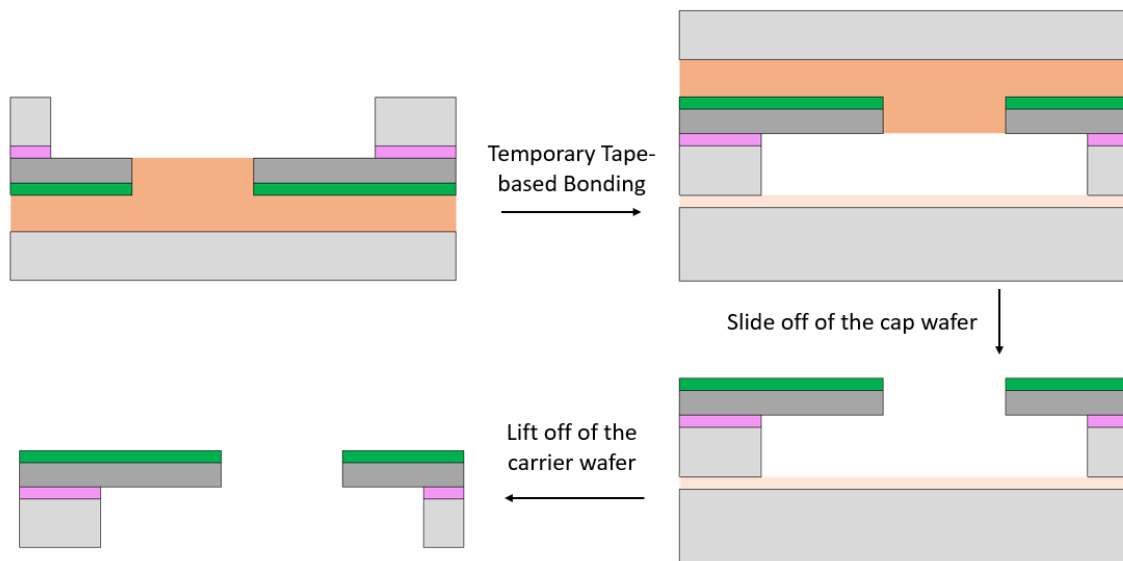


Figure 29: Scheme of the flip-flop process: (a) temporary tape-based bonding to allow the handling on the back side; (b) slide off of the cap wafer; (c) lift off of the carrier wafer.

Temporary Tape-based Bonding is employed to bond the carrier wafer to the back side of the device wafer. Firstly, the adhesive tape is applied to the carrier wafer at room temperature. Then, the carrier wafer is bonded to the back side of the device wafer at temperatures lower than 100°C applying pressure with the bond top chuck. The possibility to perform temporary bonding at low temperatures is fundamental to avoid the softening of the polymer adhesive employed to bond the cap wafer to the device wafer.

Commonly, the debonding of the cap wafer occurs by slide off of the cap wafer, as it is illustrated in Figure 30. The stack is heated to a temperature above the softening point of the polymer to reduce its viscosity [38]. The temperature depends on the polymeric adhesive used, commonly at temperatures around 160 °C the viscosity is sufficiently low to enable debonding. As mentioned before, this step is critical because free-standing structures could break due to the forces applied. Therefore, the velocity of sliding must be accurately set up to avoid cracking. After debonding, the front side of the device wafer is cleaned with dodecene to remove the polymeric residual.

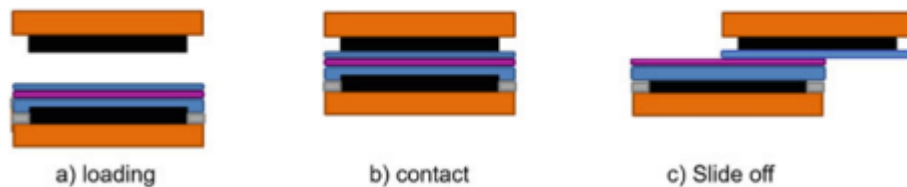


Figure 30: Schematic illustration of slide off of the cap wafer. [31]

The carrier wafer is removed from the device wafer by lift off, as shown in Figure 31. In order to perform lift off of the carrier wafer, the adhesive forces of the tape must be reduced. The release can occur either by heating or UV irradiation. In the first case, the stack is heated to temperatures around 200 °C. Once the adhesive forces are reduced, the carrier wafer is lifted. This process is less critical than the debonding of the cap wafer, due to the different temporary bonding employed. Temporary polymer-based bonding is employed when the following processes are not performed in harsh conditions. Because after this process only slide off of the cap wafer is performed, it is fundamental that the adhesion forces of the tape are sufficiently high at slide off temperatures.

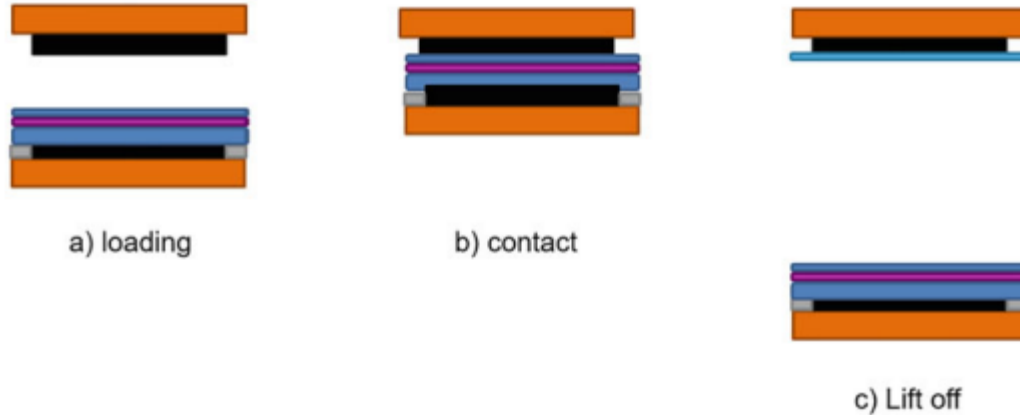


Figure 31: Schematic illustration of lift off of the carrier wafer. [31]

References

¹ B. Vigna, P. Ferrari, F. F. Villa, E. Lasalandra, S. Zerbini; *Silicon Sensors and Actuators*; Springer; chapter 2: "Epitaxy" (2022).

² E.J. Ng, S. Wang, D. Buchman, C.-F. Chiang, T.W. Kenny, H. Muenzel, M. Fuertsch, J. Marek, U.M. Gomez, G. Yama, G. O'Brien; *Ultra-stable Epitaxial Polysilicon Resonators*; Solid-State Sensors, Actuators, and Microsystems Workshop, Hilton Head Island, 271–274 (2012).

³ M. Fuertsch, M. Offenber, H. Munzel, J. Morante; *Comprehensive study of processing parameters influencing the stress and stress gradient of thick polysilicon layers*, Micromachining and Microfabrication, 130 – 141 (1997).

⁴ P.J. French; *Polysilicon: a versatile material for microsystems*; Sensors and Actuators A 99, 3–12 (2002).

⁵ J. Son, H. Lee; *Contact-Area-Changeable CMP Conditioning for Enhancing Pad Lifetime*; Appl. Sci. 11, 3251 (2021).

⁶ H. Lee, D. Lee, H. Jeong; *Mechanical Aspects of the Chemical Mechanical Polishing Process: A Review*; International Journal of Precision Engineering and Manufacturing 17, 525-536 (2016).

⁷ H. O. Pierson; *Handbook of chemical vapor deposition*; Noyes Publications (1999).

⁸ B. Vigna, P. Ferrari, F. F. Villa, E. Lasalandra, S. Zerbini; *Silicon Sensors and Actuators*; Springer; chapter 3: "Thin Film Deposition" (2022).

⁹ N. Sharma, M. Hooda, S. K. Sharma; *Synthesis and Characterization of LPCVD Polysilicon and Silicon Nitride Thin Films for MEMS Applications*; Journal of Materials (2014).

-
- ¹⁰ M. Tilli, T. Motooka, V. Airaksinen, S. Franssila, M. Paulasto-Kröckel, V. Lindroos; *Handbook of Silicon Based MEMS Materials and Technologies*; Elsevier; chapter 6: “Thin Films on Silicon” (2015).
- ¹¹ P.J. French, P.M. Sarro, R. Mallée, E.J.M. Fakkeldij, R.F. Wolffenbuttel; *Optimization of a low-stress silicon nitride process for surface-micromachining applications*; *Sensors and Actuators A* 58, 149 – 157 (1997).
- ¹² J. G. E. Gardeniers and H. A. C. Tilmans, C. C. G. Visser; *LPCVD silicon-rich silicon nitride films for applications in micromechanics, studied with statistical experimental design*; *J. Vac. Sci. Technol. A* 14(5), 2879 – 2892 (1996).
- ¹³ M. J. Madou; “Manufacturing Techniques for Microfabrication and Nanotechnology”; Volume II; CRC Press; chapter 7: “Physical and Chemical Vapor Deposition—Thin Film Properties and Surface Micromachining” (2011).
- ¹⁴ M. Maeda, K. Ikeda; *Stress evaluation of radio-frequency-biased plasma enhanced chemical vapor deposited silicon nitride films*; *Journal of Applied Physics* 83, 7, 3865 – 3870 (1998).
- ¹⁵ M. Ohring; *Material Science of Thin Films*; Academic Press; chapter 4: “Chemical Vapor Deposition” (1992).
- ¹⁶ K.-S. Chen, X. Zhang, S.-Y. Lin; *Intrinsic stress generation and relaxation of plasma-enhanced chemical vapor deposited oxide during deposition and subsequent thermal cycling*; *Thin Solid Films* 434, 190–202 (2003).
- ¹⁷ J. Rodriguez, C. Dominguez-Tagle, F. Munoz, A. Llobera; *Mechanical properties of PECVD silicon oxide films suitable for integrated optics applications*; *Proceedings of SPIE* Vol. 3953, 142 - 149 (2000).
- ¹⁸ B. Vigna, P. Ferrari, F. F. Villa, E. Lasalandra, S. Zerbin; *Silicon Sensors and Actuators*; Springer; chapter 6: “Optical Lithography” (2022).
- ¹⁹ M. Tilli, T. Motooka, V. Airaksinen, S. Franssila, M. Paulasto-Kröckel, V. Lindroos; *Handbook of Silicon Based MEMS Materials and Technologies*; Elsevier; chapter 20: “MEMS Lithography” (2015).
- ²⁰ M. J. Madou; *Manufacturing Techniques for Microfabrication and Nanotechnology*; Volume II; CRC Press; chapter 1: “Photolithography” (2011).
- ²¹ S. M. Sze; *Dispositivi a semiconduttore: comportamento fisico e tecnologia*; Hoepli; chapter 11: “Litografia e attacco chimico” (1991).
- ²² M. J. Madou; *Manufacturing Techniques for Microfabrication and Nanotechnology*; Volume II; CRC Press; chapter 3: “Dry Etching” (2011).
- ²³ F. Karouta; *A practical approach to reactive ion etching*; *J. Phys. D: Appl. Phys.* 47 (2014).
- ²⁴ A. Sankaran, M. J. Kushner; *Fluorocarbon plasma etching and profile evolution of porous low-dielectric-constant silica*; *Applied Physics Letters* 82, 12, 1824 – 1826 (2003).
- ²⁵ T. E. F. M. Standaert, C. Hedlund, E. A. Joseph, G. S. Oehrlein, T. J. Dalton; *Role of fluorocarbon film formation in the etching of silicon, silicon dioxide, silicon nitride, and amorphous hydrogenated silicon carbide*; *Journal of Vacuum Science & Technology A* 22, 53 (2004).

-
- ²⁶ V. M. Donnelly, A. Kornblit; *Plasma etching: Yesterday, today, and tomorrow*; J. Vac. Sci. Technol. A 31, 5 (2013).
- ²⁷ B. Vigna, P. Ferrari, F. F. Villa, E. Lasalandra, S. Zerbinì; *Silicon Sensors and Actuators*; Springer; chapter 5: “Deep Silicon Etch” (2022).
- ²⁸ M. Tilli, T. Motooka, V. Airaksinen, S. Franssila, M. Paulasto-Kröckel, V. Lindroos; *Handbook of Silicon Based MEMS Materials and Technologies*; Elsevier; chapter 21: “Deep Reactive Ion Etching” (2015).
- ²⁹ Z. A. S. Mohammed, M. A. S. Olimpo, D. P. Poenar, S. Aditya; *Smoothing of scalloped DRIE trench walls*; Materials Science in Semiconductor Processing 63, 83–89 (2017).
- ³⁰ F. Marty, L. Rousseau, B. Saadany, B. Mercier, O. Français, Y. Mita, T. Bourouin; *Advanced etching of silicon based on deep reactive ion etching for silicon high aspect ratio microstructures and three-dimensional micro- and nanostructures*; Microelectronics Journal 36, 673–677 (2005).
- ³¹ B. Vigna, P. Ferrari, F. F. Villa, E. Lasalandra, S. Zerbinì; *Silicon Sensors and Actuators*; Springer, chapter 11: “Wafer-to-Wafer Bonding” (2022).
- ³² P. Ramm, J. J.-Q. Lu, M. M. V. Taklo; *Handbook of Wafer Bonding*; Wiley (2012).
- ³³ F. Niklaus, P. Enoksson, E. Kalvesten, G. Stemme; *Low-temperature full wafer adhesive bonding*; J. Micromech. Microeng. 11, 100–107 (2001).
- ³⁴ H. Ito; *Chemically Amplified Resists: Past, Present, and Future*; Proc. of SPIE 3678 (1999).
- ³⁵ H. Ito; *Development of New Advanced Resist Materials for Microlithography*; Journal of Photopolymer Science and Technology 21, 4, 475 – 491 (2008).
- ³⁶ B. Jung, C. Ober, M. Thompson; *Deprotection reaction kinetics in chemically amplified photoresists determined by sub-millisecond post exposure bake*; Proc. of SPIE 8325 (2012).
- ³⁷ S. Malik, J. Eisele, A. Whewell, L. Ferreira, T. Holt, M. Bowden; *Post-Exposure Bake Temperature Consideration for High Activation Energy Resist Systems*; Journal of Photopolymer Science and Technology 13, 4, 513 – 518 (2000).
- ³⁸ Z. Mo, F. Wang, J. Li, Q. Liu, G. Zhang, W. Li, C. Yang, R. Sun; *Temporary Bonding and Debonding in Advanced Packaging: Recent Progress and Applications*; Electronics, 12 (2023).

4 | Characterization of thin films

Due to the large use of thin films in MEMS and microelectronics, it is fundamental to employ several characterization techniques during the processing of devices. Commonly, the characterization of thin films involves the measurement of thickness, stress, refractive index, resistivity, chemical composition, and morphology. These measurement techniques are needed for both process control and process development. In process control, it is important to measure the properties of films to verify the stability of well-established deposition recipes. For instance, before the actual deposition on the product wafer, the film is previously deposited on a test wafer to measure its properties, such as thickness, and to assure that they are included in the control range. Differently, in process development, measurements are employed to verify that the variation of some process parameters results in the optimization of the deposition process.

In this chapter, only thickness and curvature measurements are discussed since this work is focused on the mechanical properties of thin films. Moreover, the measurement of deflection of released structures is discussed since it is employed in the cantilever deflection method to evaluate the local residual stress of thin films.

4.1. Thickness measurement

In MEMS industry, the measurement of thin films' thickness is commonly performed by optical techniques such as ellipsometry and reflectometry, which are both non-destructive and characterized by high accuracy. Ellipsometry and reflectometry are both indirect measurement techniques which employ theoretical models to fit the experimental data [1]. The theoretical data (x_{calc}) are calculated from the parameters of the model, which are correlated with the thickness and the optical properties of the thin film. The theoretical model is fit to the experimental data (x_{exp}) varying the model's parameters, while the *goodness of fit* (GOF) is calculated as follows:

$$GOF = 1 - \frac{1}{N} \sqrt{\sum_{i=1}^N (x_{exp,i} - x_{calc,i})^2}$$

where N is the amount of experimental data collected.

In order to be confident about the analysis, sometimes the results are compared with a direct thickness characterization using electron microscopy (i.e., SEM or TEM). However, it is important to underline that this is a destructive characterization. In this work ellipsometry is employed to

measure the thickness of the thermal oxide layer by using the tool Therma-Wave OP3290, while reflectometry to measure the thickness of the thin films deposited on the EPI Poly layer by using the tool N&K 3000 Analyzer. The working principles of ellipsometry and reflectometry are discussed in the following paragraphs.

4.1.1. Ellipsometry

Ellipsometry is an optical technique employed to evaluate the optical properties and the thickness of thin films. The working principle of the measurement is based on the change in polarization of a previously polarized incident light beam after being reflected from the thin film. The change in polarization depends on the optical properties and the thickness of the film, however it is not possible to directly correlate these parameters. Ellipsometry is an indirect method in which theoretical models are fitted to experimental data. Therefore, it is fundamental to use a proper model to represent the physical system that is under characterization.

The general elliptical polarization is shown in Figure 32. The electric field is composed of two components: E_p and E_s , which are respectively parallel and perpendicular to the plane of incidence of light. The polarization state is characterized by two parameters: $\tan\psi$ and Δ . The first parameter represents the ratio between the amplitudes of E_p and E_s , while the second one is the phase difference between the two components. From the general case of elliptical polarization, the linear polarization is obtained for $\Delta=0$ or π [2].

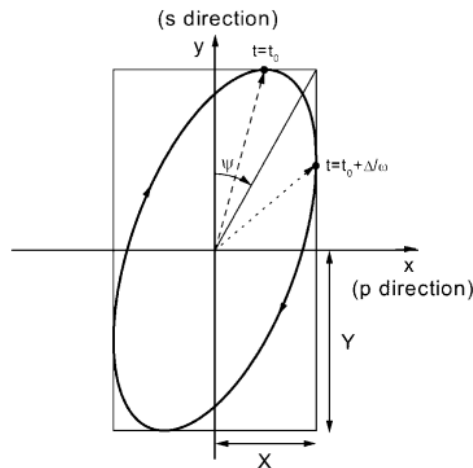


Figure 32: Scheme of elliptical polarization of light. [2]

In Figure 33, the general configuration of ellipsometry is illustrated.

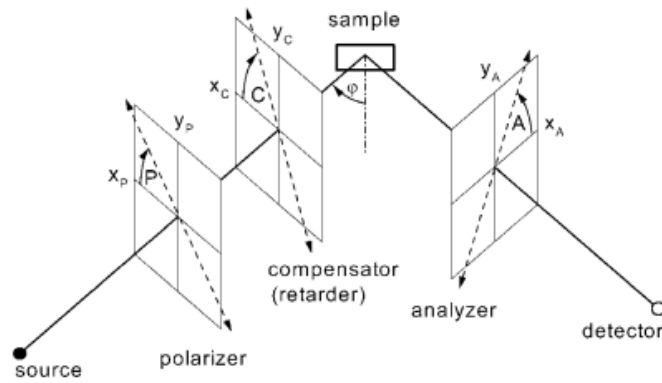


Figure 33: Schematic illustration of ellipsometry. [2]

An unpolarized monochromatic light beam is generated from a source and then it passes through a polarizer (P). The components of light perpendicular to the transmission axis of the polarizer are absorbed, therefore the beam is linearly polarized. Then, light is transmitted through the compensator (C), which has a fast transmission axis and a slow transmission axis. Consequently, the polarization of the light beam changes from linear to elliptical. After the incidence on the sample at the angle φ , the reflected beam passes through a second polarizer, which is called analyzer (A), before reaching the detector [3,4,5]. Depending on the configuration, the compensator could be absent. The ellipsometric parameters $\tan \psi$ and Δ of the reflected beam are determined by modifying the positions of the transmission axes of the polarizer, the compensator and the analyzer enabling the calculation of the complex reflection coefficient (ρ) [2,6]:

$$\rho = \tan \psi e^{i\Delta}$$

The parameter ρ is characteristic of the system. It depends on the angle of incidence, the wavelength, the thickness and the refractive indices of the ambient, the film and the substrate. As mentioned before, ellipsometry is an indirect method for the evaluation of the thickness of thin films. Theoretical models of the sample are employed to fit the experimental data. The model to employ is chosen considering several aspects: it has to be a physically realistic model, the calculated spectra must be in good agreement with the experimental data (high value of GOF), and the confidence limits should be sufficiently low [7].

4.1.2. Reflectometry

As far as the characterization of thin films is concerned [4], reflectometry represents an alternative to ellipsometry. These two techniques differ since in reflectometry the analysis is

based on the reflectance spectrum over a wide range of wavelengths instead of the polarization state of the reflected beam [1]. Similarly to ellipsometry, the thickness of the thin film is measured indirectly employing experimental data and a fitting of theoretical models.

The reflectometer measures the ratio between the intensity of the reflected beam and the intensity of the incident white light beam, yielding the experimental reflectance spectrum. Reflectance at a specific wavelength (λ_i) is a function of the thickness of the thin film (d) and the real and the imaginary parts of the complex index of refraction (n and k) at λ_i . For a wide range of thin films, the theoretical reflectance spectrum is obtained from the Forouhi-Bloomer dispersion equations [8]. The thickness and the optical properties of the film are obtained by fitting the theoretical spectrum to the experimental spectrum, maximizing the GOF. Figure 34 shows a reflectometry spectrum, in which the theoretical spectrum is fit to the experimental spectrum.

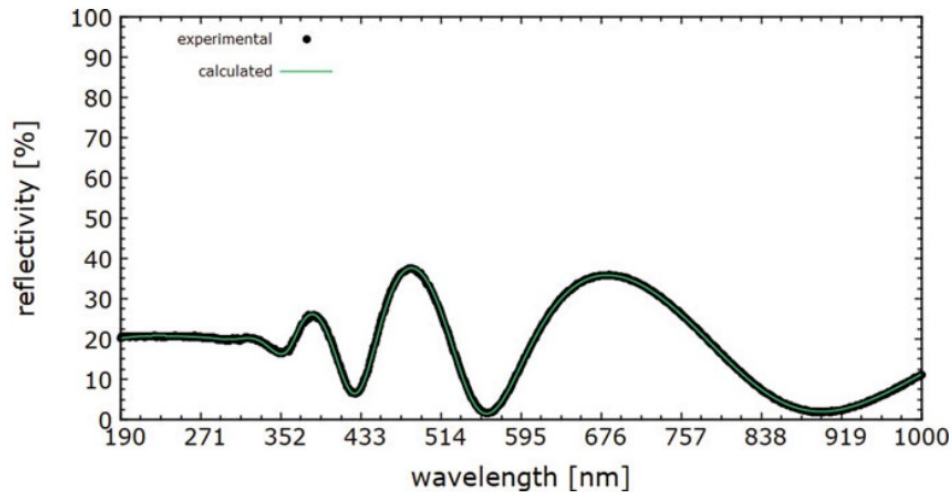


Figure 34: Example of a reflectometry spectrum in which the theoretical spectrum is properly fit to the experimental spectrum. [1]

4.2. Curvature measurement for stress evaluation

The residual stress of thin films is commonly evaluated by measuring the curvature of the wafer after the deposition of a film. As discussed in section 2.3, the residual stress and the curvature are related by Stoney's equation [9]:

$$\sigma_f = \left(\frac{E_s}{1 - \nu_s} \right) \frac{t_s^2}{6\rho t_f}$$

The curvature of the wafer is measured employing the *scanner laser method* [10]. This optical technique consists in the reflection of an incident laser beam from the surface of the wafer, which must be mirror-like. As shown in Figure 35, the incident laser beam is scanned along a diameter

of the wafer, while the angular deflection 2θ of the reflected beam from the incident direction is measured by a detector as a function of the position (r) along the scanning diameter.

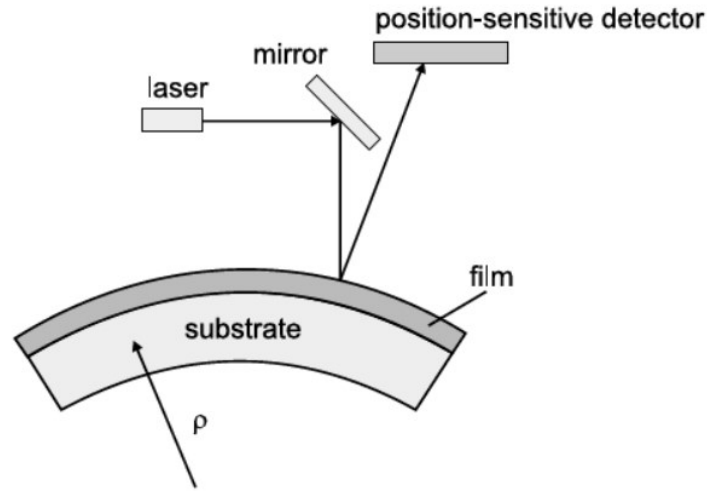


Figure 35: Schematic illustration of the curvature measurement by scanning laser method. [10]

The curvature (κ) is measured from the angle of reflection (θ) by the following equation:

$$\kappa = \frac{1}{\rho} = \frac{d\theta(r)}{dr}$$

The measured radius of curvature is substituted in Stoney's equation, enabling the estimation of the mean residual stress. Since wafers are not flat, which means that their radius of curvature is not infinite, the curvature of the wafer must be calculated also before the deposition of the thin film to avoid the influence of the pre-deposition curvature on the residual stress estimation [11]. Therefore, Stoney's equation is rewritten as follows:

$$\sigma_f = \left(\frac{E_s}{1 - \nu_s} \right) \frac{t_s^2}{6t_f} \left(\frac{1}{\rho} - \frac{1}{\rho_0} \right)$$

where ρ_0 is the curvature of the wafer before the deposition of the thin film.

As discussed in section 2.3, Stoney's equation assumes that the deformation of the wafer is spherical, which means that the radius of curvature is equal in all directions. However, this assumption is commonly not respected. Thus, the radius of curvature is usually measured along several diameters, while the mean value is used in the equation.

Although the scanning laser method is a non-local technique, some tools can perform a local evaluation of the residual stress by applying Stoney's equation using the radius of curvature of a portion of the scanning path instead of the entire diameter. However, in literature several articles

state that the local application of Stoney's equation gives incorrect results for non-uniform stress distributions [12,13].

In this work, the scanning laser method is compared to the cantilever deflection method. The tool KLA-Tencor Flexus FLX5500 is employed to evaluate the mean residual stress of the thin films by using Stoney's equation, while the tool Frontier Semiconductor FSM 128 C2C is employed to evaluate the local residual stress by applying the Stoney's equation locally.

4.3. Measurement of the deflection of released structures

As a consequence of the residual stress, released structures show an out-of-plane deflection, which can be measured by visible light interferometry. Interferometry is an optical technique based on the wave interference phenomenon. Commonly, the tool configuration is based on the Michelson's interferometer, whose scheme is shown in Figure 36. It presents two different arms: the reference arm and the measurement arm. The beam generated from the light source is equally split by a beam splitter in two beams: the beam reference (in the reference arm) and the beam sample (in the measurement arm). The first one is reflected from a reference metal-coated mirror, while the second one is reflected from the sample [14].

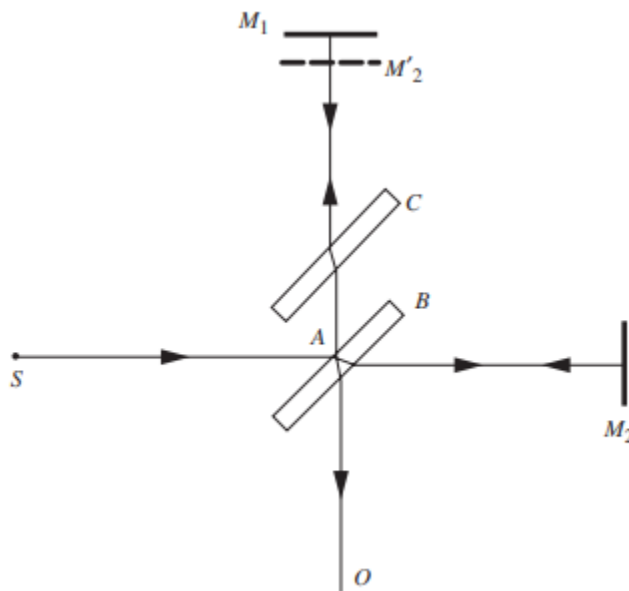


Figure 36: Configuration of the Michelson's interferometer. [14]

Considering a single layer structure, reflection occurs at the interfaces between air and the top surface and between the bottom surface and the air below. Then, the reflected beams from the sample and the reflected beam from the reference recombine. Due to the difference in optical

path, an interference spectrum (called interferogram) is obtained from the detector. Using a Fast Fourier Transform (FFT), the interferogram (frequency domain) is converted into the Fourier spectrum (time domain) [15]. The Fourier spectrum is characterized by several intensity peaks at different distances from the reference, each peak is referred to the signal coming from the reflection at a specific interface.

The profile of released structures is obtained by multiple acquisitions along the profile line, analyzing how the position of a specific peak changes in the Fourier spectrum. Plotting the distance of the chosen peak as a function of the position along the profile line, the deflection of the structure can be evaluated. The tool Rudolph Technologies NSX 330 is employed to obtain the profile of deflected cantilevers, as shown in Figure 37, enabling the measurement of their deflection after being released.

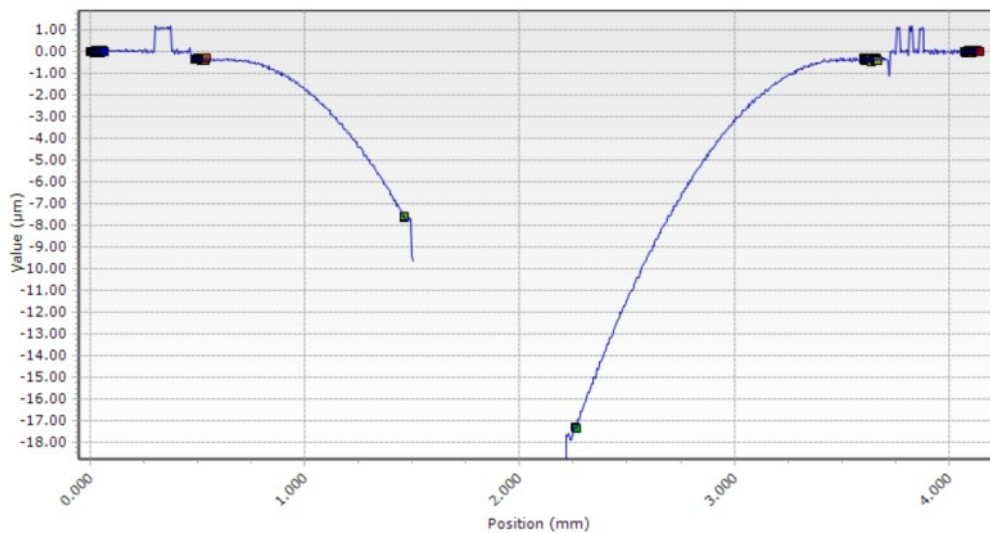


Figure 37: Downward bent cantilevers' profile obtained from visible light interferometry by using the tool Rudolph Technologies NSX 330.

References

¹ B. Vigna, P. Ferrari, F. F. Villa, E. Lasalandra, S. Zerbini; *Silicon Sensors and Actuators*; Springer; chapter 4: "Thin Film Characterization and Metrology" (2022).

² H. G. Tompkins, E. A. Irene; *Handbook of ellipsometry*; Springer; chapter 1: "Polarized Light and Ellipsometry" (2005).

-
- ³ M. Ohring; *The Material Science of Thin Films*; Academic Press; chapter 6: “*Characterization of Thin Films*” (1992).
- ⁴ D. K. Schroder; *Semiconductor Material and Device Characterization*; John Wiley & Sons, Inc.; Third edition; chapter 10: “*Optical Characterization*” (2006).
- ⁵ D. Gonçalves, E.A. Irene; *Fundamentals and Applications of Spectroscopic Ellipsometry*; Quim. Nova, Vol. 25, No. 5, 794-800 (2002).
- ⁶ K. Hassani, K. Abbaszadeh; *Thin film characterization with a simple Stokes ellipsometer*; Eur. J. Phys. 36 (2015).
- ⁷ K. Vedam; *Spectroscopic ellipsometry: a historical overview*; Thin Solid Films 313-314 (1998).
- ⁸ A. R. Forouhi; *Optical dispersion relations for amorphous semiconductors and amorphous dielectrics*; Physical Review B, 34, 10, 7018-7025 (1986).
- ⁹ G. G. Stoney; *The tension of metallic films deposited by electrolysis*; Proc. R. Soc. London A 82, 172-173 (1909).
- ¹⁰ L. B. Freund, S. Suresh; *Thin Film Materials: Stress, Defect Formation and Surface Evolution*; Cambridge University Press; chapter 2: “*Film stress and substrate curvature*” (2004).
- ¹¹ C.-L. Tien, T.-W. Lin; *Thermal expansion coefficient and thermomechanical properties of SiN_x thin films prepared by plasma-enhanced chemical vapor deposition*; Applied Optics 51, 30, 7229-7235 (2012).
- ¹² D. Ngo, X. Feng, Y. Huang, A.J. Rosakis, M.A. Brown; *Thin film/substrate systems featuring arbitrary film thickness and misfit strain distributions. Part I: Analysis for obtaining film stress from non-local curvature information*; International Journal of Solids and Structures 44, 1745-1754 (2007).
- ¹³ M. Zhu, P. B. Kirby; *Governing equation for the measurement of nonuniform stress distributions in thin films using a substrate deformation technique*; Appl. Phys. Lett. 88, 171903 (2006).
- ¹⁴ P. Hariharan; *Optical Interferometry*; 2nd Edition; Elsevier Science & Technology; chapter 2: “*Two-Beam Interference*” (2003).
- ¹⁵ J. Jin, J. W. Kim, C.-S. Kang, J.-A. Kim, S. Lee; *Precision depth measurement of through silicon vias (TSVs) on 3D semiconductor packaging process*; Optics Express 20, 5, 5011-5016 (2012).

5 | Theoretical model for stress evaluation from cantilever deflection

In section 4.2 it was described the common method to measure the mean stress of a film [1] based on Stoney's equation [2]. Despite being a simple and fast approach to calculate the residual stress, this method presents several limitations:

- The residual stress is considered uniform.
- It does not allow the measurement of the stress gradient.
- It does not evaluate the effect of the post-deposition processes.
- It cannot measure the residual stress in multi-layer stacks.

Firstly, stress is considered uniform along the wafer, neglecting a possible center-to-edge variability since it does not allow a local analysis. Secondly, it is not possible to calculate the stress gradient of the layer since the stress is assumed uniform across the thickness. Studying only the curvature of the wafer could cause a misleading of the out-of-plane deformation of a released structure. As it was shown by Kilinc et al. [3], from a wafer with a negligible curvature (i.e., infinite radius of curvature), it is possible to obtain a deflected free-standing cantilever since its deflection is dependent on the stress gradient. Vice versa, a free-standing cantilever obtained from a warped wafer may not show a relevant tip deflection if the stress gradient is negligible. Considering a wafer with a monolayer deposited on top of it, the curvature of the wafer depends on both the residual stress and the stress gradient of the deposited layer. On the contrary, the deflection of a released monolayer cantilever depends only on the stress gradient since the residual stress causes an in-plane deformation. It is possible to evaluate only the as-deposited residual stress since the analysis of the effects of post-deposition processes is usually not allowed [4]. Finally, Stoney's Equation cannot be employed to study multi-layer stacks.

When a cantilever is released, the mean residual stress is relieved by an in-plane deformation, while the stress gradient is relieved by an out-of-plane deformation [3,5]. The presence of a stress gradient results in a net bending moment, which causes the bending of the cantilever. Figure 38 shows the deflection of a single-layer cantilever depending on the stress gradient. A positive stress gradient leads to an upward deflection because the tensile stress on the top side is relieved by contraction, while the compressive stress on the bottom side is relieved by dilatation. On the contrary, a negative stress gradient leads to a downward deflection.

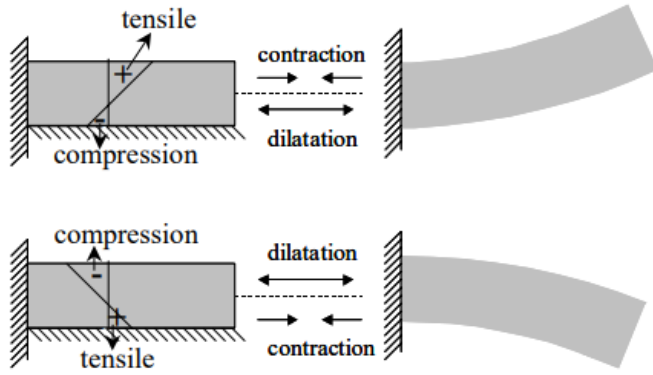


Figure 38: Deflection of a cantilever beam upon positive and negative stress gradient. [5]

Employing visible light interferometry, as mentioned in section 4.3, it is possible to measure the deflection of the bent cantilever. Considering a cantilever with N films on top of a base layer (Figure 39), the resulting bending moment can be written as:

$$M = \int_{y_0}^{y_1} (\sigma_0 + \nabla\sigma_0 y) w (y - y_c) dy + \sum_{j=1}^N \int_{y_j}^{y_{j+1}} \left(\sigma_j + \nabla\sigma_j \left(y - y_j - \frac{t_j}{2} \right) \right) w (y - y_c) dy \quad (5.1)$$

where σ_0 and $\nabla\sigma_0$ are respectively the mean stress and the stress gradient of the base layer, σ_j , $\nabla\sigma_j$ and t_j the mean stress, the stress gradient and the thickness of the j -th film, w the width of the cantilever, while y_c the neutral axis of the section. This equation is general, depending on the configuration of the cantilever it can be simplified.

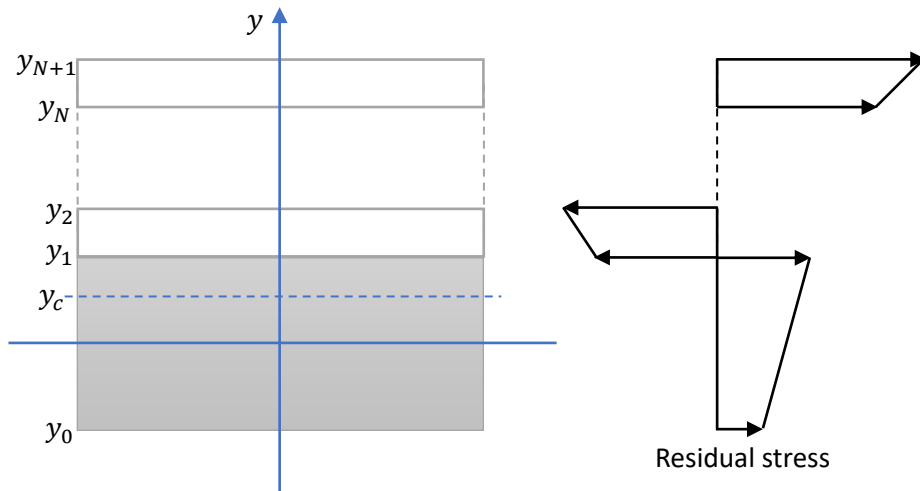


Figure 39: Section of a multi-layer cantilever with the residual stress of each layer.

5.1. Single-layer cantilever

Considering a cantilever made just by the base layer, the stress profile can be represented with Eq. 2.2. The general equation of the bending moment can be written for this specific case. Only the term related with the base layer should be considered and the neutral axis is placed at the center of the cantilever (thus, y_c is equal to zero). Due to the position of the neutral axis, the bending moment depends only on the stress gradient of the layer. The simplified version of Eq. 5.1 is:

$$M = \int_{y_0}^{y_1} \nabla\sigma_0 w y^2 \cdot dy \quad (5.2)$$

Solving the integral, the net bending moment can be written as:

$$M = \frac{\nabla\sigma_0}{12} w t_0^3 = \frac{\sigma_{0,1} - \sigma_{0,2}}{12} w t_0^2 \quad (5.3)$$

where $\sigma_{0,1}$ and $\sigma_{0,2}$ are respectively the residual stress at the top and at the bottom of the base layer, while t_0 is the thickness.

According to the *small deflection theory* of solid mechanics, if the deflection is lower than the 10% of the beam's length, the bending moment acting on a cantilever beam fixed at $x=0$ can be expressed as follows:

$$M = EI \frac{d^2z}{dx^2} \quad (5.4)$$

Where z is the deflection along the x -axis, while I is the moment of inertia. The differential equation is solved by applying the following boundary conditions [6]:

$$z|_{x=0} = 0$$

$$\left. \frac{dz}{dx} \right|_{x=0} = 0$$

It results in Eq. 5.5, in which the deflection is written as a function of the bending moment.

$$z = \frac{M x^2}{EI} \quad (5.5)$$

Replacing the bending moment with Eq. 5.3 and the moment of inertia with $I = w t_0^3 / 12$ in Eq.5.5, the stress gradient is calculated from the deflection δ at the tip of the cantilever (i.e., at $x = L$) as follows:

$$\nabla\sigma_0 = 2 \frac{E}{L^2} \delta \quad (5.6)$$

5.2. Bi-layer cantilever

Considering a cantilever made of a base layer and a thin film (Figure 40), it is possible to evaluate the residual stress of the thin film from the deflection of the cantilever upon release. Since the layer on top of the base layer is a thin film (in this work the films are characterized by a thickness included in the range 0.1–0.5 μm), the residual stress is considered constant across its thickness, neglecting the stress gradient of the thin film ($\nabla\sigma_1$).

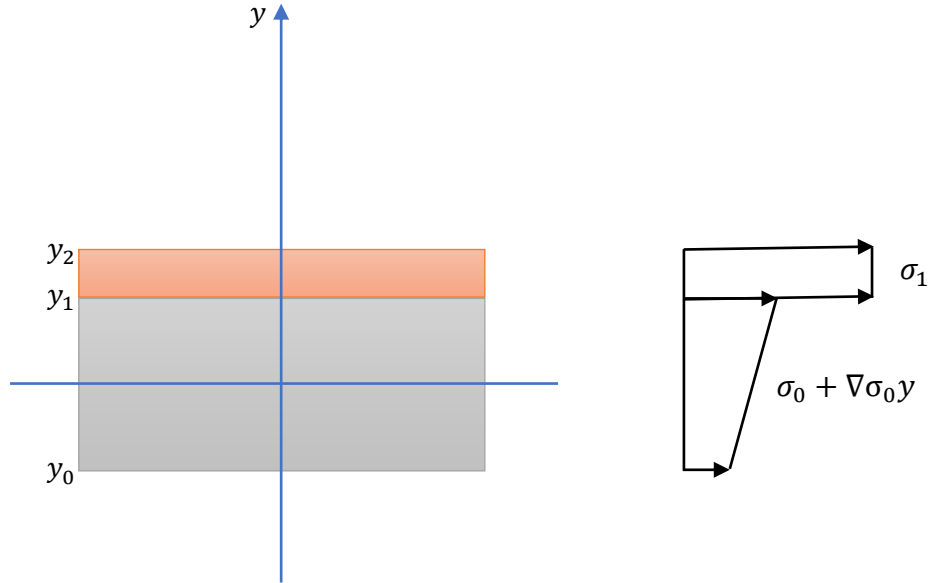


Figure 40: Scheme of the bi-layer cantilever with the residual stress of the thin film and the base layer.

According to the method proposed by Min and Kim [7], the residual stress of the thin film is calculated comparing the deflection of the bi-layer cantilever with the deflection of a single-layer cantilever, composed only of the base layer. The presence of the additional layer changes the moment of inertia and the neutral axis of the cantilever. In order to study the behavior of the cantilever, an equivalent single-layer cantilever is used. The equivalent single-layer cantilever is obtained by considering a cantilever made just by the base layer material with a different width of the additional layer to maintain the same deflection of the bi-layer cantilever at a certain bending moment. Therefore, the shape of the section is no longer rectangular, as it is shown in Figure 41. The equivalent width (w_e) of the additional layer can be calculated using Eq. 5.7:

$$w_e = \frac{E_1}{E_0} w \quad (5.7)$$

where E_1 and E_0 are respectively the Young's moduli of the additional layer and the base layer, while w is the actual width of the cantilever.

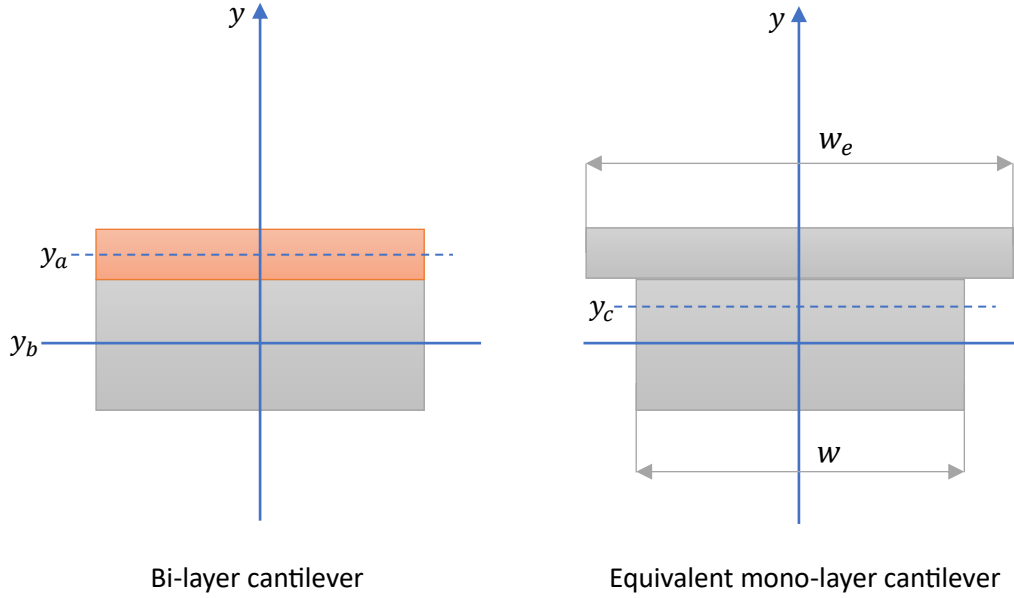


Figure 41: Section of the equivalent single-layer cantilever made by the material of the base layer.

The neutral axis of the bi-layer cantilever (y_c) can be calculated from the geometry of the equivalent section, using the following equation:

$$y_c = \frac{y_b w t_0 + y_a w_e t_1}{w t_0 + w_e t_1} \quad (5.8)$$

where y_b is the neutral axis of the base layer, while y_a is the neutral axis of the additional layer. As shown in Figure 40, the zero of the y -axis was chosen at the middle of the base layer, therefore the value of y_b is equal to zero since the neutral axis of a single-layer rectangular section is placed at half of its thickness. For the same reason, the neutral axis of the additional layer is:

$$y_a = \frac{t_0 + t_1}{2}$$

The moment of inertia of the equivalent section (I_c) is calculated as follows:

$$I_c = I_b + w t_0 (y_c - y_b)^2 + I_a + w_e t_1 (y_c - y_a)^2 \quad (5.9)$$

where I_b and I_a are respectively the moments of inertia of the base layer and the additional layer. The net bending moment acting on the bilayer cantilever after release (M_c) is calculated using Eq. 5.10, which is obtained from Eq. 5.1.

$$\begin{aligned}
M_c &= \int_{y_0}^{y_1} (\sigma_0 + \nabla\sigma_0 y) w(y - y_c) dy + \int_{y_1}^{y_2} \sigma_1 w(y - y_c) dy \\
&= -\sigma_0 w y_c t_0 + \nabla\sigma_0 w \frac{t_0^3}{12} + \sigma_1 w t_1 \left(\frac{t_1}{2} + \frac{t_0}{2} - y_c \right) \quad (5.10)
\end{aligned}$$

As mentioned above, the residual stress of the additional layer is calculated by comparing the deflection of the bi-layer cantilever with the deflection of the single-layer cantilever. The bending moment acting on the single-layer cantilever (M_b) is obtained by Eq. 5.3, as previously discussed. Eq. 5.5 is used to obtain the bending moment as a function of the deflection at the tip of the cantilever (δ), by substituting z with δ and x with L . Thus, M_c and M_b can be written as:

$$M_c = \frac{2E_0}{L^2} I_c \delta_c \quad (5.11)$$

$$M_b = \frac{2E_0}{L^2} I_b \delta_b \quad (5.12)$$

where δ_c and δ_b are respectively the deflection at the tip of the bilayer cantilever and the single-layer cantilever. Considering Eq. 5.10 and Eq. 5.3, the difference between M_c and M_b is:

$$M_c - M_b = \sigma_1 w t_1 \left(\frac{t_1}{2} + \frac{t_0}{2} - y_c \right) - \sigma_0 w y_c t_0 \quad (5.13)$$

Replacing M_c and M_b in Eq. 5.13 with Eq. 5.11 and Eq. 4.12, the residual stress in the thin film can be written as:

$$\sigma_1 = \frac{\left(2 \frac{E_0}{L^2} \right) (I_c \delta_c - I_b \delta_b) + \sigma_0 w t_0 y_c}{w t_1 \left(\frac{t_1}{2} + \frac{t_0}{2} - y_c \right)} \quad (5.14)$$

Apart from δ_c , δ_b and σ_0 , all the parameters in Eq. 5.14 are known. The deflections are measured by visible light interferometry, while the residual stress of the base layer (σ_0) is evaluated by using Stoney's equation.

References

¹ L. B. Freund, S. Suresh; *Thin Film Materials: Stress, Defect Formation and Surface Evolution*; Cambridge University Press; chapter 2: "Film stress and substrate curvature" (2004).

² G. G. Stoney; *The tension of metallic films deposited by electrolysis*; Proc. R. Soc. London A 82, 172-173 (1909).

³ Y. Kilinc, U. Unal, B. E. Alaca; *Residual stress gradients in electroplated nicker thin films*; *Microelectronic Engineering* 134, 60–67 (2015).

⁴ C.-W. Baek, Y.-K. Kim, Y. Ahn, Y.-H. Kim; *Measurement of the mechanical properties of electroplated gold thin films using micromachined beam structures*; *Sensors and Actuators A* 117, 17–27 (2005).

⁵ T. Van der Donck, J. Proost, C. Rusu, K. Baert, C. Van Hoof, J.-P. Celis, A. Witvrouw; *Effect of deposition parameters on the stress gradient of CVD and PECVD poly-SiGe for MEMS applications*; *Proceedings of SPIE* 5342, 8–18 (2004).

⁶ A. K. Chinthakindi, D. Bhusari, B. P. Dusch, Jürgen Musolf, B. A. Willemsen, E. Prophet, M. Roberson, P. A. Kohl; *Electrostatic Actuators with Intrinsic Stress Gradient*; *Journal of Electrochemical Society* 149, H139 - H145 (2002).

⁷ Y.-H.Min, Y.-K. Kim; *In situ measurement of residual stress in micromachined thin films using a specimen with composite-layered cantilevers*; *J. Micromech. Microeng.* 10, 314–321 (2000).

6 | Fabrication and characterization of test structures

In this chapter, the fabrication of the test structures and the measurement of the residual stress from cantilever deflection are detailed. The test structure is composed of an array of twelve cantilevers, as it is shown in Figure 42. The six cantilevers on the left of the structure are 1270 μm long, while the other six are 829 μm long. The width of the cantilevers is equal to 187 μm . This layout enables the comparison of the results obtained analyzing cantilevers of different lengths. For the same wafer, the results obtained using cantilevers of the same array are expected to be in agreement. The total number of test structures across the wafer is twenty-six and they are arranged on the wafer as shown in Figure 43. The minimum edge exclusion (i.e., the distance between the edge of the wafer and the position of the farthest test structure from the center of the wafer) is equal to 12 mm.

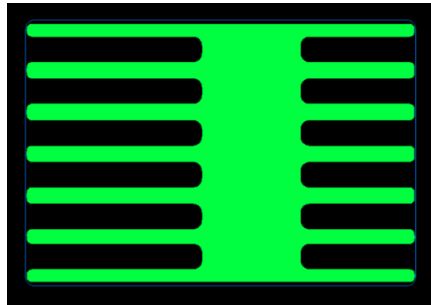


Figure 42: GDS image of the test structure.

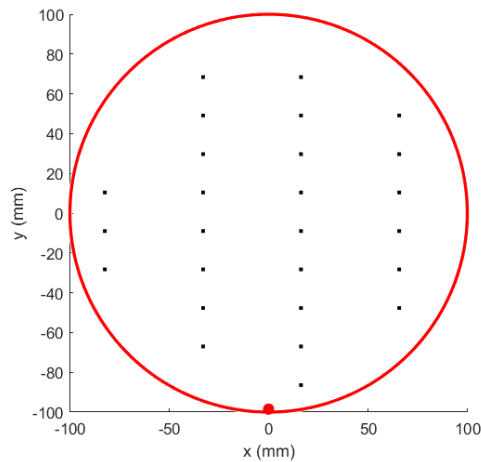


Figure 43: Arrangement of the twenty-six test structures on wafer.

In Table 2, the three lots of wafers used in this work are listed.

Table 2: Lots of wafers used in this work and the measurements performed for each lot.

Lot number	Number of wafers	Purpose
1	5	<ul style="list-style-type: none"> Measurement of the the stress gradient of the base layer in EPI Poly.
2	25	<ul style="list-style-type: none"> Measurement of the residual stress of the following four thin films: <i>LPCVD SiN tens</i>, <i>PECVD USG</i>, <i>PECVD SiN +170</i>, <i>PECVD SiN -150</i>.
3	25	<ul style="list-style-type: none"> Measurement of the residual stress of the following four thin films: <i>PECVD SiN -150 B</i>, <i>PECVD SiN -350</i>, <i>PECVD SiON</i>, <i>LPCVD SiN comp</i>.

Lot 1 has been used to evaluate the stress gradient of the EPI Poly base layer. Therefore, single-layer cantilevers are fabricated thus enabling the calculation of the stress gradient from their deflection (section 5.1). For all the five wafers of lot 1, the thickness of the EPI Poly layer is 20 μm .

Two lots have been dedicated to the study of cantilevers composed of two layers: the base layer and a dielectric film deposited on top. Lot 2 is used to measure the residual stress of four different dielectric thin films. The lot presents a split in the thickness of the EPI Poly base layer:

- 20 μm thick from laser mark (LM) 1 to 13.
- 10 μm thick from LM 14 to 25.

Table 3 lists the thin films deposited on each wafer of lot 2 and their nominal values of thickness and stress. The *control range*, which is the range in which the residual stress must be included when testing the deposition process, is provided with both the thickness and the nominal residual stress. The names of the film recipes refer to the deposition technique employed, and the material deposited. In cases where different films are made of the same material and are deposited with the same technique, a reference to the nominal residual stress of the film is added. For example, the recipe *PECVD SiN +170* refers to a silicon nitride film deposited by PECVD, which has a nominal residual stress equal to 170 MPa. On the wafers LM 13 and 14 the deposition of the thin film has been skipped since the deflection of the reference single-layer cantilevers in EPI Poly is required to calculate the residual stress of the thin films. LM 13 is the reference wafer for bi-layer cantilevers with a 20 μm thick EPI Poly layer, while LM 14 for bi-layer cantilevers with a 10 μm thick layer.

Table 3: Split in deposition for the wafers of lot 2.

LM	Thickness of EPI Poly (μm)	Thin film recipe	Nominal thickness of the thin film (\AA)	Nominal residual stress of the thin film (MPa)
1 - 3	20	LPCVD SiN tens	3000 ± 100	$+600 \pm 40$
4 - 6	20	PECVD USG	4000 ± 200	-80 ± 20
7 - 9	20	PECVD SiN +170	1400 ± 40	$+170 \pm 70$
10 - 12	20	PECVD SiN -150	3000 ± 100	-150 ± 30
13	20			
14	10			
15 - 17	10	LPCVD SiN tens	3000 ± 100	$+600 \pm 40$
18 - 20	10	PECVD USG	4000 ± 200	-80 ± 20
21 - 23	10	PECVD SiN +170	1400 ± 40	$+170 \pm 70$
24 - 25	10	PECVD SiN -150	3000 ± 100	-150 ± 30

Lot 3 has been processed with a different split of thin films deposited on top of the base layer. Table 4 lists the thin films deposited on each wafer of lot 3 and their nominal values of thickness and stress.

Table 4: Split in deposition for the wafers of lot 3.

LM	Thickness of EPI Poly (μm)	Thin film recipe	Nominal thickness of the thin film (\AA)	Nominal residual stress of the thin film (MPa)
1 - 3	20	PECVD SiN -150 B	3000 ± 150	-150 ± 50
4 - 6	20	PECVD SiN -350	3000 ± 100	-350 ± 30
7 - 9	20	PECVD SiON	5000 ± 250	-100 ± 50
10 - 12	20	LPCVD SiN comp	2100 ± 60	-100 ± 40
13	20			
14	10			
15 - 17	10	PECVD SiN -150 B	3000 ± 150	-150 ± 50
18 - 20	10	PECVD SiN -350	3000 ± 100	-350 ± 30
21 - 23	10	PECVD SiON	5000 ± 250	-100 ± 50
24 - 25	10	LPCVD SiN comp	2100 ± 60	-100 ± 40

6.1. Fabrication of test structures

The simplified scheme of the process flow employed to fabricate the test structures is shown in Figure 44.

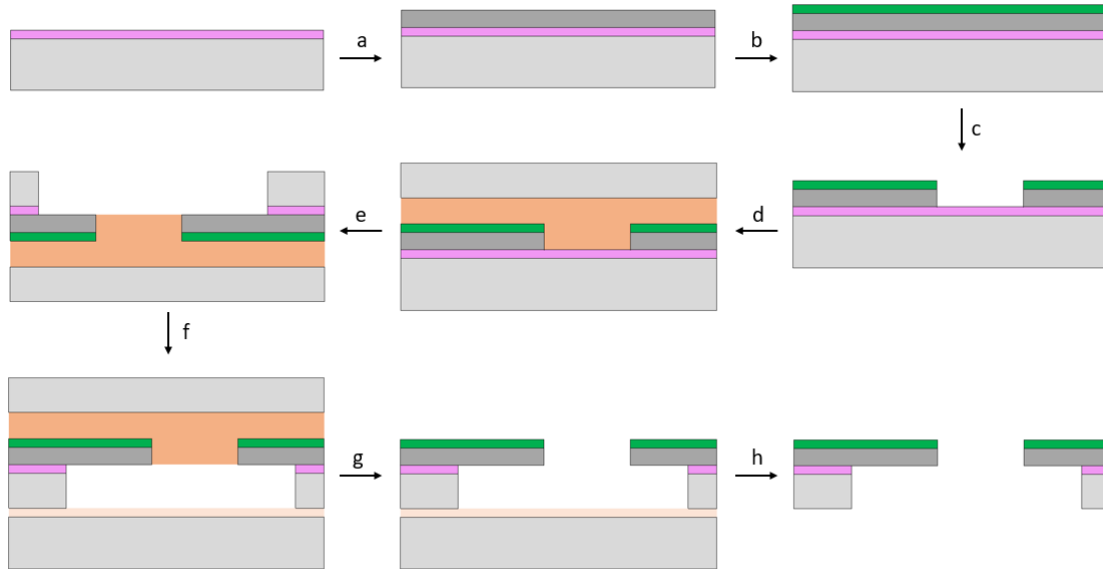


Figure 44: Simplified process flow for the fabrication of the test structure: (a) growth of the EPI Poly layer; (b) deposition of the thin film by CVD; (c) etching of the thin film by RIE and of the EPI Poly layer by Bosch process; (d) polymer-based temporary bonding of the cap wafer; (e) etching of the silicon substrate by Bosch process and of the thermal oxide layer by dry etching; (f) tape-based temporary bonding of the carrier wafer; (g) debonding of the cap wafer by slide off; (h) debonding of the carrier wafer by lift off.

The EPI Poly base layer is grown on an 8" mono-silicon wafer Si(100) with a 1 μm thick thermal silicon oxide layer on top of it. The growth occurs in a single-wafer epitaxial reactor at 1186 $^{\circ}\text{C}$ using trichlorosilane as precursor. Since EPI Poly is characterized by high roughness, a CMP step is then employed to obtain a mirror-like surface. A target of 3 μm of EPI Poly thickness is removed by polishing, thus 23 μm thick and 13 μm thick layers are grown to obtain respectively the target values of 20 μm and 10 μm after polishing.

The dielectric thin film is deposited on top of the polished EPI Poly layer by CVD techniques. In Table 5 the deposition conditions of the thin films are summarized. *LPCVD SiN tens* and *LPCVD SiN comp* films are deposited in a vertical furnace at 780 $^{\circ}\text{C}$ using dichlorosilane (DCS) and ammonia (NH_3) as precursors. The ratio DCS/ NH_3 is higher in the recipe *LPCVD SiN comp*. Two different tools are employed in the PECVD depositions, which will be referred to as tool A and tool B. Tool A is a single-wafer chamber tool, therefore each wafer is processed in the same deposition chamber. Significant variations of the residual stress between different wafers with the same film are not expected. Differently, tool B is a double-chamber tool and thus two wafers are processed in parallel. In this case, differences in residual stress between films deposited on

the first and on the second heater are expected. *PECVD USG* films are deposited at 350 °C from silane and nitrous oxide in tool A. *PECVD SiN +170* and *PECVD SiN -150 B* films are both deposited from silane, ammonia and nitrogen in tool B at 400 °C. *PECVD SiN -150* and *PECVD SiN -350* films are deposited from silane and nitrogen in tool A at 350 °C. *PECVD SiON* films are deposited from silane, nitrous oxide, ammonia and nitrogen in tool B at 400 °C.

After the deposition of the thin film, its thickness is measured by employing the tool N&K 3000 Analyzer, fitting the experimental data with a theoretical model which considers the presence of the EPI Poly and the thermal silicon oxide layers under the thin film.

Table 5: Deposition parameters for the thin films deposited.

Thin film recipe	Temperature (°C)	Precursors
LPCVD SiN tens	780	SiCl ₂ H ₂ , NH ₃
LPCVD SiN comp	780	SiCl ₂ H ₂ , NH ₃
PECVD USG	350	SiH ₄ , N ₂ O
PECVD SiN +170	400	SiH ₄ , NH ₃ , N ₂
PECVD SiN -150	350	SiH ₄ , N ₂
PECVD SiN -150 B	400	SiH ₄ , NH ₃ , N ₂
PECVD SiN -350	350	SiH ₄ , N ₂
PECVD SiON	400	SiH ₄ , N ₂ O, NH ₃ , N ₂

The front side is patterned by optical lithography employing a mask aligner tool. Firstly, the wafer is treated with hexametildisilazane vapor to improve the adhesion of the photoresist. Then a positive I-line photoresist, thus sensitive to a wavelength equal to 365 μm, is deposited by spin coating, obtaining a 7 μm thick layer. A soft bake at 100 °C occurs to remove the solvent from the resist. Since high resolutions are not required, in proximity exposure is employed. During the development step, an aqueous base developer with TMAH is used. In this case, one lithographic mask is used for both the etching of the dielectric film and the EPI Poly layer; therefore, the hard bake step is avoided because during deep silicon etching the photoresist must not be sloped. Both silicon nitride and silicon oxide thin films are etched by RIE using a plasma chemistry composed of CHF₃, CF₄, O₂ and Ar. The Bosch process is employed to perform the deep silicon etching of the EPI Poly exposed on the front side. After the removal of the dielectric film and the EPI Poly layer, the resist residual is removed by oxygen plasma.

In order to process the back side of the wafer, a 500 μm thick cap wafer is bonded by temporary polymer-based bonding. The adhesive polymer is spin coated on the surface of the wafer, obtaining a 60 μm layer. The bonding occurs at 150 °C to overcome the glass transition temperature of the polymer. The cap wafer and the device wafer are lapped to respectively reduce their thickness from 500 μm to 400 μm and from 715 μm to 385 μm. The pattern of cavities

on the back side of the device wafer, which corresponds with the arrays of cantilevers on the front side, is defined by optical lithographic employing a mask aligner tool. A chemically amplified photoresist is spin coated on the back side, obtaining a 17 μm thick layer. After exposure, two post exposure bake steps occur at 105 $^{\circ}\text{C}$ and at 90 $^{\circ}\text{C}$ to activate the reaction between the photoacid and the pendant group in the polymeric chains of the photoresist. Then, the exposed regions of the photoresist are removed by an aqueous solution with TMAH. The cavities are opened by employing the Bosch process and by etching the thermal oxide layer using a plasma chemistry composed of Ar and CF_4 . In order to handle the wafer during the removal of the cap wafer, a carrier wafer is bonded on the back side of the device wafer by temporary tape-based bonding at 80 $^{\circ}\text{C}$. Then, the debonding of the cap wafer occurs by slide off at 160 $^{\circ}\text{C}$ to soften the adhesive polymer. Slide off is performed by applying a tangential loading equal to 90 N parallel to the length of the cantilevers. Then, the front side is cleaned from the residuals of the polymeric adhesive by using dodecene. Finally, the carrier wafer is removed by lift off at 200 $^{\circ}\text{C}$.

The process flow employed resulted appropriate to fabricate the test structure. In particular, during the debonding of the cap wafer by slide off, which is the most critical step, the cantilevers did not break consequently the tangential force applied. However, wafers LM 8, 17 and 24 of lot 2 and LM 1 of lot 3 broke during the handling of the lot.

6.2. Measurement setup

The deflection of the cantilevers is measured by visible light interferometry, using the tool Rudolph Technologies NSX 330. For each of the twenty-six structures, the deflections of one 1270 μm long cantilever and one 829 μm long cantilever are measured since it is assumed that for each structures the residual stress is uniform. The profile of the bent cantilevers is obtained by multiple acquisitions of the out-of-plane deflection (z coordinate) along the profile line which is traced along the two cantilevers at the top of the test structure (Figure 45). Each acquisition is taken every 5 μm along the profile line.

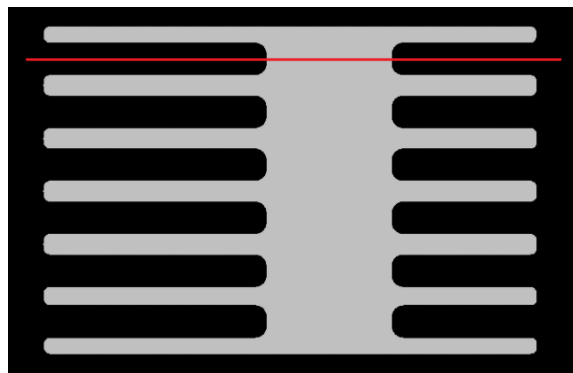


Figure 45: Profile line (red line) along which the profile of the bent cantilevers is obtained.

The zero of the z coordinate is set at the fixed end of cantilevers. Therefore, negative values of deflection are obtained from downward bent cantilevers, while positive values from upward bent cantilevers. For each acquisition, the out-of-plane deflection is obtained from the signal of the Fourier spectrum related to the interface between air and the top surface of the cantilever. The tip deflection is taken at a distance of $50\ \mu\text{m}$ from the actual free end of the cantilever in order to avoid the diffraction effect at the edges [1] and it is obtained from the mean value between two consecutive acquisitions. Therefore, during the calculation of the residual stress of the thin film by using Eq. 5.14, it is fundamental to replace the length of the cantilever (L) with a value of the x coordinate equal to L minus $50\ \mu\text{m}$. Otherwise, the absolute value of residual stress would be underestimated since the deflection at the actual free end of the cantilever is higher than the value measured. Similarly, also in the calculation of the stress gradient of the EPI Poly layer by Eq. 5.6, the term L in the denominator is replaced by L minus $50\ \mu\text{m}$. The uncertainty in the measurement of deflection is considered equal to $0.1\ \mu\text{m}$.

6.3. Calculation of residual stress

In order to calculate the local residual stress of a thin film by Eq. 5.14, several assumptions are made:

- a) The residual stress of the EPI Poly layer is uniform across the entire wafer.
- b) The thickness of the EPI Poly layer is uniform across the entire wafer.
- c) The thickness of the thin film is uniform across the entire wafer.
- d) The stress gradient of the EPI Poly layer and the residual stress of the thin film are locally uniform in the region of the test structure.
- e) The distribution of the stress gradient of the EPI Poly layer is the same for wafers from the same lot.

The average residual stress of the EPI Poly film is measured by the tool KLA-Tencor Flexus FLX5500. The measurement is performed on three test wafers where EPI Poly layers with different thicknesses (target values: $13\ \mu\text{m}$, $18\ \mu\text{m}$ and $23\ \mu\text{m}$) are grown employing the same recipe used in the process flow of the lots. The residual stress is measured right after the growth by the scanner laser method on the mirror-like backside of the wafer since the front side is characterized by high roughness. The measurement occurs along four different diameters: the residual stress of the layer is considered as the average of the values obtained along each diameter. It should be noted that the sign of residual stress given as an output by the tool must be reversed since the measurement is performed on the back side. After the growth, the thickness is reduced by CMP respectively to $10\ \mu\text{m}$, $15\ \mu\text{m}$ and $20\ \mu\text{m}$. The residual stress is measured again for the three test wafers by using KLA-Tencor Flexus FLX5500. The measurement is performed on the front side along four diameters. The value of residual stress in Eq. 5.14 refers to the stress measured after

CMP, because it is employed in the fabrication of the test structures. However, a relevant effect of CMP on the residual stress of EPI Poly is not expected. Assumption (a) is required since it is not possible to calculate the residual stress of the EPI Poly layer from the measurement of the deflection of the single-layer cantilevers in lot 1. As mentioned in section 5.1, the measurement of the deflection of single-layer cantilevers allows only the calculation of the stress gradient.

Assumption (b) is validated by measuring the thickness of the EPI Poly layer by infrared (IR) light interferometry in nine points of the wafer. The analysis of the uniformity of the thickness of EPI Poly post-CMP is performed on wafers LM 1, 6, 11, 12, 13, 14, 15, 19 and 25 of lot 2 and on wafers LM 1, 10, 13, 14 and 25 of lot 3. From the measured data, the uniformity is evaluated by the term “non-uniformity” which is calculated as the standard deviation over the mean value in percentage. Higher values of non-uniformity are related to a lower thickness uniformity of the layer. The thickness non-uniformity of the EPI Poly layer is around 1%, validating assumption (b). Similarly, assumption (c) is validated by measuring the thickness of the thin film by reflectometry in forty-nine points of the wafer, employing the tool N&K 3000 Analyzer. The measurement is performed on wafers LM 1, 4, 7 and 10 of lot 2 respectively for the films *LPCVD SiN tens*, *PECVD USG*, *PECVD SiN +170* and *PECVD SiN -150*; while on wafers LM 1, 4, 7 and 10 of lot 3 respectively for the films *PECVD SiN -150 B*, *PECVD SiN -350*, *PECVD SiON* and *LPCVD SiN comp*. The thickness non-uniformity of the thin film is in general around 1%, validating assumption (c). The results are considered as the reference thickness of the films in the calculation of the residual stress due to the high repeatability of the deposition processes. Assumption (d) is validated by measuring the deflection of the totality of cantilevers in six different test structures for wafers LM 10 and 13 of lot 2. Five of the six test structures analyzed are placed near the edges, while the other one is placed near the center of the wafer. Since for each test structure the standard deviation of the cantilever deflection is lower than the uncertainty in the measurement (0.1 μm), just the deflections of one 1270 μm long cantilever and one 829 μm long cantilever are measured for each test structure.

The deflection of single-layer cantilevers in EPI Poly is fundamental to calculate the residual stress of the thin film in bi-layer cantilevers. In single-layer cantilevers, the deflection is directly related to the stress gradient of the layer. Since the stress gradient of the base layer affects the deflection of the bi-layer cantilever, the deflection of the single-layer cantilever is measured to evaluate the local stress gradient of the layer. An analysis on the distribution of the stress gradient across the EPI Poly layer is performed on the five wafers of lot 1 to validate assumption (e). The stress gradient is calculated from the deflection of single-layer cantilevers by using Eq. 5.6.

The residual stress (σ_1) of the thin films deposited on the wafers of lot 2 and lot 3 is calculated from the deflection of the bi-layer cantilevers by using Eq. 5.14:

$$\sigma_1 = \frac{\left(2 \frac{E_0}{L^2}\right) (I_c \delta_c - I_b \delta_b) + \sigma_0 w t_0 y_c}{w t_1 \left(\frac{t_1}{2} + \frac{t_0}{2} - y_c\right)}$$

The terms in the equation are detailed in section 5.2. For each test structure, the measurement occurs along the profile line traced at the top of the structure. For both lots, the value of deflection of the single-layer cantilever in EPI Poly is taken from wafer LM 13 for bi-layer cantilevers with a 20 μm thick base layer and from LM 14 for bi-layer cantilevers with a 10 μm thick base layer. The stress gradient of the EPI Poly layer cannot be assumed as uniform; therefore, the local deflection of the single-layer cantilevers is used in the equation instead of the average deflection. In the calculation of the residual stress from a certain test structure, the value of deflection of the single-layer cantilever refers to the respective test structure of the reference wafer placed in the same spot. Therefore, it is assumed that the EPI Poly layers on the wafers of the same lot are characterized by the same stress gradient distribution. In Table 6, the values of Young's modulus used in the residual stress calculation for the EPI Poly layer and the thin films are listed. The Young's modulus of *LPCVD SiN* is taken from literature [2], while for the EPI Poly layer and the other thin films the values are provided based on experimental data acquired by STMicroelectronics R&D process team. The uncertainty in the results of residual stress due to the propagation of the uncertainty of the deflection measurement is calculated in accordance with the "Guide to the expression of uncertainty in measurement" [3].

Table 6: Young's modulus of EPI Poly and the thin films deposited.

	EPI Poly	LPCVD SiN	PECVD SiN	PECVD USG	PECVD SiON
Young's modulus (GPa)	$1.6 \cdot 10^2$	$2.6 \cdot 10^2$ [2]	$1.8 \cdot 10^2$	$0.7 \cdot 10^2$	$0.7 \cdot 10^2$

In order to prove the accuracy of this method, the results obtained from cantilevers with a 20 μm thick EPI Poly layer will be compared with the results from cantilevers with a 10 μm thick layer in section 7.5. Similarly, the results obtained from 1270 μm long cantilevers and from 829 μm long cantilevers will be compared in section 7.6.

6.4. Characterization by the scanning laser method

As discussed in section 4.2, the scanning laser method is the reference technique employed to evaluate the residual stress in thin films. This method allows the evaluation of the average residual stress across the entire wafer from its curvature by using the Stoney's equation. The results of the cantilever deflection method will be compared with the results of the scanning laser

method in section 7.8. Since the cantilever deflection method is a local technique, the mean residual stress across the wafer is calculated to compare the two methods. The scanning laser method is employed by using the tool KLA-Tencor Flexus FLX5500. The measurement is performed on test wafers, on which for each recipe the thin films are deposited by using the exact same tools employed for lot 2 and lot 3. The curvature of the wafer is measured along four different diameters and the edge exclusion is equal to 20 mm.

Finally, the results of the cantilever deflection method will be compared with the results of the local evaluation of the residual stress by the scanning laser method in section 7.8. The tool Frontier Semiconductor FSM 128 C2C is employed to evaluate the local residual stress in the thin film from the local curvature of the wafer. The scanning path is divided in 0.8 mm long intervals; the local residual stress is calculated by the Stoney's equation from the curvature of the wafer in each interval. The analysis is limited to the recipe *LPCVD SiN tens* and it is performed on four different diameters of the test wafers. The edge exclusion is equal to 10 mm.

References

¹ J. Jin, J. W. Kim, C.-S. Kang, J.-A. Kim, S. Lee; Precision depth measurement of through silicon vias (TSVs) on 3D semiconductor packaging process; *Optics Express* 20, 5, 5011-5016 (2012).

² W.-H. Chuang, T. Luger, R. K. Fetting, R. Ghodssi; *Mechanical property characterization of LPCVD silicon nitride thin films at cryogenic temperatures*; *Journal of Microelectromechanical systems* 13, 5, 870 – 879 (2004).

³ *Evaluation of measurement data - Guide to the expression of uncertainty in measurement*; Joint Committee for Guides in Metrology (2008).

7 | Results and discussion

Figure 46 shows a SEM image of the test structure at the end of the process flow, where it is possible to observe the free-standing cantilevers and the cavity opened on the backside of the wafer.



Figure 46: SEM image of the test structure at the end of the process flow.

In the following sections, the analyses performed to validate the assumptions made in section 6.3, the values and the distributions of residual stress calculated from the test structures fabricated on wafers of lot 2 and lot 3 are shown and discussed. Finally, the cantilever deflection method is compared with the scanning laser method.

7.1 Residual stress of the EPI Poly layer

The thickness and the residual stress of the EPI Poly layer before and after the CMP step are listed in Table 7 for three test wafers.

Table 7: Thickness and residual stress of the EPI Poly layer before and after the CMP step for three test wafers.

	Thickness before CMP (μm)	Residual stress before CMP (MPa)	Thickness after CMP (μm)	Residual stress after CMP (MPa)
Test wafer 1	13.10	-3	9.89	-4
Test wafer 2	17.90	-2	14.81	-2
Test wafer 3	22.98	-1	20.05	-1

The average thickness of the EPI Poly layer, measured by IR light interferometry, is respectively 13.10 μm , 17.90 μm and 22.98 μm . The residual stress of each layer measured before performing CMP is respectively -3 MPa, -2 MPa and -1 MPa. The decrease of the compressive stress with thickness towards a condition of “zero-stress” for the 23 μm layer is in agreement with ST experimental reference data [1].

For each test wafer, the average thickness of the EPI Poly layer after CMP is respectively: 9.89 μm , 14.81 μm and 20.05 μm ; while the residual stress is respectively -4 MPa, -2 MPa and -1 MPa. As expected, relevant variations in residual stress do not occur after performing CMP. In the calculation of the residual stress of the thin film, the residual stress of the EPI Poly layer is considered -4 MPa for cantilevers with a 10 μm base layer and -1 MPa in case of a 20 μm thick base layer.

7.2 Validation of the assumptions in the calculation of residual stress

As discussed in section 6.3, the thickness of the EPI Poly and the thickness of the thin film are assumed uniform across the entire wafer, while the residual stress is assumed locally uniform in the region of each test structure. These assumptions are validated in this section.

The average thickness and the thickness non-uniformity of the EPI Poly layer of wafers LM 1, 6, 11, 12, 13, 14, 15, 19 and 25 of lot 2 are listed in Table 8.

Table 8: Mean thickness and thickness non-uniformity of the EPI Poly layer of wafers LM 1, 6, 11, 12, 13, 14, 15, 19 and 25 of lot 2.

	Mean thickness (μm)	Thickness non-uniformity (%)
LM 1	19.99	0.8
LM 6	19.99	1.0
LM 11	20.04	0.7
LM 12	19.99	1.0
LM 13	20.14	0.9
LM 14	10.03	1.0
LM 15	10.00	0.8
LM 19	10.02	1.1
LM 25	9.96	1.1

The low values of thickness non-uniformity (around 1%) validate the assumption of uniform thickness of EPI Poly across the whole wafer. Due to the high repeatability of the process, the results are in accordance with the target value. Therefore, in the calculation of the residual stress of the thin film, the thickness of the EPI Poly layer is taken as the average between the results from wafers LM 1, 6, 11, 12 and 13 (20.03 μm) in the case of bi-layer cantilevers with a 20 μm

thick base layer. Similarly, in the case of bi-layer cantilevers with a 10 μm thick base layer, the thickness of the EPI Poly layer is taken as the average of the results from wafers LM 14, 15, 19 and 25 (10.00 μm).

The average thickness and the thickness non-uniformity of the EPI Poly layer of wafers LM 1, 10, 13, 14 and 25 of lot 3 are listed in Table 9.

Table 9: Mean thickness and thickness non-uniformity of the EPI Poly layer of wafers LM 1, 10, 13, 14 and 25 of lot 3.

	Mean thickness (μm)	Thickness non-uniformity (%)
LM 1	19.95	1.0
LM 10	20.02	1.0
LM 13	20.00	1.1
LM 14	9.96	1.0
LM 25	9.99	1.1

Similarly to lot 2, the thickness non-uniformity is around 1%. For lot 3 the thickness of the EPI Poly layer is taken as the average thickness of LM 1, 10 and 13 (19.99 μm) for wafers from LM 1 to LM 13, while as the average thickness of LM 14 and 25 (9.98 μm) for wafers from LM 14 to LM 25.

The thickness analysis of the thin films deposited on wafers LM 1 (*LPCVD SiN tens*), LM 4 (*PECVD USG*), LM 7 (*PECVD SiN +170*) and LM 10 (*PECVD SiN -150*) of lot 2 and LM 1 (*PECVD SiN -150 B*), LM 4 (*PECVD SiN -350*), LM 7 (*PECVD SiON*) and LM 10 (*LPCVD SiN comp*) of lot 3 are respectively listed in Table 10 and Table 11.

Table 10: Mean, maximum and minimum thickness, thickness range, thickness non-uniformity and nominal thickness of the thin films deposited on wafers LM 1, 4, 7 and 10 of lot 2.

	Thin film	Mean thickness (\AA)	Maximum thickness (\AA)	Minimum thickness (\AA)	Thickness range (\AA)	Thickness non-uniformity (%)	Nominal thickness (\AA)
LM 1	LPCVD SiN tens	3009	3046	2948	98	1.0	3000
LM 4	PECVD USG	3970	4062	3923	139	0.8	4000
LM 7	PECVD SiN +170	1413	1445	1382	63	1.1	1400
LM 10	PECVD SiN -150	3044	3080	3029	51	0.3	3000

Table 11: Mean, maximum and minimum thickness, thickness range, thickness non-uniformity and nominal thickness of the thin films deposited on the wafers LM 1, 4, 7 and 10 of lot 3.

	Thin film	Mean thickness (Å)	Maximum thickness (Å)	Minimum thickness (Å)	Thickness range (Å)	Thickness non-uniformity (%)	Nominal thickness (Å)
LM 1	PECVD SiN -150 B	3090	3176	3038	139	1.4	3000
LM 4	PECVD SiN -350	2934	3006	2897	109	0.7	3000
LM 7	PECVD SiON	5010	5116	4952	164	0.9	5000
LM 10	LPCVD SiN comp	2170	2224	2093	131	2.1	2100

The difference between the mean thickness and the nominal thickness is generally in the order of nanometers, which confirms the high accuracy of the deposition processes. The assumption of uniform thickness is validated by low values of non-uniformity (around 1% or even lower) and by ranges between the maximum and the minimum thickness around 10 nm in the worst cases.

For six test structures of wafers LM 10 and 13 of lot 2, the deflection of the totality of the cantilevers in the array is measured. The mean, the maximum and the minimum deflection and the standard deviation for each test structure analyzed on wafer LM 10 are listed in Table 12, while the results for each test structure analyzed on wafer LM 13 are listed in Table 13.

Table 12: Mean, maximum and minimum deflection, and standard deviation of the six 1270 μm long cantilevers in each test structure analyzed for wafer LM 10 of lot 2.

Test Structure	Mean deflection (μm)	Maximum deflection (μm)	Minimum deflection (μm)	Standard deviation (μm)
#1	-1.1	-1.1 \pm 0.1	-1.2 \pm 0.1	0.04
#2	-1.3	-1.3 \pm 0.1	-1.4 \pm 0.1	0.03
#3	-1.0	-0.9 \pm 0.1	-1.0 \pm 0.1	0.03
#4	-1.3	-1.2 \pm 0.1	-1.4 \pm 0.1	0.05
#5	-1.2	-1.1 \pm 0.1	-1.3 \pm 0.1	0.06
#6	-1.4	-1.4 \pm 0.1	-1.5 \pm 0.1	0.01

Table 13: Mean, maximum and minimum deflection, and standard deviation of the six 1270 μm long cantilevers in each test structure analyzed for wafer LM 13 of lot 2.

Test Structure	Mean deflection (μm)	Maximum deflection (μm)	Minimum deflection (μm)	Standard deviation (μm)
#1	1.7	1.8 \pm 0.1	1.6 \pm 0.1	0.06
#2	1.5	1.6 \pm 0.1	1.4 \pm 0.1	0.06
#3	1.5	1.5 \pm 0.1	1.4 \pm 0.1	0.03
#4	1.5	1.5 \pm 0.1	1.4 \pm 0.1	0.04
#5	1.7	1.8 \pm 0.1	1.7 \pm 0.1	0.05
#6	1.6	1.7 \pm 0.1	1.5 \pm 0.1	0.07

For the totality of the test structures analyzed, the standard deviation of the cantilever deflection is lower than the uncertainty of the measurement (0.1 μm). This result is valid for both LM 10 and LM 13. Therefore, the deflection of just one cantilever for each test structure on the wafer is measured to calculate the local residual stress of the thin film, assuming that the residual stress of the thin film and the stress gradient of the EPI Poly layer are locally uniform in the region of the test structure.

7.3. Stress gradient of the EPI Poly layer

The deflection of one 1270 μm long cantilever is measured for each test structure of the five wafers of lot 1. The mean, the maximum and the minimum deflection and the deflection range are listed in Table 14 for each wafer of the lot.

Table 14: Mean, maximum and minimum deflection, and deflection range of the 1270 μm long cantilevers for each wafer of lot 1.

	Mean deflection (μm)	Maximum deflection (μm)	Minimum deflection (μm)	Deflection range (μm)
LM 1	1.9	2.2 \pm 0.1	1.7 \pm 0.1	0.5
LM 2	1.9	2.1 \pm 0.1	1.7 \pm 0.1	0.4
LM 3	1.9	2.1 \pm 0.1	1.6 \pm 0.1	0.5
LM 4	1.9	2.1 \pm 0.1	1.7 \pm 0.1	0.4
LM 5	1.9	2.2 \pm 0.1	1.7 \pm 0.1	0.5

The local stress gradient of the EPI Poly layer is calculated for each test structure from the local deflection by using Eq. 5.6. The mean, the maximum and the minimum stress gradient and the stress gradient range are calculated and listed in Table 15 for each wafer.

Table 15: Mean, maximum and minimum stress gradient, and stress gradient range of the EPI Poly layer calculated from the 1270 μm long cantilevers for each wafer of lot 1.

	Mean stress gradient (MPa/ μm)	Maximum stress gradient (MPa/ μm)	Minimum stress gradient (MPa/ μm)	Stress gradient range (MPa/ μm)
LM 1	0.41	0.46 \pm 0.02	0.36 \pm 0.02	0.10
LM 2	0.41	0.46 \pm 0.02	0.36 \pm 0.02	0.10
LM 3	0.41	0.45 \pm 0.02	0.35 \pm 0.02	0.10
LM 4	0.41	0.46 \pm 0.02	0.37 \pm 0.02	0.09
LM 5	0.41	0.47 \pm 0.02	0.37 \pm 0.02	0.10

The stress gradient distribution of the EPI Poly layer is analyzed by using a contour plot from the local values of stress gradient referred to the coordinates of the respective test structures. Figure

47 shows the contour plots of the stress gradient distribution for the five wafers of lot 1. In the maps, the notch of the wafer is represented by the red dot at (0; -100).

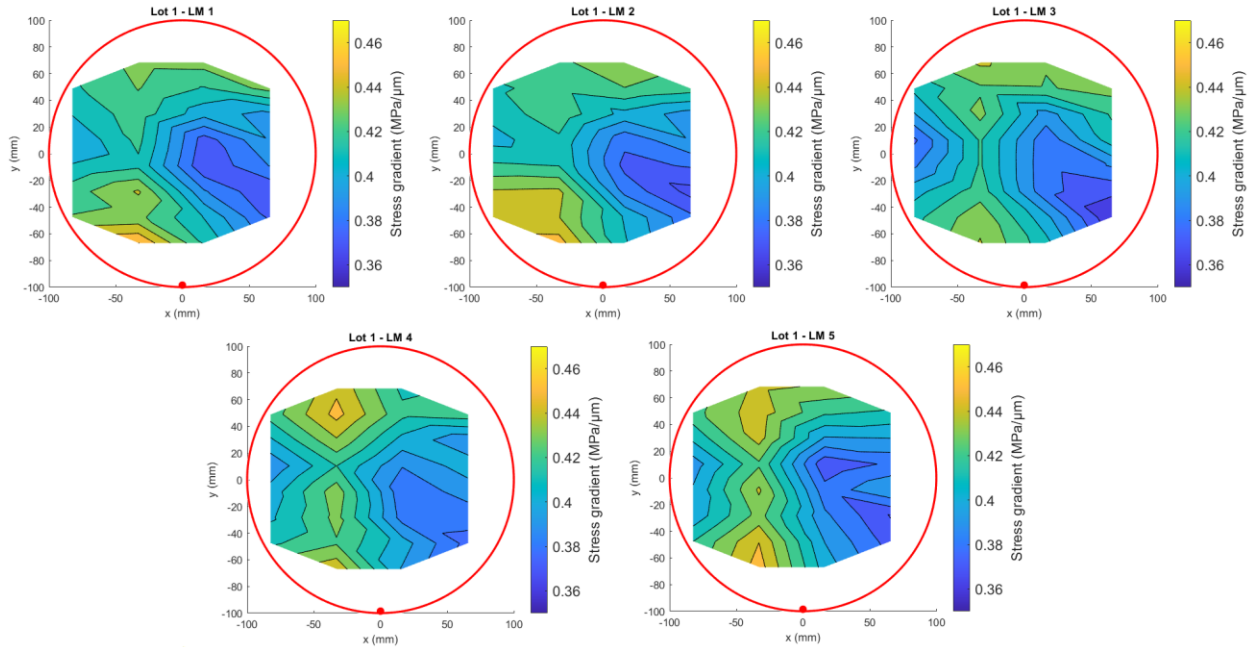


Figure 47: Stress gradient distribution of the EPI Poly layer for the wafers of lot 1 calculated from the 1270 μm long cantilevers.

From Table 15, it can be noted that the wafers are characterized by almost the same values of mean, maximum and minimum stress gradient, and stress gradient range. The range between the maximum and the minimum stress gradient (around 0.10 MPa/ μm) is in the same order of magnitude of the stress gradient. Therefore, it is not allowed to assume that the stress gradient of the EPI Poly layer is uniform across the wafer, as shown in Figure 47. Moreover, the stress gradient distribution is similar for all the wafers, which suggests that in general wafers from the same lot are characterized by the same stress gradient distribution. Therefore, in the calculation of residual stress from a certain test structure the deflection of the single-layer cantilever is taken from the corresponding test structure on the reference wafer. The reference wafer is needed to substitute in Eq. 5.10 the stress gradient of the base layer, which is an unknown term, with the deflection of a single-layer cantilever, which is measurable.

7.4. Residual stress of thin films: lot 2

In this section, the residual stress of the thin films deposited on the wafers of lot 2 is calculated locally from the deflection of the bi-layer cantilevers with a 20 μm thick EPI Poly base layer. The

deflection of the respective single-layer cantilevers in EPI Poly is measured locally on wafer LM 13.

7.4.1. Residual stress of LPCVD SiN tens

The residual stress of *LPCVD SiN tens* thin film is calculated locally from each test structure of wafers LM 1, 2 and 3. The mean, the maximum and the minimum residual stress, and the stress range are listed in Table 16 for each wafer.

Table 16: Mean, maximum and minimum residual stress, and stress range of the “LPCVD SiN tens” film deposited on wafers LM 1, 2 and 3 of lot 2.

	Mean residual stress (MPa)	Maximum residual stress (MPa)	Minimum residual stress (MPa)	Stress range (MPa)
LM 1	545	567 ± 8	519 ± 8	48
LM 2	540	563 ± 8	512 ± 8	51
LM 3	542	564 ± 8	498 ± 8	66

In Figure 48, the residual stress measured from the deflection of the cantilevers on wafers LM 1, 2 and 3 is compared with the nominal residual stress of the deposition recipe (600 MPa), represented by a red line. The control range of the nominal value (± 40 MPa) is represented by two red dashed lines.

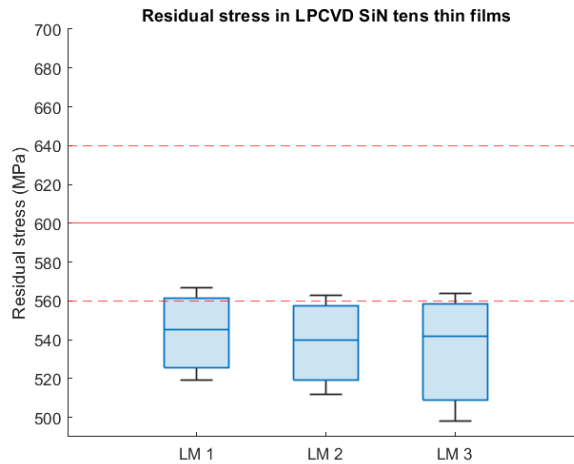


Figure 48: Comparison of the mean residual stress of the “LPCVD SiN tens” film and its range for wafers LM 1, 2 and 3 of lot 2 with the nominal stress and the control range.

Table 16 shows a significant correspondence between the mean and the maximum residual stress of the three wafers, which are respectively around 542 MPa and 565 MPa. A slight discrepancy in

the minimum residual stress is observed for LM 3 compared to LM 1 and LM 2, affecting the stress range which is higher for LM 3. The measured values of residual stress are lower than the nominal value, as it is shown by Figure 48. In particular, the mean residual stress is not included in the control range for all the three wafers since it is lower than the lower limit (560 MPa).

The distribution of the residual stress in the analyzed area of the wafer is represented by a contour plot in Figure 49 for wafers LM 1, 2 and 3.

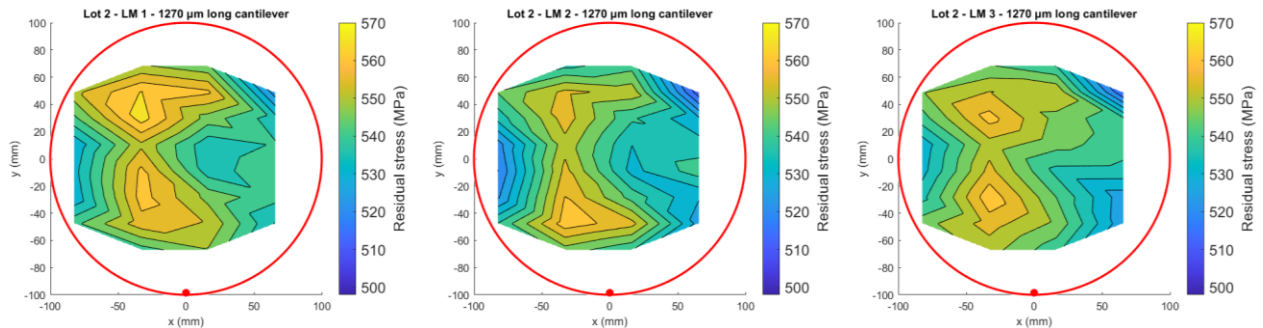


Figure 49: Residual stress distribution of the “LPCVD SiN tens” film across the analyzed area for wafers LM 1, 2 and 3 of lot 2 calculated from the 1270 μm long cantilevers.

The residual stress distribution is similar for all the three wafers. The regions on the center-left of the analyzed area (referred to a notch-down position) are characterized by a higher tensile stress (around 560 MPa), while the regions towards the edge are in general characterized by a lower stress (around 520 MPa). The distribution does not appear centrosymmetric; therefore, it is not possible to define a general center-to-edge variability. Since in the LPCVD reactor the wafers are processed simultaneously, similar stress distributions were expected; the dynamic of the LPCVD deposition is not expected to generate a centrosymmetric pattern. The accordance in the stress distribution in Figure 49 shows the ability of the cantilever deflection method in representing the residual stress locally. Slight variations in residual stress between the wafers are expected since they are placed in different positions of the reactor boat.

7.4.2. Residual stress of PECVD USG

The residual stress of *PECVD USG* thin films is calculated locally from each test structure of wafers LM 4, 5 and 6. The mean, the maximum and the minimum residual stress and the stress range are listed in Table 17 for each wafer.

Table 17: Mean, maximum and minimum residual stress and stress range of the “PECVD USG” films deposited on wafers LM 4, 5 and 6 of lot 2.

	Mean residual stress (MPa)	Maximum residual stress (MPa)	Minimum residual stress (MPa)	Stress range (MPa)
LM 4	-96	-86 ± 6	-104 ± 6	19
LM 5	-95	-85 ± 6	-103 ± 6	18
LM 6	-95	-84 ± 6	-105 ± 6	21

In Figure 50, the residual stress measured from the deflection of the cantilevers on wafers LM 4, 5 and 6 is compared with the nominal residual stress of the deposition recipe (-80 MPa), represented by a red line. The control range of the nominal value (± 40 MPa) is represented by two red dashed lines.

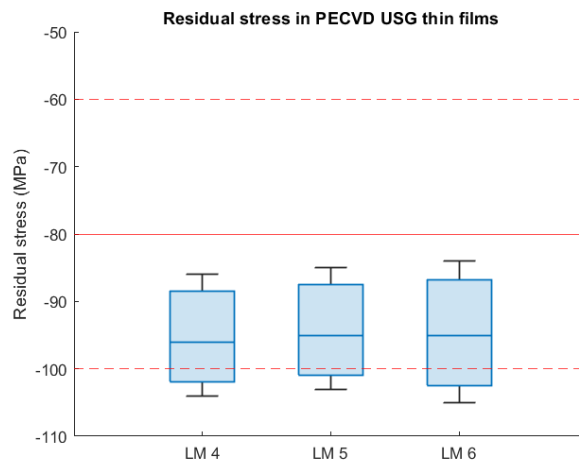


Figure 50: Comparison of the mean residual stress of the “PECVD USG” film and its range for wafers LM 4, 5 and 6 of lot 2 with the nominal stress and the control range.

Table 17 shows a significant correspondence between the mean, the maximum and the minimum residual stress of the three wafers, which are respectively around -95 MPa, -85 MPa and -104 MPa. Although the mean residual stress is more compressive than the nominal value, it is included in the control range, as it is shown in Figure 50. However, the minimum measured values of residual stress are lower than the lower limit of the control range (-100 MPa). This case shows the relevance of the local evaluation of the residual stress. Employing a non-local technique as the scanning laser method, the thin film passes the control test since the mean residual stress is included in the control range. However, in some regions of the wafer the residual stress exceeds the control limits.

The distribution of residual stress in the analyzed area of the wafer is obtained by a contour plot and it is shown in Figure 51 for wafers LM 4, 5 and 6.

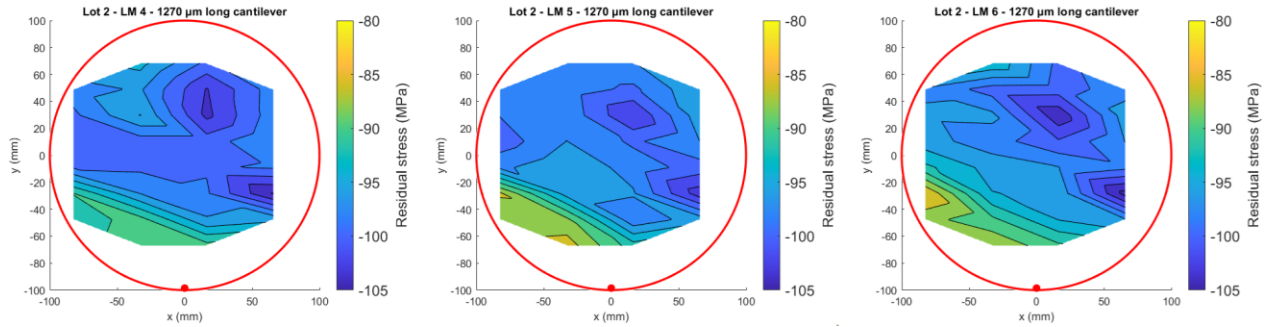


Figure 51: Residual stress distribution of the “PECVD USG” film across the analyzed area for wafers LM 4, 5 and 6 of lot 2 calculated from the 1270 μm long cantilevers.

The residual stress distribution is similar for all the three wafers. The distribution is not clearly centrosymmetric; however, the central region is characterized by a more compressive residual stress (around -100 MPa). In the region near the edge on the notch side of the wafer, the residual stress is slightly less compressive (around -90 MPa). Since the PECVD chamber employed is a single-wafer reactor, the three wafers were not processed simultaneously. The fact that the residual stress distribution is similar for all the three cases confirms that thin films deposited in the same chamber are characterized by similar stress distributions.

7.4.3. Residual stress of PECVD SiN +170

The residual stress of PECVD SiN +170 thin films is calculated locally from each test structure of wafers LM 7 and 9. The mean, the maximum and the minimum residual stress and the stress range are listed in Table 18 for each wafer.

Table 18: Mean, maximum and minimum residual stress and stress range of the “PECVD SiN +170” films deposited on wafers LM 7 and 9 of lot 2.

	Mean residual stress (MPa)	Maximum residual stress (MPa)	Minimum residual stress (MPa)	Stress range (MPa)
LM 7	142	161 \pm 17	105 \pm 17	56
LM 9	142	165 \pm 17	99 \pm 17	66

In Figure 52, the residual stress measured from the deflection of the cantilevers on wafers LM 7 and 9 is compared with the nominal residual stress of the deposition recipe (170 MPa), represented by a red line. The control range of the nominal value (± 70 MPa) is represented by two red dashed lines.

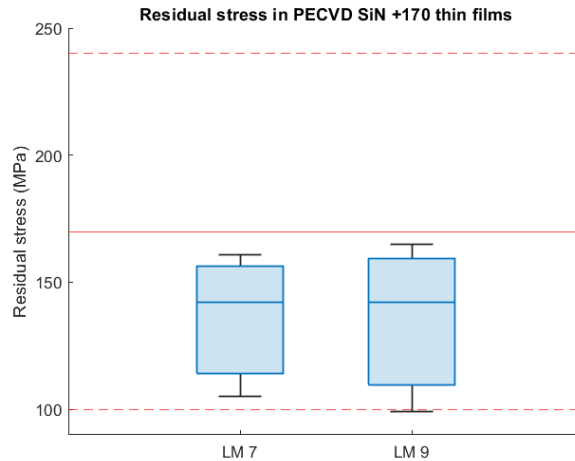


Figure 52: Comparison of the mean residual stress of the “PECVD SiN +170” film and its range for the wafers LM 7 and 9 of lot 2 with the nominal stress and the control range.

The mean, the maximum and the minimum residual stress of the two wafers are in accordance: respectively around 142 MPa, 163 MPa and 102 MPa. The mean residual stress is less tensile than the nominal value. The results are in accordance with the specifications of the recipe since they are included in the control range, as it is shown by Figure 52.

The distribution of residual stress in the analyzed area of the wafer is obtained by a contour plot and it is shown in Figure 53 for wafers LM 7 and 9.

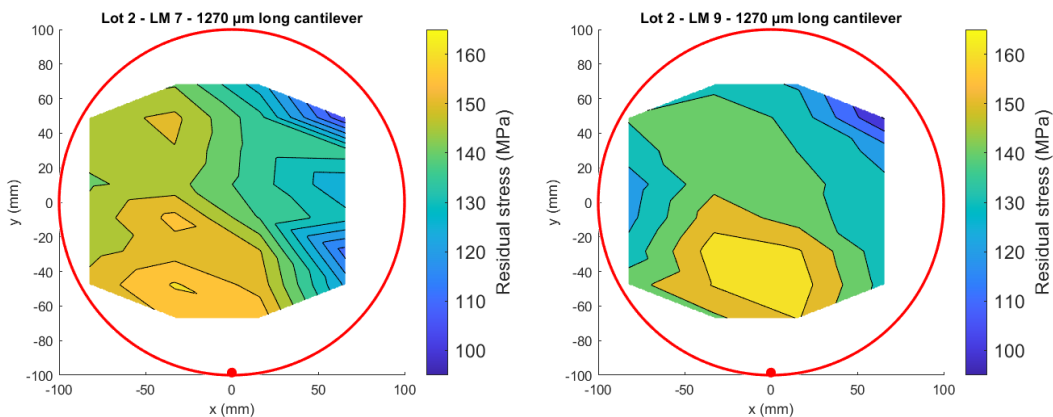


Figure 53: Residual stress distribution of the “PECVD SiN +170” film across the analyzed area for wafers LM 7 and 9 of lot 2 calculated from the 1270 μm long cantilevers.

The residual stress distribution is similar for both wafers. The region of the analyzed area towards the notch side is characterized by a more tensile residual stress (around 160 MPa). As mentioned

in section 6.1, PECVD SiN +170 is deposited employing a tool in which two wafers are processed simultaneously in two different chambers. The wafers LM 7 and LM 9 were processed in one chamber, while LM 8 was processed in the other one. The tight correspondence in the values and the distribution of the residual stress was expected for LM processed in the same chamber, while some small variations were expected for LM 8 due to the use of another deposition chamber.

7.4.4. Residual stress of PECVD SiN -150

The residual stress of PECVD SiN -150 thin films is calculated locally from each test structure of wafers LM 10, 11 and 12. The mean, the maximum and the minimum residual stress and the stress range are listed in Table 19 for each wafer.

Table 19: Mean, maximum and minimum residual stress and stress range of the “PECVD SiN +170” films deposited on wafers LM 10, 11 and 12 of lot 2.

	Mean residual stress (MPa)	Maximum residual stress (MPa)	Minimum residual stress (MPa)	Stress range (MPa)
LM 10	-131	-113 ± 8	-149 ± 8	36
LM 11	-132	-115 ± 8	-153 ± 8	38
LM 12	-135	-119 ± 8	-149 ± 8	30

In Figure 54, the residual stress measured from the deflection of the cantilevers on wafers LM 10, 11 and 12 is compared with the nominal residual stress of the deposition recipe (-150 MPa), represented by a red line. The control range of the nominal value (± 30 MPa) is represented by two red dashed lines.

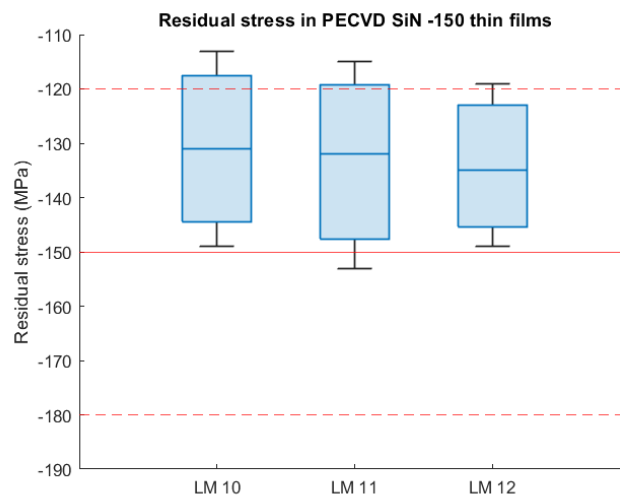


Figure 54: Comparison of the mean residual stress of the “PECVD SiN -150” film and its range for wafers LM 10, 11 and 12 of lot 2 with the nominal stress and the control range.

Table 19 shows a significant correspondence between the mean, the maximum and the minimum residual stress of the three wafers, which are respectively around -133 MPa, -116 MPa and -150 MPa. The mean residual stress is less compressive than the nominal value, but it is included in the control range, as it is shown in Figure 54. However, the maximum measured values of residual stress are higher than the upper limit of the control range (-120 MPa). In this respect it is important to recall that the film passes the deposition control test when the residual stress is measured by a non-local technique, even if in some regions of the wafer the residual stress exceeds the control limits.

The distribution of residual stress in the analyzed area of the wafer is obtained by a contour plot and it is shown in Figure 55 for wafers LM 10, 11 and 12.

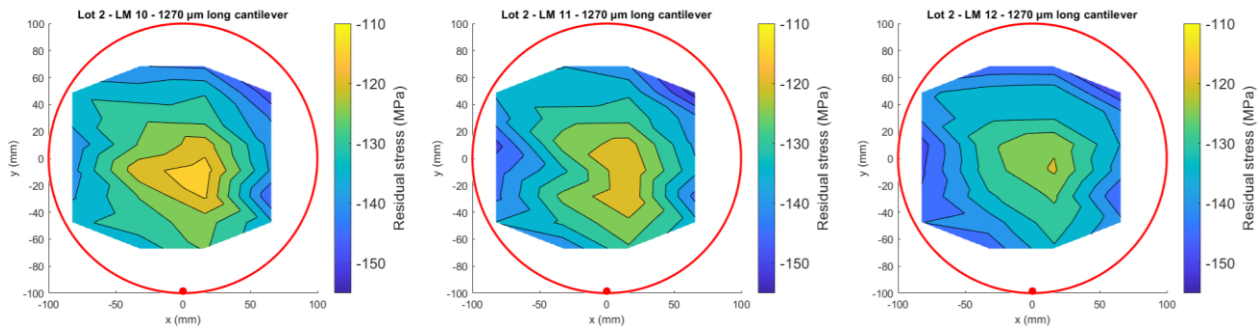


Figure 55: Residual stress distribution of the “PECVD SiN -150” film across the analyzed area for wafers LM 10, 11 and 12 of lot 2 calculated from the 1270 μm long cantilevers.

The residual stress distribution is similar for all the three wafers. In this case, the distribution can be approximated as clearly centrosymmetric as expected for plasma driven deposition. In the central region of the wafer the residual stress is less compressive (around -115 MPa) while it becomes more compressive towards the edges. The center-to-edge variability is around 35 MPa.

7.5. Comparison between cantilevers of different thicknesses

In this section, the results obtained from wafers with a 20 μm thick EPI Poly layer are compared with the results obtained from wafers with a 10 μm thick EPI Poly layer of lot 2. The comparison is made analyzing only the 1270 μm long cantilevers. The mean, the maximum and the minimum residual stress and the stress range for each wafer with a 10 μm thick base layer of lot 2 are calculated and listed in Table 20.

Table 20: Mean, maximum and minimum residual stress and stress range of the thin films deposited on the wafers of lot 2 with a 10 µm thick EPI Poly layer.

Thin film	Wafer	Mean residual stress (MPa)	Maximum residual stress (MPa)	Minimum residual stress (MPa)	Stress range (MPa)
LPCVD SiN tens	LM 15	595	612 ± 2	553 ± 2	59
PECVD USG	LM 18	-106	-95 ± 1	-111 ± 1	17
	LM 19	-106	-96 ± 1	-112 ± 1	16
	LM 20	-106	-94 ± 1	-113 ± 1	19
PECVD SiN +170	LM 21	190	211 ± 4	164 ± 4	46
	LM 22	144	166 ± 4	117 ± 4	49
	LM 23	182	201 ± 4	160 ± 4	41
PECVD SiN -150	LM 25	-148	-133 ± 2	-165 ± 2	32

For all the wafers with a 10 µm thick base layer, the uncertainty of the local stress is lower than in the case of a 20 µm thick base layer. This is due to a lower propagation of the uncertainty of the measurement of cantilever deflection. Since a lower thickness of the base layer means a lower moment of inertia of the cantilever section, the variation of deflection consequently a certain variation of stress is higher for cantilevers with a 10 µm thick base layer than for cantilevers with a 20 µm thick base layer. Therefore, they are less affected by the uncertainty of the measurement of deflection.

The comparison of the results from wafers of the same deposition split is performed only for *PECVD SiN +170* and *PECVD USG* films. In the case of *PECVD USG*, wafers LM 18, 19 and 20 are characterized by almost the same mean, maximum and minimum residual stress, in agreement with the results from wafers with a 20 µm thick base layer. Differently, in the case of *PECVD SiN +170* the results of LM 22 differ from LM 21 and LM 23. This discrepancy, which is in the order of tens of MPa, could be due to the tool employed in the deposition of the film. As mentioned above, the *PECVD SiN +170* film is deposited in a tool which presents two deposition chambers working in parallel mode.

For each film, the mean, the maximum and minimum residual stress and the stress range calculated from wafers with a 10 µm thick EPI Poly layer are compared with the respective results obtained from wafers with a 20 µm thick base layer. In particular, the results in Table 20 are compared with the results in Table 16 for the *LPCVD SiN tens* film, in Table 17 for the *PECVD USG* film, in Table 18 for the *PECVD SiN +170* film and in Table 19 for the *PECVD SiN -150* film. For all the films on a 10 µm thick base layer, the residual stress is more tensile in the case of tensile films and more compressive in the case of compressive films. Although the higher uncertainty of the results from wafers with a 20 µm thick base layer affects the comparison, a discrepancy around tens of MPa must be due to other causes. One possible explanation is that one of the assumptions of the calculation affects the results differently depending on the thickness of the base layer. It must be noted that in the case of the *PECVD SiN +170* film, only the wafer LM 22 should be compared with the wafers LM 7 and LM 9 since for these wafers the deposition process occurred

in the same chamber. Therefore, in the case of *PECVD SiN +170* film the results seem in accordance.

Apart from the *LPCVD SiN tens* film, the residual stress distributions of the wafers with a 10 μm thick base layer and a 20 μm thick base layer are in accordance. The stress distribution of the *PECVD USG* film on wafers LM 18, 19 and 20 is shown in Figure 56. Comparing the plots in Figure 56 with the plots in Figure 51 (20 μm thick EPI Poly), it can be observed the accordance in the variation of stress across the wafer.

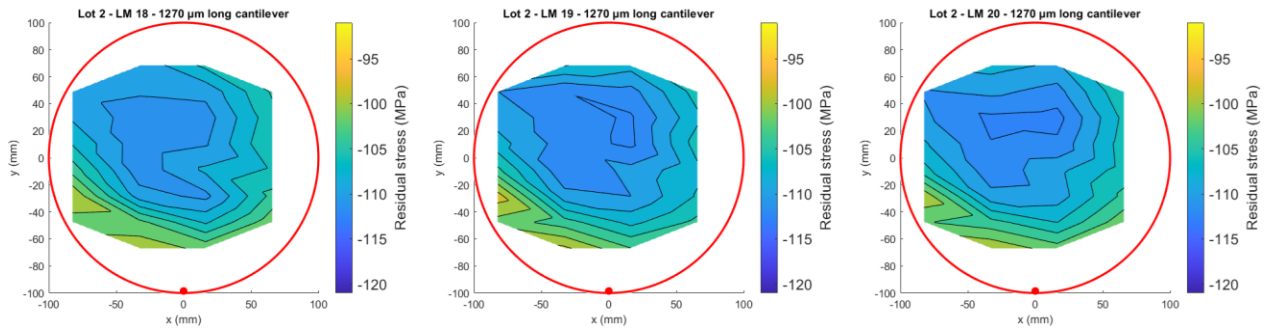


Figure 56: Residual stress distribution of the “*PECVD USG*” film across the analyzed area for wafers LM 18, 19 and 20 of lot 2 calculated from the 1270 μm long cantilevers.

The residual stress distribution of the *LPCVD SiN tens* film on wafer LM 15 is shown in Figure 57. Differently from LM 1, 2 and 3 (Figure 49), the distribution appears more centrosymmetric with a higher tensile stress (around 600 MPa) at the center of the wafer.

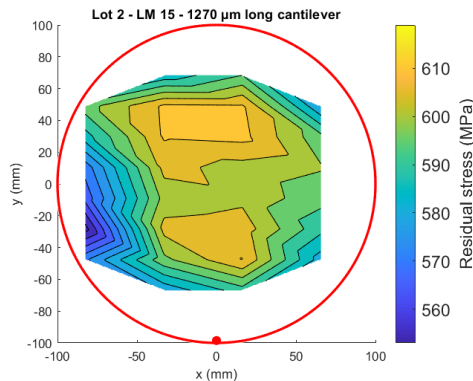


Figure 57: Residual stress distribution of the “*PECVD SiN -150*” film across the analyzed area for wafer LM 15 of lot 2 calculated from the 1270 μm long cantilevers.

The stress distribution of the *PECVD SiN +170* film for wafers LM 21, 22 and 23 is shown in Figure 58. As discussed above, the mean residual stress of LM 22 is less compressive. This information

could be obtained also from the scanning laser method. However, the cantilevers' deflection method enables the comparison of the residual stress variation across the film. It can be noted that the stress distribution of LM 22 is similar to the stress distributions of LM 21 and LM 23.

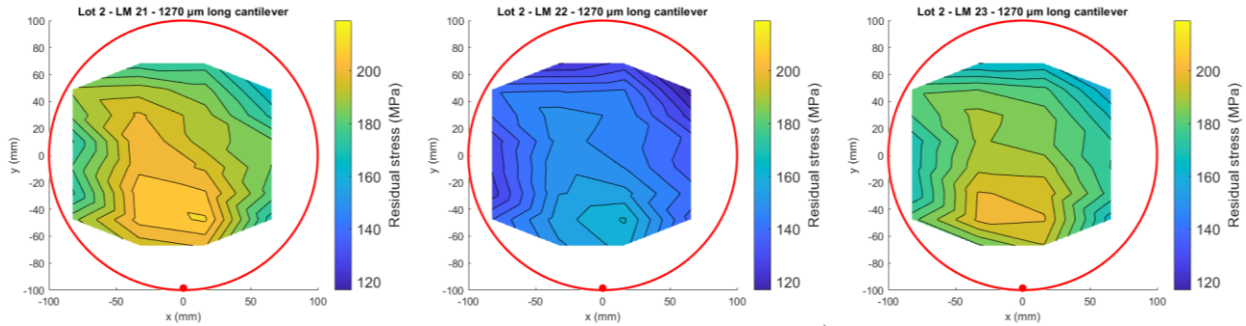


Figure 58: Residual stress distribution of the “PECVD SiN +170” film across the analyzed area for wafers LM 21, 22 and 23 of lot 2 calculated from the 1270 μm long cantilevers.

7.6. Comparison between cantilevers of different lengths

In this section, the results obtained from the 1270 μm long cantilevers are compared with the results obtained from the 829 μm long cantilevers. The mean, the maximum and the minimum residual stress and the stress range calculated from the 829 μm long cantilevers for each wafer of lot 2 with a 20 μm thick base layer are listed in Table 21.

Table 21: Mean, maximum and minimum residual stress and stress range of the films deposited on the wafers with a 20 μm thick EPI Poly layer of lot 2 calculated from the 829 μm long cantilevers.

Thin film	Wafer	Mean residual stress (MPa)	Maximum residual stress (MPa)	Minimum residual stress (MPa)	Stress range (MPa)
LPCVD SiN tens	LM 1	564	588 \pm 20	539 \pm 20	50
	LM 2	575	598 \pm 20	536 \pm 20	62
	LM 3	574	600 \pm 20	529 \pm 20	72
PECVD USG	LM 4	-99	-84 \pm 15	-110 \pm 15	26
	LM 5	-98	-85 \pm 15	-106 \pm 15	22
	LM 6	-97	-85 \pm 15	-111 \pm 15	26
PECVD SiN +170	LM 7	149	183 \pm 41	123 \pm 41	59
	LM 9	149	185 \pm 41	101 \pm 41	84
PECVD SiN -150	LM 10	-137	-117 \pm 19	-170 \pm 19	53
	LM 11	-135	-116 \pm 19	-161 \pm 19	46
	LM 12	-139	-122 \pm 19	-168 \pm 19	46

In the case of 829 μm long cantilevers the uncertainty of the local residual stress is higher than in the case of 1270 μm long cantilevers because for a certain variation of the deflection profile the

variation of the deflection at the tip is lower for shorter cantilevers. In the case of wafers with a 20 μm thick base layer, the uncertainties in the local stress calculated from 829 μm long cantilevers are in the order of tens of MPa. Therefore, the results from 1270 μm long cantilevers and from 829 μm long cantilevers of the same wafer are compared for wafers with a 10 μm thick base layer. The mean, the maximum and the minimum residual stress and the stress range calculated from the 829 μm long cantilevers for each wafer of lot 2 with a 10 μm thick base layer are listed in Table 22.

Table 22: Mean, maximum and minimum residual stress and stress range of the films deposited on the wafers with a 10 μm thick EPI Poly layer of lot 2 calculated from the 829 μm long cantilevers.

Thin film	Wafer	Mean residual stress (MPa)	Maximum residual stress (MPa)	Minimum residual stress (MPa)	Stress range (MPa)
LPCVD SiN tens	LM 15	601	619 \pm 5	571 \pm 5	49
PECVD USG	LM 18	-110	-96 \pm 4	-116 \pm 4	20
	LM 19	-111	-95 \pm 4	-120 \pm 4	24
	LM 20	-108	-91 \pm 4	-116 \pm 4	25
PECVD SiN +170	LM 21	197	219 \pm 10	171 \pm 10	47
	LM 22	151	171 \pm 10	123 \pm 10	48
	LM 23	188	205 \pm 10	168 \pm 10	37
PECVD SiN -150	LM 25	-150	-132 \pm 5	-169 \pm 5	38

Considering the uncertainties, the results in Table 22 are in accordance with the values in Table 20, as expected since they refer to the same wafers. Moreover, also the residual stress distributions calculated from 829 μm long cantilevers are in accordance with the distributions obtained from 1270 μm long cantilevers of the same wafers. This is valid for all the films analyzed: Figure 59 shows as an example the comparison between the stress distributions of PECVD USG obtained from the 1270 μm long cantilevers and from the 829 μm long cantilevers of wafers LM 18, 19 and 20. The fact that calculating the local residual stress of a thin film from cantilevers with different length on the same wafer gives almost the same results proves the accuracy of the cantilever deflection method. Since different lengths of the cantilevers give the same results, the geometry of the cantilevers can be designed depending on the specifications of the film which must be characterized and considering different expected deflections that might impact the measurement.

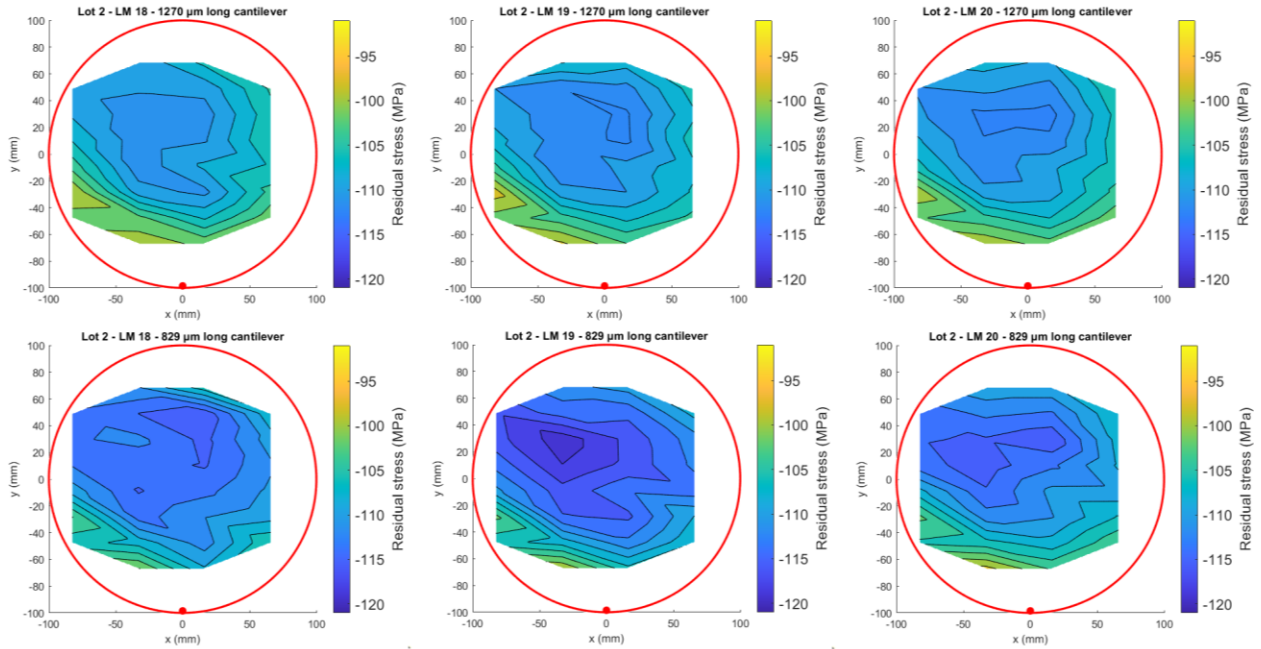


Figure 59: Comparison between the residual stress distribution obtained from the 1270 μm long cantilevers and from the 829 μm long cantilevers on the same wafer for wafers LM 18, 19 and 20 of lot 2.

7.7. Residual stress of thin films: lot 3

The local residual stress of *PECVD SiN -150 B*, *PECVD SiN -350*, *PECVD SiON*, and *LPCVD SiN comp* thin films is calculated from the measurement of the deflection of the cantilevers fabricated on the wafers of lot 3. The mean, the maximum and the minimum residual stress, and the stress range are listed in Table 23 for each wafer with a 20 μm thick EPI Poly layer, and in

Table 24 for each wafer with a 10 μm thick EPI Poly layer. Apart from the *PECVD SiN -350* film deposited on a 10 μm EPI Poly layer, the results are calculated from the deflection of the 1270 μm long cantilevers. In the case of *PECVD SiN -350* on a 10 μm EPI Poly layer, for the majority of the 1270 μm long cantilevers the deflection measurements failed due to excessive downward deflections around 25 μm . Therefore, the results are calculated from the deflection of the 829 μm long cantilevers.

Table 23: Mean, maximum and minimum residual stress, and stress range for each wafer of lot 3 with a 20 μm thick EPI Poly layer.

Thin film	Wafer	Mean residual stress (MPa)	Maximum residual stress (MPa)	Minimum residual stress (MPa)	Stress range (MPa)
PECVD SiN -150 B	LM 2	-71	-16 ± 8	-124 ± 8	108
	LM 3	-88	-44 ± 8	-137 ± 8	93
PECVD SiN -350	LM 4	-305	-285 ± 8	-326 ± 8	41
	LM 5	-302	-272 ± 8	-323 ± 8	51
PECVD SiON	LM 7	-75	-59 ± 5	-96 ± 5	37
	LM 8	-77	-46 ± 5	-104 ± 5	58
	LM 9	-75	-59 ± 5	-92 ± 5	33
LPCVD SiN comp	LM 10	-26	-15 ± 11	-53 ± 11	38
	LM 11	-23	-3 ± 11	-38 ± 11	35
	LM 12	-29	-10 ± 11	-52 ± 11	42

Table 24: Mean, maximum and minimum residual stress, and stress range for each wafer of lot 3 with a 10 μm thick EPI Poly layer.

Thin film	Wafer	Mean residual stress (MPa)	Maximum residual stress (MPa)	Minimum residual stress (MPa)	Stress range (MPa)
PECVD SiN -150 B	LM 15	-95	-31 ± 2	-148 ± 2	117
	LM 16	-106	-62 ± 2	-160 ± 2	98
	LM 17	-98	-36 ± 2	-153 ± 2	117
PECVD SiN -350	LM 18	-376	-347 ± 5	-397 ± 5	50
	LM 19	-376	-352 ± 5	-393 ± 5	41
	LM 20	-370	-348 ± 5	-391 ± 5	43
PECVD SiON	LM 21	-79	-45 ± 1	-105 ± 1	60
	LM 22	-84	-71 ± 1	-101 ± 1	30
	LM 23	-88	-52 ± 1	-118 ± 1	66
LPCVD SiN comp	LM 24	-41	-33 ± 3	-47 ± 3	14
	LM 25	-41	-34 ± 3	-55 ± 3	21

The results confirm the accordance in the residual stress of thin films of the same deposition split. The *PECVD SiN -150 B* and *PECVD SiON* films were deposited in a double-chamber tool; therefore, the differences in maximum and minimum residual stress are expected to be due to the different chambers used for the deposition process. In the case of *PECVD SiN -150 B* film, the discrepancy in the maximum residual stress is around 30 MPa. In the case of *PECVD SiON* film, the discrepancy in the maximum residual stress is more evident (around 20 MPa) in the results from

Table 24. In both cases the stress range is affected by the chamber employed, resulting in a different variability of residual stress across the wafer. However, in the case of *PECVD SiON* the mean residual stress is well aligned regardless of the deposition chamber that has been used.

The comparison between the results in Table 23 and

Table 24 confirms that the residual stress calculated from cantilevers with a 10 μm thick base layer results more compressive in case of compressive films, as expected from the analysis of lot 2.

As for lot 2, the stress distributions across the film are similar for wafers from the same deposition split. As an example, the residual stress distribution of *PECVD SiON* film is shown in Figure 60 for wafers LM 7, 8, 9, 21, 22 and 23. The stress distribution is similar for all the six wafers: the central region of the wafer is characterized by a less compressive residual stress. In particular, it is possible to notice a significant correspondence in stress distribution between wafers processed on the same chamber (LM 7, 9, 22 and LM 8, 21, 23).

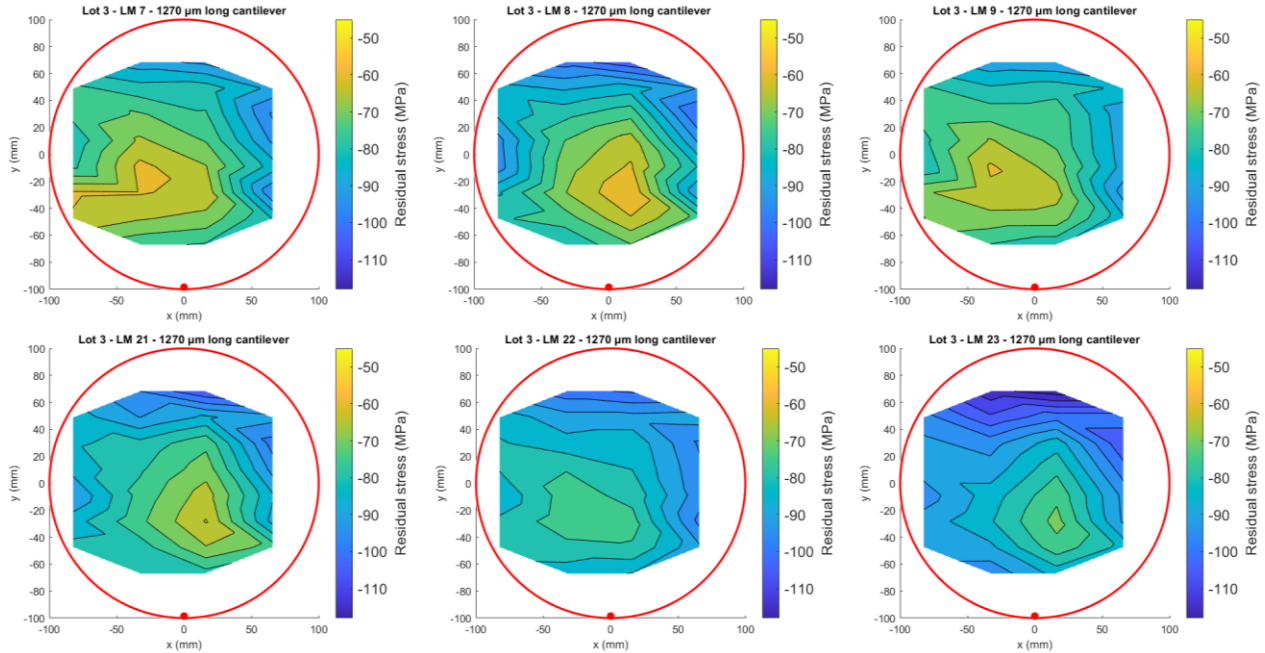


Figure 60: Residual stress distribution of the “*PECVD SiON*” film across the analyzed area for wafers LM 7, 8, 9, 21, 22 and 23 of lot 3 calculated from the 1270 μm long cantilevers.

7.8. Comparison with the scanning laser method

In this section, the results obtained from the cantilever deflection method are compared with the results of the scanning laser method performed on test wafers. The mean residual stress of the film is evaluated by a non-local measurement of the radius of curvature of the wafer along four different diameters employing the tool KLA-Tencor Flexus FLX5500. The results are listed in Table 25 alongside the average values of mean residual stress calculated for 1270 μm long cantilevers. It should be noted that in some cases the average values of mean residual stress are taken from wafers processed with the same deposition process but in different chambers.

Table 25: Comparison between the mean residual stress calculated by the scanning laser method (employing the tool KLA-Tencor Flexus FLX5500) and by the cantilever deflection method.

Thin film	Mean residual stress (MPa)		
	KLA-Tencor Flexus FLX5500	20 μm thick cantilevers	10 μm thick cantilevers
LPCVD SiN tens	610	542	595
PECVD USG	-99	-95	-106
PECVD SiN +170	154	142	172
PECVD SiN -150	-141	-133	-148
PECVD SiN -150 B	-130	-80	-100
PECVD SiN -350	-347	-304	-374
PECVD SiON	-103	-76	-84
LPCVD SiN comp	-118	-26	-41

As expected, the non-local application of Stoney’s equation gives an overall mean residual stress comparable to the cantilever deflection method. Indeed, the application of this technique is well-established in the semiconductor industry and also for MEMS fabrication, where the film stress plays a crucial role. It should be noted that a slight discrepancy was expected since the scanning laser method is performed immediately after the deposition process, while the measurement of cantilever deflection is performed after the fabrication of the test structures and therefore exposing the wafers to several process steps and their thermal budget.

As discussed in chapter 3, Stoney’s equation should be applied considering the radius of curvature of the entire wafer. However, there are some measurement tools that allow local stress analyses by applying the Stoney’s equation to the local radius of curvature between two points of the scanning path. The tool Frontier Semiconductor FSM 128 C2C is employed to evaluate the residual stress profile of the *LPCVD SiN tens* film along four different diameters for three test wafers. An example of the residual stress profile along each diameter is shown in Figure 61.

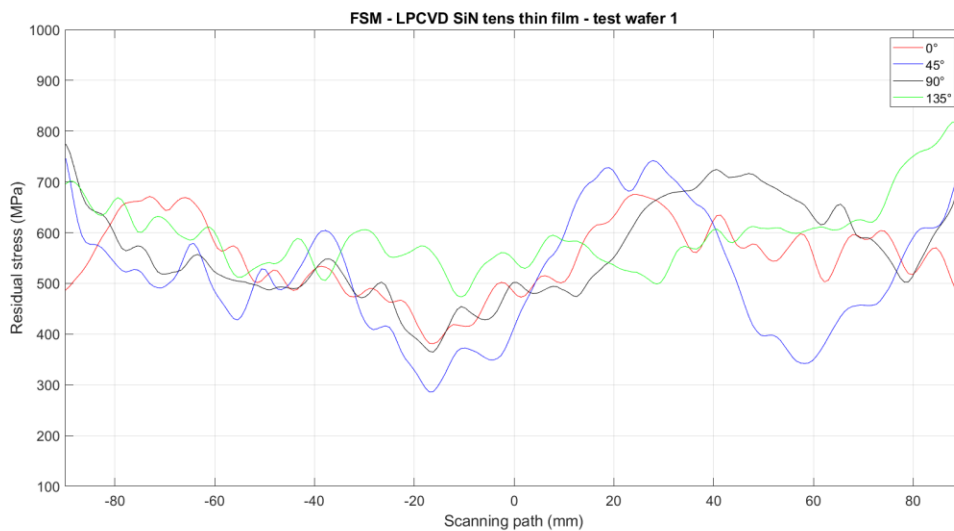


Figure 61: Residual stress profile of the “LPCVD SiN tens” film along the four diameters analyzed calculated by using the tool Frontier Semiconductor FSM 128 C2C.

From the plot, it can be noted a significant variation of the residual stress along the four diameters analyzed and, thus, a high difference between the minimum residual stress (around 300 MPa) and the maximum (around 800 MPa). This aspect is highlighted in Figure 62, where the mean residual stress and its range are plotted for wafers LM 1, 2, 3 and 15 of lot 2 and for the three test wafers analyzed with Frontier Semiconductor FSM 128 C2C, which are labelled as FSM 1, FSM 2 and FSM 3.

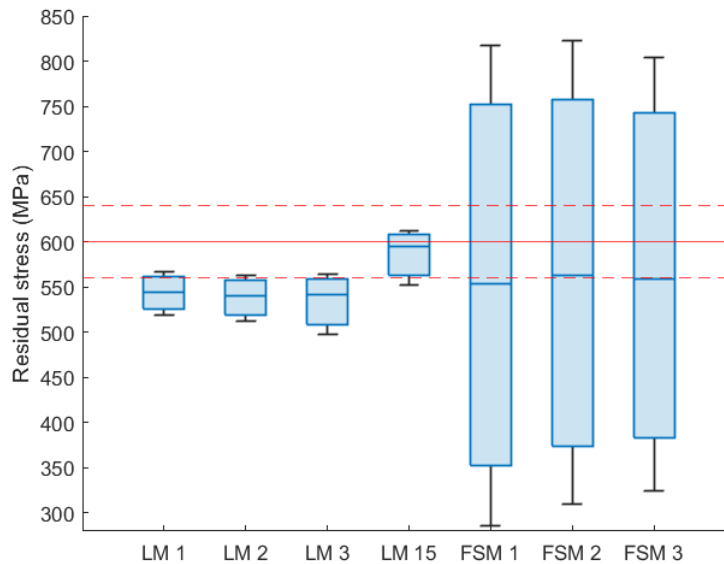


Figure 62: Comparison between the mean residual stress and the range between maximum and minimum residual stress of the “LPCVD SiN tens” film obtained by the cantilever deflection method (LM 1, 2, 3 and 15) and by the scanning laser method performed locally using the tool Frontier Semiconductor FSM 128 C2C (FSM 1, 2 and 3).

The differences in the local residual stress evaluation between the cantilever deflection method and the scanning laser method are significant. Even if the mean residual stress is comparable between the two techniques, the range between the maximum and the minimum residual stress differs by one order of magnitude. This analysis confirms that Stoney’s equation should not be applied locally without properly modifying the equation [2].

References

¹ B. Vigna, P. Ferrari, F. F. Villa, E. Lasalandra, S. Zerbini; *Silicon Sensors and Actuators*; Springer; chapter 2: “Epitaxy” (2022).

² M. Zhu, P. B. Kirby; *Governing equation for the measurement of nonuniform stress distributions in thin films using a substrate deformation technique*; Appl. Phys. Lett. 88, 171903 (2006).

8 | Conclusions

In this work, a method to evaluate the local residual stress of thin films by using MEMS test structures fabricated on 8" silicon wafers was applied on industrial CVD processes. Each test structure consists of an array of cantilevers composed of an EPI Poly base layer, which has a structural role, and the thin film deposited on top for the stress characterization. The free-standing cantilevers deflect upon release due to the unbalanced bending moment generated by the residual stress, which is calculated starting from the measurement of the cantilever deflection acquired by using visible light interferometry. The test structures were fabricated on a silicon wafer by employing a customized MEMS process flow. Differently from wafer level measurements, which evaluate exclusively the as-deposited residual stress, the measurement on the cantilever is performed at the end of a dedicated process flow and thus the thin film is characterized in a fairly realistic situation. Eight different dielectric thin films have been characterized both with conventional techniques and with the cantilever approach. The aim was to evaluate for the first time the distribution and the variability of the residual stress of each film on an 8" wafer.

8.1 Achieved results

The residual stress and stress variability of the films analyzed in this work are listed in Table 26. The results are taken from the analysis of the cantilevers with a 10 μm thick EPI Poly layer. For each film, the values of mean, maximum and minimum residual stress, stress range and stress non-uniformity are considered as the average values calculated from wafers of the same deposition split.

Table 26: Residual stress and stress variability obtained from the cantilever deflection method for each thin film analyzed in this work.

	Mean residual stress (MPa)	Maximum residual stress (MPa)	Minimum residual stress (MPa)	Stress range (MPa)	Stress non-uniformity (%)
LPCVD SiN tens	595	612	553	59	2.5
PECVD USG	-106	-95	-112	17	4.5
PECVD SiN +170	186	206	162	44	6.7
PECVD SiN -150	-148	-133	-165	32	5.7
PECVD SiN -150 B	-97	-34	-151	117	31.7
PECVD SiN -350	-374	-352	-394	45	3.0
PECVD SiON	-84	-49	-112	63	17.1
LPCVD SiN comp	-41	-34	-51	18	9.1

The obtained range between the maximum and the minimum residual stress represents a key information that can be used during the MEMS design. Moreover, this characterization provides unique insights that are intimately connected to the thin film deposition process development phase. Finally, the stress distribution on the 8" substrate can be correlated to the final mechanical and electrical characterization of fabricated MEMS devices. All the aforementioned opportunities, which were precluded with non-local stress characterization methods, are enabled by the cantilever deflection method presented in this work. Additional information has been obtained studying the effect of a split in the thickness of the EPI Poly layer (20 μm and 10 μm). Moreover, the effect of the length of the cantilevers has been also investigated.

The cantilever deflection method has also been compared to the scanning laser method, in which the mean residual stress is evaluated by Stoney's equation from the measurement of the curvature of the wafer. The two different methods provided average stress results that can be considered in good agreement within the variations associated to the different characterization processes. However, these two methods are not alternatives: the cantilevers' deflection method is required to characterize the residual stress of thin films since the stress distribution can only be evaluated by a local measurement. Differently, the scanning laser method is useful to control the deposition process in an easier and faster way during the fabrication process. The comparison with the cantilever deflection method confirms that the local application of Stoney's equation is not able to evaluate accurately the stress distribution of a thin film, while the mean residual stress is in accordance with the cantilever deflection method.

8.2 Outlooks

This work has set solid bases in the application of the cantilever deflection method to measure the residual stress of thin films. The obtained results have been demonstrated reliable and useful for an application at industrial level during the design, development and fabrication of MEMS sensors and actuators. Starting from the work that has been conducted so far, some suggestions to improve the method can be found. The cantilever geometry (i.e., the length of the cantilever and the thickness of the base layer) must be properly chosen to increase the accuracy of the measurement. The comparison between cantilevers with a 20 μm thick base layer and 10 μm thick base layer suggested that a 10 μm thick base layer is preferred due to the lower propagation of the uncertainty in the measurement of deflection. On the other hand, it must be highlighted that thinner base layers result in higher deflections, which may not be measurable by visible light interferometry. The cantilever geometry should also be chosen depending on the specifications of the film to characterize. Higher deflections are obtained from thicker and highly stressed thin films; in these cases, shorter cantilevers may be more suitable to perform the analysis. As far as the cantilever geometry is concerned, it would be recommended to integrate in the test structure layout cantilevers of different lengths. The number of test structures present in the layout should be increased to obtain more detailed maps of residual stress. The position of the test dies should

be changed to centrosymmetric to improve the evaluation of the center-to-edge variability and the sensitivity in mapping the stress distribution.

A natural follow up of this activity would be to employ this method to characterize multi-layer stacks. In this case, in the same array the cantilevers could be fabricated with a different number of thin films on top of the base layer. From each cantilever the residual stress of the film on top will be calculated considering the residual stress of the films below obtained from dedicated cantilevers. The investigation and the characterization of the residual stress in different films, regardless of the deposition technique, is expected to become more critical with the evolution of the MEMS devices towards more demanding sensing and actuation performances.